Autonomous Docking for Work Class ROVs

Petar Trslić

Supervisors: Prof Daniel Toal

Dr Gerard Dooly

Dr Edin Omerdic

Department of Electronic & Computer Engineering

University of Limerick

Submitted to the University of Limerick for the degree of

Doctor of Philosophy

March 2020

To my parents Jasna and Darko. Thank you for your endless support, inspiration, and encouragement.

Declaration

I hereby declare that except where specific reference is made to the work of others, the contents of this dissertation are original and have not been submitted in whole or in part for consideration for any other degree or qualification in this, or any other university. This dissertation is my own work and contains nothing which is the outcome of work done in collaboration with others, except as specified in the text and Acknowledgements. This dissertation contains fewer than 65,000 words including appendices, bibliography, footnotes, tables and equations and has fewer than 150 figures.

Petar Trslić

March 2020

Acknowledgements

Firstly, I would like to express my gratitude to my supervisors Prof Daniel Toal, Dr Gerard Dooly, and Dr Edin Omerdic for giving me the opportunity to conduct this research and for their guidance and support throughout my PhD studies. I would like to thank my current and former colleges from Centre for Robotics & Intelligent Systems (CRIS), Dr Matija Rossi, Dr Satja Sivcev, Dr Joseph Coleman, Cathal W. O'Donnell, Stefano Pierantozzi, Anthony Weir and Luke Robinson. Tremendous teamwork that included system integration and field testing was required to complete this research work. I would like to acknowledge the rest of the CRIS team. They provided constant support and assistance, and created an enjoyable working environment.

I would like to thank my mother Jasna, father Darko, sisters Anja, Ivana and Marija, and all friends who have tried to understand the process of going through a PhD and for providing much needed support and encouragement. Finally, for a lot of patience, and a little bit of very much needed distraction, I would like to thank my girlfriend Marija.

This material is based upon works supported by Science Foundation Ireland and industry partners Shannon Foynes Port Company and The Commissioners of Irish Lights under the MaREI Research Centres Awards 12/RC/2302_P2 & 14/SP/2740, RoboVaaS EU ERA-Net Co-fund award through Irish Marine Institute and EU Horizon 2020 research and innovation programme project EUMarineRobots under grant agreement 731103.

Abstract

This thesis describes research work in the domain of underwater robotics. It is aimed towards improving performance and achieving partial or full autonomy in the rapidly increasing underwater resident robotics field, with the emphasis on the development of a suite of technologies for autonomous Remotely operated vehicle (ROV) docking. Fundamentally resident ROVs operating from shore demand high bandwidth, zero latency communication link which is often unavailable, thus high levels of automation are needed to compensate. This is especially important for time-critical tasks such as ROV docking. In addition, the docking station provides a download/upload link, charging point, and overall mechanical protection for the resident vehicles. Therefore, the docking of the ROV at the end of a mission is one of the crucial ROV tasks and often dictates weather window extents. Research in the literature mainly focuses on the docking to a static docking station, and although docking to a docking station deployed to the seabed is part of the thesis, the emphasis is on the docking to a Tether Management System (TMS) garage suspended from the floating platform/ship. This is used as a ROV docking scenario close to that of docking to a dock on a floating production platform such as floating oil production platform, floating wind platform or floating offshore fish farm sea-cage. Typically it is difficult to compensate for all motion between the ROV and the suspended TMS/dock due to underpowered thrust, large inertia, and high drag forces, presenting a significant challenge. If the docking of a conventional work-class ROV to a suspended TMS proves successful, it presents a significant contribution and accelerates the path towards collaborative and integrated ROV and Autonomous surface vehicle (ASV) systems. This advancement will drive further improvements in the autonomous transition of the existing intervention subsea vehicles across large areas, primarily associated with the offshore wind sector. The work presented in the thesis consists of three major parts.

The first is the visual pose estimation system developed to provide accurate relative position measurements between the ROV and the docking station/TMS. The developed system is based on active light beacons asymmetrically arranged to form a unique marker, and a machine vision camera. The system is built around conventional, industry-standard subsea LED lights and camera and it has been successfully tested both in a lake and in the ocean. The additional algorithm has been developed to reduce the pose estimation errors due to the low camera sensitivity to angle measurements from longer distances. The system has been developed

for standard work-class ROV systems found throughout the sector, deployed from suspended cage type TMS.

The second is autonomous docking of an industry-standard work-class ROV to cage type TMS using a visual-based pose estimation approach. This included both, autonomous docking to static TMS deployed to the seabed, and docking to TMS suspended from the ship. Evaluation of the system has been demonstrated through completion of offshore trials in the North Atlantic Ocean during January 2019.

The third is a suspended TMS heave motion prediction method for ROV docking, based on the Adaptive Neuro-Fuzzy Inference System (ANFIS). With large ROV inertia and drag forces acting against it, the ROV is not agile enough to match a cage type TMS heaving motion. Therefore the ROV docking manoeuvre has to start before the ROV and the TMS align. This also includes matching the ROV to the docking depth that covers top or the bottom half of the TMS heave range, where TMS vertical speed is low. The method includes on-site neural network training based on previous TMS depth measurements and the TMS depth prediction. In addition, this method could be used standalone as a ROV pilot aiding tool.

Table of contents

List of figures

List of figures

List of Acronyms

ANFIS	Adaptive Neuro-Fuzzy Inference System
AR	Augmented reality
ASV	Autonomous surface vehicle
AUV	Autonomous underwater vehicle
CAPEX	Capital expenditures
CRIS	Centre for Robotics & Intelligent Systems
DOF	Degree of freedom
DP	Dynamic positioning
DS	Docking station
DVL	Doppler Velocity Log
EKF	Extended Kalman filter
FIS	Fuzzy Inference System
FOG	Fibre optics gyroscope
FOV	Field of view
H-ROV	Hybrid remotely operated vehicle
IMR	Inspection, maintenance, and repair
IMU	Inertial measurement unit
INS	Inertial navigation system
I-ROV	Inspection class remotely operated vehicle
KF	Kalman filter

LARS	Launch and recovery system
LBL	Long baseline
LLC	Low-level controllers
MAE	Mean average error
MaREI	Marine Renewable Energy Ireland
MRE	Marine Renewable Energy
O&G	Oil and Gas
OPEX	Operational expenditures
PoE	Power over Ethernet
RMSE	Root mean squared error
ROV	Remotely operated vehicle
RV	Research vessel
SBL	Short baseline
SFI	Science Foundation Ireland
TMS	Tether management system
TRL	Technology readiness level
UAV	Unmanned aerial vehicle
USBL	Ultra-short baseline
USV	Unmanned surface vehicle
UUV	Unmanned underwater vehicle

List of tables

Chapter 1

Introduction

1.1 Motivation

Due to its geographic location and climate, Ireland has exceptional Marine Renewable Energy resources (SEAI, 2010), with the government target of achieving 40% of all Irish electricity being generated from renewable sources of energy by the end of 2020 (Dineen, 2019). Thus, the development of technologies in the ocean energy field plays an important role in the Irish government's energy strategy. The same trend exists globally, with a particular focus on MRE development in other parts of northern Europe where these natural resources are widespread. Although there is a significant energy potential in wave and tidal energy production, such technologies require further R&D. On the other hand, offshore wind energy is already significantly contributing to the national grid in many countries, with UK being largest offshore wind energy producer (Fraile and Komusanac, 2019) with over 1900 operating offshore wind turbines and over 990 in construction (The Crown Estate, 2018). This has been recently followed by UK opening Offshore Wind Leasing Round 4 in October 2019, resulting in opening up the potential for at least 7 GW of new offshore wind projects in the waters around England and Wales (The Crown Estate, 2019). At the same time, Ireland's national sustainable energy authority (SEAI) long term prediction shows rapid expansion of both onshore and offshore wind energy production, with potential of 11 GW onshore and 30 GW offshore

wind energy deployed in Irish waters by 2050, and directly creating 20 000 jobs in installation, and Operation & Maintenance (O&M) tasks (SEAI, 2011).

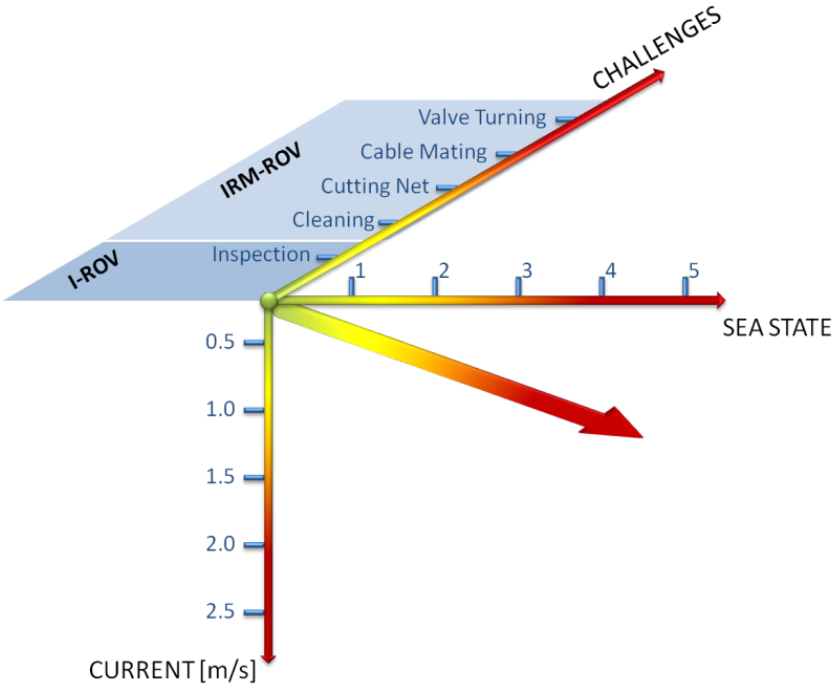

Fig. 1.1 Classification of the difficulties faced by underwater robotics as the tasks become more complex, the sea state worse, and the currents stronger. Ongoing research within this thesis and other projects in the CRIS Centre are aimed away from the origin and towards increasingly challenging scenarios.

Development of marine robotic solutions is therefore necessary to support large-scale MRE related operations, such as construction, monitoring, IMR tasks, and others. Since the MRE sector requires devices to be placed in areas of strong wind, current, and tides, marine robotics needs to evolve for such challenging environments, as shown in Fig. 1.1, in order to support the rapid expansion and roll-out of the offshore sector. In addition, in recent years the offshore wind sector pushed production platforms further off the coast, into areas of higher energy potential, following a similar development path as Oil & Gas (O&G) platforms on-shore, in shallow coastal waters, and subsequently O&G field exploitation progressing into deeper waters. Considering significant expenditures related to the cost of the surface support vessel and crew, and with the production platforms in remote locations, the cost related to inspection, maintenance, and repair tasks inevitably

rise. Those rising costs have resulted in the development and use of permanently deployed resident vehicle systems. Although the concept of permanently deployed vehicles exists in the literature for many years (McLeod, 2010), only recently have we seen the introduction of commercial resident ROV vehicles (Maslin, 2019*b*), with Oceaneering and IKM being industry leaders. However, such systems consist of a ROV and a Tether Management System (TMS) deployed to the seabed, thus the ROV operations are limited to the relatively close proximity to the seabed. For deep-water floating energy production sites, the operational depth of the ROV should be flexible due to inspection and maintenance tasks spread across the whole water column and including, cabling and anchoring on the seabed, mooring, chains and flexible risers up through the water column and floating infrastructure near the surface and above the waterline.

In addition, while resident ROVs are seen as a possible solution for O&G industry, within the MRE production field, multiple assets can be spread across more than 100 km^2, which need to be continuously inspected for condition monitoring purposes. Therefore, mobile platform to accommodate IMR tasks with significant operational radius will have to be used. This has been partially addressed through the development of resident autonomous underwater vehicles (AUV) (Albiez et al., 2015), but due to the limited intervention capabilities of AUV systems, many energy-intensive applications still require ROVs (Furuholmen et al., 2013). These restrictions have been recognized and use of collaborative platforms consisting of an autonomous surface vehicle (ASV) and ROV are seen as a potential solution. However, this approach has been so far tested only using micro-ROVs in relatively controlled environments, while commercially available solutions based on observation class ROVs exist (Offshore magazine, n.d.), significant commercial uptake of the technology is not yet recorded. One of the reasons for that is that resident ROVs are still manually operated from the shore using a remote presence approach. Such solutions fundamentally demand a high bandwidth, low latency communications link that is often unavailable further offshore. This is especially important for time-critical tasks, thus high levels of automation are needed.

One of the essential time-critical tasks in resident vehicle operation is the docking of the vehicle at the end of the mission. While the autonomous docking of unmanned underwater vehicles is a well-researched area, the main focus of research reported in the literature is on vehicle docking to a static docking station, usually deployed to the seabed. However, a TMS suspended from a surface floating platform such as a surface vessel, presents a highly dynamic system, with wave height and period dictating the viability of launch and recovery operations (Barnatt, 2013). Autonomous docking of a work-class ROV to a TMS, under such conditions, presents a significant advancement in ROV technology and opens a path towards further development of collaborative ASV-ROV solutions, which has potential to lead towards reduced IMR related costs for offshore energy production sites. With manual operations still being the standard in the offshore industry, increasing their efficiency is of great value considering how expensive and time consuming they currently are (Omerdic and Toal, 2012). These costs can have significant influences over the levelised cost of energy (LCOE) and can affect the level of overall success of expansion within the sector.

1.2 Objectives

The aim of the presented research of this thesis is the development of a suite of ROV technologies to extend current underwater robot capabilities. Considering the risks involved in ROV operations, this can be achieved through use of existing, industry proven hardware with software upgrades. The autonomy needed for a resident ROV should be achieved incrementally through automating specific tasks, while the ROV pilot role transitions towards supervisory as more and more tasks are automated.

The emphasis within this project is on the autonomous docking task for work class ROVs. The developed system needs to be implemented and tested in real-world scenarios, using industry-standard underwater robots in order to validate the feasibility of the system. As the developed solution is to be applied in the offshore

industry, the solution must be suitable for deployment on the global fleet of the work-class ROVs.

The main contributions of this thesis are:

- Identification of the gap in the current ROV technology capability for performing inspection, maintenance and repair tasks at challenging MRE site prevalent conditions.
- Development, implementation and experimental validation of a visual pose estimation solution for ROVs near sub-sea structure based on the active light marker.
- Development, implementation and real-world experimental validation of the work-class ROV docking to both static, seabed-deployed TMS, and to dynamic suspended TMS.
- Development and implementation of a suspended TMS heave motion position prediction method.
- Implementation of the method for elimination of the drift in the ROV navigation solution, utilising the developed active light marker system.

1.3 Research framework

This thesis describes research work in the domain of underwater robotics. It is aimed towards improving performance and achieving partial or full autonomy in the rapidly increasing underwater resident robotics field, with the emphasis on the development of a suite of technologies for docking of work class ROVs. The research work reported in this thesis is part of a large scale project under the Marine and Renewable Energy Ireland (MaREI) Centre research programme.

MaREI is the marine and renewable energy research, development and innovation centre supported by Science Foundation Ireland. MaREI consists of over 200 researchers spread across 12 partner institutes in Ireland, collaborating with over 50

industry partners, with the main focus of research on energy transition, climate action, and the blue economy. The MaREI scientific research programme is organized into Platforms while industry supported targeted projects are assorted into six Spokes as shown in Fig. 1.2. This thesis falls within Spoke 6. The overall goal of the spoke is to apply innovative technologies in observation and monitoring of Marine Renewable Energy (MRE) sites to protect the large investments in MRE capital infrastructure, and to operate that infrastructure for best economic energy production. The spokes are further divided into multiple Post Doctorate and PhD research projects supported by industry partners.

Fig. 1.2 Platform and Spoke Organisation of MaREI Centre.

The part of the MaREI research related to the field robotics is carried out at the Centre for Robotics and Intelligent Systems (CRIS), within the University of Limerick. The core research areas of field robotics within CRIS include:

- Development of Underwater Unmanned Vehicles (UUVs) and Unmanned Aerial Vehicles (UAVs) for marine environments.
- Underwater robotic monitoring and surveying, using vision and acoustic based sensor data for registration, positioning, navigation, and visualisation systems, to facilitate ROV operations.
- Remote presence, communications, and high-speed data security provision for remote monitoring and control of robotics operations.
- Development of autonomous and semi-autonomous robotic manipulation systems, using real-time video and high-resolution sonar systems in the control of manipulators and base robotic vehicles.

The research presented in this thesis falls within the scope of the first and the second core research area mentioned above. Marine Renewable Energy (MRE) installations offshore face challenges beyond those in offshore oil and gas due to the scale of individual installation, i.e. plant is unmanned, and MRE infrastructure must be located in areas of strong waves/current/wind. MRE installations must rely more on remote/autonomous monitoring and control (remote presence) with limited human intervention in the field. Within the CRIS group there are multiple PhD projects that contributed to the development of the ROV technology for inspection, maintenance, and repair (IMR) operations. One project included the development and testing of agile, high power-to-weight ratio inspection class ROV for close-quarters operation near the MRE infrastructures. A second project contributed to the development and application of real-time vision systems, utilising the underwater camera imaging technology for mapping, manipulation and navigation, while a third project was focused on control strategies for autonomous intervention on moving targets (MRE devices) through hydraulic manipulator arms attached to the ROV.

Research within CRIS strives towards a constant development of new underwater vehicles and extending the capabilities of existing ones is necessary.

The work described in this thesis is the outcome of an industry supported project with the aim to research, develop and implement remote presence systems to reduce the expense of deployment and support of onsite maintenance for MRE and other infrastructure offshore, particularly within the development of solutions to address and reduce the cost of ship supported robotics deployment for IMR. The industry partners on this project are Shannon Foynes Port Company and The Commissioners of Irish Lights.

1.4 Thesis structure

Chapter 2, provides an overview of trends and the state-of-the-art projects in the subject area relevant to the research presented in this thesis.

Chapter 3 gives an overview of the hardware associated with the offshore trials, presents a motion analysis of the TMS suspended from the floating platform, and discusses standard operating procedures used during the ROV operations. Each particular topic is discussed up to certain level of detail necessary for good understanding of latter chapters. For readers who are familiar with ROV operations, this chapter may possibly be skipped and the reader can refer back to it in parts later or if specific information is needed. However, for a non-familiar reader the chapter provides the essential information about the size of the system, it's dynamics, and challenges associated with ROV operations.

Chapter 4 describes a visual pose estimation system developed to provide accurate relative position measurements between the ROV and the docking station/TMS. The developed system is based on active light beacons asymmetrically arranged to form a unique marker and a machine vision camera. In addition an algorithm has been developed to reduce the pose estimation errors due to the low camera sensitivity to angle measurements at larger ranges. The system has been developed for standard work-class ROV systems found throughout the sector and deployed with suspended

cage type TMS. The system is built around conventional, industry-standard subsea LED lights and camera, and it has been successfully tested both, in the laboratory and in the ocean.

Chapter 5 presents autonomous docking of an industry-standard work-class ROV to cage type TMS using a visual-based pose estimation approach. The chapter covers both, autonomous docking to static TMS deployed to the seabed, and to the best of the author's knowledge, the first autonomous docking of a work-class ROV to a suspended TMS from a floating platform. Evaluation of the system has been demonstrated through completion of offshore trials in the North Atlantic Ocean during January 2019. The subject matter within this chapter has been published by the author (see Appendix D) (Trslic et al., 2020).

Chapter 6 describes a suspended TMS heave motion prediction method for ROV docking, based on the Adaptive Neuro-Fuzzy Inference System (ANFIS). During the manual docking, a ROV pilot is able to predict the dynamic position of the docking station and estimate heave motion based on the observations of the motion over the time period for a few heave cycles before attempting to dock. A similar approach is presented in this chapter with an ANFIS based solution for TMS heave motion prediction. The method includes on-site neural network training based on previous TMS depth measurements and the TMS depth prediction. In addition, this method could be used standalone as a ROV pilot aiding tool. The method presented in this chapter has been published by author (see Appendix D) (Trslić, Omerdic, Dooly and Toal, 2020).

Chapter 7 discusses the use of an LED based subsea location marker attached to a known structure within the offshore field, for ROV position update. Since resident vehicles for IMR tasks usually operate in partially structured environments, the position and orientation of known structures with a low-cost navigational marker can be used to eliminate drift in the ROV navigation system when close to the target. The system has been tested in the real-world environment and the results of the research have been reported by author (see Appendix D) (Trslić, Weir, Riordan, Omerdic, Toal and Dooly, 2020).

The thesis concludes with Chapter 8, by offering a summary and discussion of the presented work and the key contributions achieved by it. The chapter also provides descriptions and suggestions for further developments in the presented work and the research area.

This thesis is supplemented by several appendices. Appendix A describes a control architecture of the work-class ROV Étaín, while Appendix B contains technical specification of the ROV, and Appendix C contains technical specification of the ROV navigation system solution components. Appendix D lists the key publications that emanated from the work presented in this thesis.

Chapter 2

Background

2.1 Introduction

There is constant growth in the world's energy consumption and an ever-increasing focus on energy security and diversification, with an emphasis on having energy production within home territorial regions. Economic expansion brings increased demand for all fuels and we have seen all variants grow at above-average rates (Dudley, 2019). In offshore power generation this increased demand is followed by expansion of deep-water O&G sector (Murawski et al., 2020; Offshore magazine, 2019), where significant energy potential exists. This trend comes from a number of contributing factors including: need for increased energy farm footprint, technological advancements in ROV/AUV industry and significant savings in deep-water capital expenditure (CAPEX) and operational expenditure (OPEX) costs compared to 2014 levels (Mordor Intelligence, 2019). The same trend is followed by Marine Renewable Energy (MRE) sector with offshore wind platforms being placed in remote offshore locations which typically offer more stable wind regimes (Hannon et al., 2019). Although higher energy potential and cost savings have resulted in deep-water sites becoming commercially viable, the costs associated with operations, maintenance, and repair are inevitably increasing with the move into deeper offshore regions. In downtime/failures, due to the remoteness of the production platform and associated transit times, weather windows for inspection, maintenance, and repair

operations are significantly reduced. This represents a substantial issue in reducing and maintaining projected OPEX costs.

One of the primary OPEX costs, including ROV deployment, is support vessel day rates. Traditionally, subsea IMR activities are carried out using a work-class hydraulic remotely operated vehicle. The vehicles are tethered and controlled directly from a surface support vessel and generally incur significant expenditures associated with the cost of the vessel and crew. The day rate of an offshore maintenance vessel with a crew and equipped with ROV typically reaches at $100,000 or more (Christ and Sr, 2013; Statoil, 2017). One of the primary restriction in terms of ROV operations and associated operational weather windows, is in the launch and recovery of the vehicle (Duncan, 1986). These restrictions are recognized within the offshore energy production industry and as a solution to the problems resident, permanently deployed underwater vehicles are emerging as a potential solution to overcome these problems, expand operation weather windows and reduce OPEX costs. Using a permanently deployed vehicle, real-time, surface weather independent, onsite remote piloting is possible near the seabed. This opens the path to year-round operations without the need for expensive vessels onsite and with reduced personnel transfers (OSJ, 2018). The recognized limitations, together with advancements in ROV technology, battery technology, and the partial coverage of the North Sea and the Gulf of Mexico area with a high-bandwidth, and relatively low latency 4G network (Tampnet, 2018), has led to the significant development of commercial resident ROV and resident Hybrid ROV (H-ROV) systems (Maslin, 2019*b*).

2.2 Resident ROVs and Hybrid ROVs (H-ROVs)

ROVs have been the workhorse of the oil & gas industry since their introduction in the early 1970s. However, the resident ROV concept is only recent, being born out of unprecedented cost saving demand for O&G and global expansion of the offshore wind sector (IEA, 2019). There are various research and development projects globally investigating this concept, some with significant collaboration and

investment from both the oil & gas and the MRE industry sector. Some major investments in work-class resident ROV systems are led by Equinor (formerly Statoil). Oceaneering developed the resident ROV solution E-ROV for Equinor (Equinor, 2019; Oceaneering, 2019). The E-ROV system consists of a work-class ROV and tether management system stationed on the seabed, with a fully integrated communication system buoy on the surface. The power is supplied through submerged battery pack which can be scaled up or down, depending on operational requirements. This system represents an intervention ROV system, which is mobile and can be redeployed relatively easily. Based on E-ROV, Oceaneering also released details of a new vehicle, hybrid ROV (H-ROV) called Freedom, currently under development (*Freedom ROV | Oceaneering [Video file]*, 2019; Oceaneering, 2018). Freedom represents a concept move towards a system in a resident hybrid ROV/AUV format. While in AUV mode, this system would be primarily mobile through the limited onboard power while moving between multiple sites spread around the operational field. After Freedom approaches the site, it reconnects to a subsea charging and communication station and allows for a real-time ROV piloting.

The other major industrial research project in resident systems is ongoing between Equinor and IKM. Through this collaboration IKM developed a large resident system for heavy intervention in an O&G field called R-ROV (IKM Subsea, 2018; UT2, 2018). It consists of a Launch and Recovery System (LARS) and power supply system deployed on a floating platform (e.g. O&G platform) with a TMS and docking station deployed to the seabed. The communication channel to the shore-based ROV operating centre is provided through satellite uplink/downlink (Robinson et al., 2018), 4G mobile network or in some cases fibre optic cable piggybacked on existing pipeline infrastructure. IKM Subsea were one of the first commercial entities to bring this from the proof-of-concept prototype stage to full operational system enactments. IKM developed their fully electric Merlin UCV ROV, modifying their manipulator protocols along with umbilical connectors for shore-based distance piloting and long-term deployment (MacDonald and Torkilsden, 2019). This was developed and deployed under a breakthrough ten-year contract for Equinor's Visund and Snorre

B field assets where one resident ROV system was included for deployment onsite (MacDonald and Torkilsden, 2016).

There are several ongoing resident H-ROV development projects like Oceaneering's Freedom, based around vehicle platforms able to transition between ROV and AUV mode, which are in different stages of development and technology readiness level (TRL) phases. The primary advantage of this resident hybrid ROV concept is that the vehicle can unplug itself, operate in the AUV mode and autonomously move location to a second subsea resident station, covering relatively long distances with the onboard battery pack. Once a resident station is reached the ROV reconnects for power and data transfer. This concept has been around for years and collaboration between the Cybernetix, IFREMER and The University of Liverpool led to the development of Swimmer AUV (Evans et al., 2001), being one of the first to demonstrate the functionality of the H-ROV solution. Swimmer is a large AUV shuttle which served as a mother vessel to a work class ROV (Tito and Rambaldi, 2009). The AUV has been able to autonomously navigate and dock to the docking stations deployed to the seabed and connected to the surface facility supplying power and communications. Once the AUV is docked, power is supplied to the ROV and a real-time data and a video communication channel is established between the ROV operator and the vehicle. However, with developments in battery technology which allow for a higher energy density storage, and with a ROV design being more hydrodynamic, the ROVs today are able to transverse larger distances operating in AUV mode without the mother vessel.

Hybrid ROVs were originally developed for high-risk scientific operations. The Nereus Hybrid Underwater Vehicle has been developed based on the collaboration between the Woods Hole Oceanographic Insitution (WHOI), the John Hopkins University and the U.S. Navy Space and Naval Warfare Systems. The vehicle developed in 2007 has been specifically designed for deep water operations (Bowen et al., 2008), which led to the successful observation and sampling operations in the Challenger Deep of the Mariana Trench (Whitcomb et al., 2010). The vehicle could be configured prior to launch to operate either in AUV or ROV mode. In AUV mode

the vehicle has been used for sea floor mapping using cameras and sonars, while in ROV mode the vehicle was operated real-time via optical fibre cable deployed from the supporting surface vehicle. The use of lightweight optical cable has been necessary since conventional steel-reinforced cables are self-supporting in sea water up to 7,000 m while Kevlar based umbilical result in large-diameter cables requiring large cable handling systems and introducing high cross-section drag. Although, the concept of using optical fibre for ROVs has been presented before (Aoki et al., 1999), the Nereus has been among the pioneers of a long-range fiber-optics tether based hybrid ROVs.

Followed by the success of the Nereus, WHOI developed another hybrid vehicle for under-ice operations called ROV Nereid-UI (Bowen et al., 2014). The vehicle rated to 2,000 m has been designed to operate both in AUV mode for survey operations, or in tethered ROV mode for tele-operated sampling and intervention operations, using up to 20 km of lightweight optical fibre tether. While under ice, in case of the damaged tether, the vehicle can be operated in semi-autonomous mode using low-bandwidth dual-band acoustic communications system.

The H-ROV Ariane has been developed by IFREMER for near-bottom work in fragile environments such as coral reefs (Brignone et al., 2015; Raugel et al., 2019). Ariane is a 2,500 m depth rated vehicle designed to be operated from a non DP capable surface vessel in order to reduce operational costs. The vehicle is able to operate in AUV mode both for a survey tasks, or as a safety fallback strategy in case of tether rupture. While in ROV mode, the vehicle is unlike the previously described hybrid ROV systems, operated through reusable fiber-optic tether deployed from the ROV itself. In the case of tether entanglement, the vehicle is equipped with pyrotechnic fibre cutter for emergency tether cut. The vehicle then switches to AUV mode and performs pre-planned homing/surfacing manoeuvres relying on the acoustic link. Recently similar systems with extended autonomous capabilities, have been under development by major ROV producers for inspection and intervention tasks around distributed subsea energy production related assets.

Table 2.1 Key resident ROV and Hybrid-ROV projects.

Project leader	Project name	ROV type and class	ROV power	Docking station	Communication with the control centre	Project status	System capabilities
Oceaneering, Equinor	E-ROV	Resident Hybrid ROV, Work-class	Through tether	Cage-type TMS, seabed deployed	Surface buoy with 4G network	Project started in 2017. System fully developed. Initial tests performed in July 2019	Intervention and inspection tasks, manipulator-related activities
Oceaneering, Equinor	Freedom	Resident Hybrid ROV, Work-class	Through tether + Onboard battery pack	Multiple distributed docking stations, seabed deployed	Surface buoy with 4G network	Project started in 2018. Early development phase	Intervention and inspection tasks, manipulator-related activities, pipeline surveys
IKM, Equinor	R-ROV	Resident ROV, Work-class	Through tether	Modified cage-type TMS with open top, seabed deployed	Optical fibre to the shore, satellite link, 4G network from deployment platform	Project started in 2016. System fully developed, deployed and continuously tested at Equinor's Snorre B platform	Drilling and wells related work, valve operation
Saipem, Equinor	Hydrone-R	Resident Hybrid ROV, Work-class	Through tether + onboard battery pack	Seabed deployed	N/A	Project started in 2017. System in late development phase. Initial trials performed in July 2019.	Intervention and inspection tasks, light construction capabilities
Saipem, Equinor	Hydrone-W	Resident ROV, Work-class	Through tether	N/A	N/A	Early development phase. First trials planned for 2021	Heavy duty work-class capabilities
Modus Seabed Intervention, Osbit	AVISIoN	Resident Hybrid ROV, Inspection-class	Onboard battery pack	Seabed deployed	N/A	Project started in 2014. Late development phase	Autonomous solution for inspection and survey of wind farm subsea infrastructure
IFREMER, Cybernetix, University of Liverpool	SWIMMER	Resident AUV shuttle + ROV, Work-class	Onboard battery pack for AUV, ROV through tether once AUV docked	Multiple distributed docking stations, seabed deployed	Optical fibre to shore	System developed in 2001	R&D platform for scientific research
IFREMER	ARIANE	Hybrid ROV, Work-class	Onboard battery pack	Launched and recovered manually from a ship	Reusable optical fibre	System fully developed in 2015	Near-bottom work in fragile environments
WHOI, John Hopkins University, Center for Coastal and Ocean Mapping	Nereid-UI	Hybrid ROV, Work-class	Onboard battery pack	Launched and recovered manually from a ship	Sacrificial optical fibre	System fully developed in 2014	Under-ice operations, Inspection and intervention
WHOI, John Hopkins University, U.S. Navy Space	Nereus	Hybrid ROV, Inspection-class	Onboard battery pack	Launched and recovered manually from a ship	Sacrificial optical fibre	System fully developed in 2007	Scientific deep-water operations, observation and sampling, sea-floor mapping

Saipem is working on the Hydrone family of three different resident unmanned underwater vehicles. The concept has been presented in 2017. (*Under the Sea | Hydrone | Saipem [Video file]*, 2017), and has been continuously developed since (Maslin, 2019*a*; UT2, 2018). Hydrone-R is the first vehicle to be launched in the market as an intervention ROV with light construction work capabilities, and with first tests carried out in July 2019 (Saipem, 2019). The vehicle can be remotely controlled from shore and can operate in tethered or wireless mode using underwater wireless optical modems (Caiti et al., 2016*a*; Leon et al., 2017; Sonardyne, 2020). Also, it is designed to navigate up to 10 km in AUV mode. The development of this ROV led to the multi-million subsea service contract between Saipem and Equinor at Njord field in the Norwegian Sea (McPhee, 2019), which is the first confirmed site for Saipem's subsea UUVs. The second ROV from the Hydrone family is Hydrone-W. It presents a resident work-class ROV for heavy duty tasks, permanently connected to a subsea tether management system. However, the project is in early development phase and is expected to be developed and tested in 2021 (Beckman, 2019). The third vehicle is Hydrone-S, which presents an advanced, resident AUV used for the collection of data from a large number of subsea sensors spread around offshore energy production field. The vehicle is heavily based on the FlatFish resident AUV developed in partnership between DFKI, Senai Cimatec and Shell company (Zagatti et al., 2018), for autonomous visual inspection, tracking pipelines, hovering around the subsea structures and returning to the deployed docking station in order to recharge and transfer gathered data. The FlatFish project has been entrusted to Saipem in 2018 for further development and is expected to be commercially ready in 2020 (Energy Northern Perspective, 2019).

Another ongoing resident H-ROV project is based on collaboration between Modus Seabed Intervention, Osbit and Offshore Renewable Energy (ORE) Catapult (Modus, 2019). The system is based on a commercial ROV/AUV platform Saab Seaeye Sabertooth (Saab, 2019), which previously has been continuously developed under Clean sea project in partnership with Eni (Buffagni et al., 2014; Grasso et al., 2016). The goal of the Modus based project is to develop an autonomous solution for

inspection and survey of offshore wind farm subsea infrastructure. However, while a seabed dock has been developed, and system deployment and docking trials from floating docking station has been announced (Catapult, 2018), the outcome of the trials has not been reported yet.

While the majority of H-ROV projects are based on evolved traditional ROV platforms, the Eelume project by Kongsberg (Liljebäck and Mills, 2017), and Aquanaut by Houston Mechatronics (Manley et al., 2018) present a different approach to the H-ROV industry. The Eelume vehicle is based on a chain of joints, payload modules and thruster modules. With a snake-like, modular vehicle for navigating through tight places, an additional redundancy and shape-changing ability has been achieved, which allows the vehicle to act as a robot arm when needed. On the other hand, Aquanaut has a shape-shifting morphology which gives the vehicle the ability to operate in two different modes. While in Survey/Transit mode the vehicle adopts hydrodynamic, torpedo-like shape for efficient transit, while upon arriving at a work site the vehicle switches to Intervention mode and adopts the shape of a work-class ROV. The vehicle has been tested so far only in the laboratory conditions and it is yet to be seen it's performance in the real-world environment.

In general, there is a significant uptake in resident ROV technology, and with the rapid expansion of the offshore sector more diverse resident ROV projects are expected to be seen. However, as shown in Table 2.1, one thing in common to all projects mentioned in this section is a static docking station deployed to the seabed. While such systems are seen as a viable solution for O&G platforms in relatively shallow water, deep-water energy production sites, and especially MRE production fields with assets distributed over large area, demand a different UUV approach to continuous condition monitoring and intervention tasks.

2.3 Challenges in deep-water energy production sites

With the move of the energy production sites into deep water regions, the costs related to IMR operations are increasing, and this should be addressed. This may not be

overcome simply through predictive maintenance due to the growth in infrastructure planned within the future offshore blue economy (Toal et al., 2010).

The resident ROV systems may seem as a viable solution for deep-water IMR tasks, however such systems consist of a ROV and a TMS deployed to the seabed. Therefore, the ROV operations are limited and can be undertaken only in relatively close proximity to the seabed TMS. Since the IMR tasks in deep-water energy production sites can range from the floating infrastructure near the surface to cabling, cable risers and chains, down to moorings and seabed infrastructure, the operational depth of the ROV should be flexible. In addition, geographic spread of infrastructure assets in the MRE sector, which is currently undergoing huge expansion, creates additional concerns, with IMR tasks on a large area demanding more vessels, thus introducing higher OPEX. This has been partially addressed through the development of resident autonomous underwater vehicles (Albiez et al., 2015; Gilmour et al., 2012). However, due to the limited intervention capabilities of resident AUV systems, many energy-intensive applications still require ROVs (Furuholmen et al., 2013). These limitations have been recognized and the use of a collaborative ASV-ROV platform seems like a potential solution (Fahrni et al., 2018; Lachaud et al., 2018), with a small number of commercial solutions already available.

Marine Tech developed unmanned surface vehicle RSV Sea Observer equipped with an inspection-class ROV (I-ROV) for offshore subsea monitoring (*MarineTech - RSV Sea Observer [Video file]*, 2017). The USV is based on fully electric, approximately 4 metres long inflatable platform designed for offshore operations in up to 1.5 m swell, which can accommodate 250 kg of payload. The surface vehicle is equipped with a dynamic positioning system, and is able to achieve a maximum transition speed of 10 knots. However, the vehicle is designed to operate only in a coastal area with minimal sea state, and provides only observation capabilities while the maximum operating range is 5 km.

As part of the Autonomous Robotic Intervention System for Extreme Maritime Environments (ARISE) project the system consisting of a C-Worker 7 ASV and an I-ROV Saab Seaye Falcon has been developed. C-Worker 7 is a 7.2 m long

ASV equipped with radio and satellite communications and designed for direct, semi-autonomous or autonomous control. With a moonpool size 2.5 m x 1 m it is suitable to launch and recover inspection class ROV and provide up to 2 kW of power for payloads (L3 ASV, n.d.). The ROV system onboard provides observation and light intervention capabilities. The system is designed to be used in a hazardous environment such as for jacket and hull inspection. The proof of the concept has been demonstrated in 2019 (L3 ASV, 2020), with the second phase of the project leading towards further ROV launch and recovery capability (ASV Global, 2020).

Following the technical paper presented by TechnipFMC and Total on opportunities and challenges of operating ROV-USV platforms (Lachaud et al., 2018), the ECA GROUP demonstated a similar system in 2019 using the I-ROV H300V and an unmanned surface vehicle the USV Inspector (ECA Group, 2019). The ROV system provides observation and light intervention capabilities. However, this system is under development, and it is used as a proof of the concept system. The ROV deployment is still performed manually without the TMS with the tether being managed manually. Once deployed, the ROV is operated in a free-swimming mode.

Various other cooperative ASV-ROV projects have been demonstrated (Conte et al., 2016; Gray and Schwartz, 2016), with ASV-ROV collaborative platform being tested only using observation class ROVs, and with the ROVs being launched and recovered directly, without a docking station. The most recent ROV-ASV project has been introduced in February this year. The project named Armada is led by Ocean Infinity (Offshore Engineer, 2020). The goal of the project is to built a fleet of large unmanned surface vehicles/ships, each equipped to perform various data acquisition and intervention tasks. Depending on the task, each vehicle will be equipped with various sensor payloads and capable of deploying state-of-the-art AUV or ROV systems. However, this project is only in conceptual phase.

Although it has been shown in this section that there is an interest in collaborative ASV-ROV platforms, significant commercial uptake of this technology has not been recorded yet. Fundamentally such solutions are still operated from shore and demand a high bandwidth, low latency communication link. While partial

availability of 4G mobile networks in the North Sea and in the Gulf of Mexico helps to drive the industry (Maslin, 2019*b*), such a communication link is in most cases unavailable, especially at deep-water offshore energy production sites. Therefore, to achieve the level of agility needed for resident ROVs in subsea domains and within time-critical tasks, these communication issues need to be addressed. High levels of automation, through onboard sensor technologies, machine learning, computer vision, and advanced control and navigation approaches can provide an alternate to the high-bandwidth communication link requirements for remote on shore piloting solution (Dooly et al., 2016). One of the time-critical tasks in resident ROV and AUV operations is the docking of the system back into the docking station at the end of a mission, with the DS providing an overall mechanical protection, charging point and download/upload link. This task is a particularly crucial part of all UUV operations and likely represents the primary task which will dictate the full system operating window, especially if heaving DS suspended from a floating platform is considered.

2.4 Autonomous UUV docking

Since autonomous docking has been one of the main tasks in resident AUV operations in order to extended operational duration on site, most research in the literature on the automation of subsea vehicle docking procedures has been focused on resident AUV platforms. There are various reasons for resident AUV deployment, however all resident AUV solutions include recharging and data exchange without recovering the vehicle to the surface. One of the first autonomous AUV docking systems have been proposed for long-term oceanographic sampling purposes (Curtin et al., 1993). Cowen et al. (1997) developed autonomous docking to a funnel shaped receptacle based on a single underwater light mounted on the docking station, using quadrant detector and optical terminal guidance for AUV control. The system worked using a similar principle to a heat-seeking air-to-air missile, with the system constantly

trying to keep the target (light source) roughly centered horizontally and vertically in the image plane.

In the same year, the docking system to an interesting pole-based omnidirectional docking station, based only on acoustic bearing and range rate measuring system has been suggested by Singh et al. (1997). When the vehicle starts the homing procedure its USBL system is continuously trying to null the bearing to the dock. If the dock is missed the range rate to the dock undergoes sign reversal, thus the AUV has missed the dock.

Another docking system using the acoustic positioning has been presented by Smith (1997). The inverted short-baseline (SBL) system, with baseline length approximately 6 m and three beacons arranged in a star and anchored to the seabed, has been used to estimate relative AUV position. However, the system has been designed for slow-approaching vehicles with approaching speed less than 1 m/s. A homing and docking approach using electromagnetic guidance has been suggested by Feezor et al. (2001). The system has been developed to provide accurate position and orientation measurement at the final stage of the docking manoeuvre, and compared to the high frequency acoustic systems at the time, this system provided higher update rates and more accuracy. In addition, unlike the acoustic systems, this system did not suffer from additional complexities when operating close to the seabed or the surface, however operating range of the system has been 30 m.

In the same year, Evans et al. (2001) presented innovative acoustic imaging system for autonomous docking of the SWIMMER AUV to docking station. The system has been based on two orthogonally mounted sonars on the AUV. The images acquired from the sonars were compared with simulated sonar data using CAD model, sonar model and estimated position data, to generate true, updated position. This system was further upgraded with vision based system as part of ALIVE project (Evans et al., 2003), using edge detection to detect features which are compared with 3D CAD models and used to estimate the vehicle position in the final docking phase. A further vision based system reported by Brignone et al. (2007), with video

processing algorithm used passive checkerboard markers to estimate relative AUV position, with sonar performance further optimised using passive sonar markers.

Pan-Mook Lee et al. (2003) demonstrated autonomous docking to a funnel shaped receptacle using active light beacons which has been further improved (Park et al., 2009). Five beacons attached to the docking station have been used as markers, and with the camera attached to the nose of the AUV, the relative position between the docking station and the vehicle has been calculated. At the same time Carreras et al. (2003) demonstrated the vision localization method for underwater robots in structured environment, allowing for real-time computation of all six degrees of freedom along with the vehicle velocities. The system has been based on visually coded passive marker (similar to augmented reality marker today) which has been recognized using the vision system.

Autonomous docking using USBL to estimate funnel-shaped DS position, using Doppler Velocity Log (DVL) velocity and altitude information on the AUV, has been demonstrated by Allen et al. (2006). A similar system has been developed and reported in Hobson et al. (2007) and McEwen et al. (2008). Another approach looking at fusing data from the vision system, DVL, and Fibre Optics Gyroscope (FOG), using Extended Kalman Filter (EKF), has been presented in Krupinski et al. (2008) and Krupinski et al. (2009). This approach has been further extended by Vallicrosa et al. (2016) and Palomeras et al. (2018) which added USBL and depth measurements to navigation filter further improving vehicle localization capabilities. Acoustic localization has been used at long ranges from the DS, visual pose estimation based on four active light beacons has been used for close range pose estimation, while pose estimation on passive Augmented Reality (AR) markers has been used for the final approach.

More recently, Li et al. (2015) presented an algorithm for AUV docking based on visual pose estimation using two cameras. The method used active light beacons attached to the docking station. During the docking, the algorithm operates in one of two operating modes depending on the number of lights acquired using two cameras. While two cameras added to redundancy and precision of the system, Li

concluded that the method suffered from the long computational interval (1.5-2.5 s), thus additional dead-reckoning navigation system such as DVL, should aid the navigation solution. However, this problem has been addressed in Zhong et al. (2019) using a fast binocular localisation method.

2.4.1 Autonomous UUV docking to a moving docking station

As shown in the previous section,the autonomous docking of UUVs is a well-researched area with various approaches demonstrated throughout the years. However, the main focus in the literature is on docking to a static docking station, usually deployed to the seabed. A TMS suspended from a surface platform such as a surface vessel, presents a highly dynamic system, with a surface platform being the main source of TMS motion, and with wave height and period dictating the viability of launch and recovery operations (Barnatt, 2013). Although docking of UUVs to a moving docking station has been reported, the research is mainly focused on AUV docking and on compensation of disturbances in the horizontal plane (e.g., cross-current), while assuming minimal docking station heave oscillations.

Fixed-wing depressor-based docking solution is presented by Raspante (2012), where a funnel shaped DS is attached to the depressor and towed by a surface vehicle at a constant speed, while the AUV intercepts the docking station and performs the docking.

On the other hand, docking of an AUV into a compliant docking station attached to a ship hull, using USBL and optical guidance, has been reported by Rigaud and Nicolas-Meunier (2015). The USBL has been used for long range relative position estimation, while at close range the optical homing system, based on the recognition of LED light beacons pattern has been used.

A USV-based automated launch and recovery system (LARS) for AUVs has been presented in Sarda and Dhanak (2017). The recovery system is based on the deployment of a thin line with a depressor wing from the surface vessel, whereas the AUV is equipped with a pincer-type mechanism for latching. Recovering of an AUV by another AUV in shallow water has been presented in Liu et al. (2019). The

system consists of a “mother” AUV with a funnel shaped docking station attached to its body, designed to accommodate launch and recovery of the “daughter” AUV. Docking to an active docking station is presented in Yazdani et al. (2019). The paper presents a cooperative guidance system for the AUV docking, whereas the system consists of a funnel shaped receptacle with an active heading adjustment.

However, despite considerable achievements both in academia and the UUV industry, suitable autonomous work-class ROV docking solution to allow the IMR tasks while acknowledging all the challenges, has not been developed, integrated or tested yet.

2.5 Closing remarks

This chapter has summarized the relevant background and presented a comprehensive overview of the projects related to resident UUV field with emphasis on resident ROV solutions.

By analysing the literature in underwater unmanned vehicles development, it is clear that resident vehicles have been a popular topic for many years, but only recently are seen, by offshore energy production companies, as a viable solution for the reduction of OPEX costs in offshore production fields. This has been followed by a significant uptake of commercial interest in resident ROV systems, with various research projects targeting different problems within the field, resulting in significant investment into development of projects, which are mostly at the early technology readiness level phase. However, with offshore wind and O&G platforms being pushed into deeper offshore regions where higher energy potential exists, current resident ROV systems consisting of a TMS deployed to the seabed are not able to cover a whole range of IMR tasks performed across the whole water column. O&G production platforms in deeper water locations employ floating structures and offshore wind technology R&D is developing floating wind solutions to enable wind energy in deeper waters. IMR tasks on infrastructure must thus cater with anchors, flexible risers, moorings and large floating structures. There is a need for resident

ROVs to be deployed from higher up in the water column, and there is a requirement for ROV systems and their associated docking stations and TMS systems to be deployed on or from these floating structures. This can be done with TMS and DS built onto the submerged part of the floating structures or the DS and TMS suspended from the floating structure to the desired working depth with the TMS acting as a clump weight to compensate for a cross-section drag. This leaves an unfilled gap between the current solutions and the ones required by growing offshore energy production sector.

Moreover, while resident ROV solution partially meets the O&G inspection, maintenance, and repair requirements, the marine renewable energy production field due to the multiple assets distributed over large areas demands a different approach, and as a possible solution collaborative platform consisting of ROV and ASV has emerged. However, many of the examples in the literature fail to address some of the fundamental barriers to the significant rollout of this technology into commercial sectors. Essentially these solutions demand high bandwidth, low-latency communication channel to shore and are still manually operated through the remote presence approach. Although such communication link is essential for time-critical tasks, it is often not available. To close this gap, the autonomy needed for a resident ROV should be achieved incrementally through automating specific tasks, while the ROV pilot role transitions towards supervisory as more and more tasks are automated.

One of the essential time-critical tasks is docking of the vehicle at the end of the mission. Considering heaving DS suspended from a floating platform (e.g. ASV), this task is even more time-critical. However, suitable autonomous ROV docking solutions are not available. Solving this problem would accelerate uptake in resident ROV technology and would open a path towards future development of collaborative ASV-ROV platforms, which potentially leads to reduced IMR costs for offshore energy production sites.

Chapter 3

Standard operating procedures and Tether Management System (TMS) motion analysis

3.1 Introduction

This chapter provides an overview of the hardware used for the offshore trials, discusses the behaviour of a TMS suspended from the floating surface vessel, and gives insight in the standard operating procedures during the ROV docking. The chapter can be read in two ways, depending on the reader's background. The reader familiar with offshore ROV operations may quickly read through Section 3.2 to get familiar with the system used during the offshore trials, while the rest of the chapter can be skipped and consulted as needed. Otherwise the reader is advised to read through the chapter and encouraged to refer back to its contents as necessary as the reader progresses through the thesis.

Section 3.2 provides an overview of the hardware and supporting equipment involved in the offshore trials. The relationship between the surface vessel motion and the suspended TMS motion is given in Section 3.3, which also serves as a foundation for Chapter 6. Since the autonomous docking of the ROV is one of the

main contributions of this thesis, it is necessary to have an understanding of the standard, manual docking procedure first, which is therefore the topic of Section 3.4.

3.2 Hardware

Fig. 3.1 shows the experimental setup used for autonomous docking. Industry standard equipment was utilised with upgraded, in house developed control systems. The Centre for Robotics and Intelligent Systems (CRIS), University of Limerick ROV system consists of a control cabin, launch and recovery system (LARS), tether management system, and the remotely operated vehicle, ROV Étaín itself. Technical specifications of the system components are given in Table 3.1. The Research Vessel (RV) Celtic Explorer of the (Irish) Marine institute was used throughout the offshore trials (Institute, 2019) .

Table 3.1 Technical specification of the system.

	Description	Dimensions LxWxH [m]	Weight [t]
Control Cabin	Reinforced container used as ROV control centre	6 x 2.4 x 2.4	6.5
LARS	A - frame type, 2200 m steel reinforced umbilical, ϕ 25.4 mm	5.5 x 2.8 x 3.2	12
TMS	Cage type, 400 m soft tether, ϕ 21 mm	2.9 x 1.8 x 2.5	2.1
ROV	Middle size ROV capable of inspection, maintenance and repair tasks	2.1 x 1.3 x 1.25	1.1
Ship	Research Vessel	Length - 66 m	Displacement - 2425 t

The ROV is controlled from a control cabin used as the control centre aboard the research vessel. Power is supplied from the ship, while the connection between the cabin and the TMS and ROV is established through 2.2 km of steel reinforced umbilical with embedded fibre optic cable. The LARS is a conventional A-frame type, hydraulically operated.

3.2.1 Remotely operated vehicle (ROV)

Both remotely operated vehicles (ROVs) and autonomous underwater vehicles(AUVs) are considered part of the unmanned underwater vehicles (UUVs) family. AUVs are battery-powered vehicles usually used for survey missions such as detailed seafloor

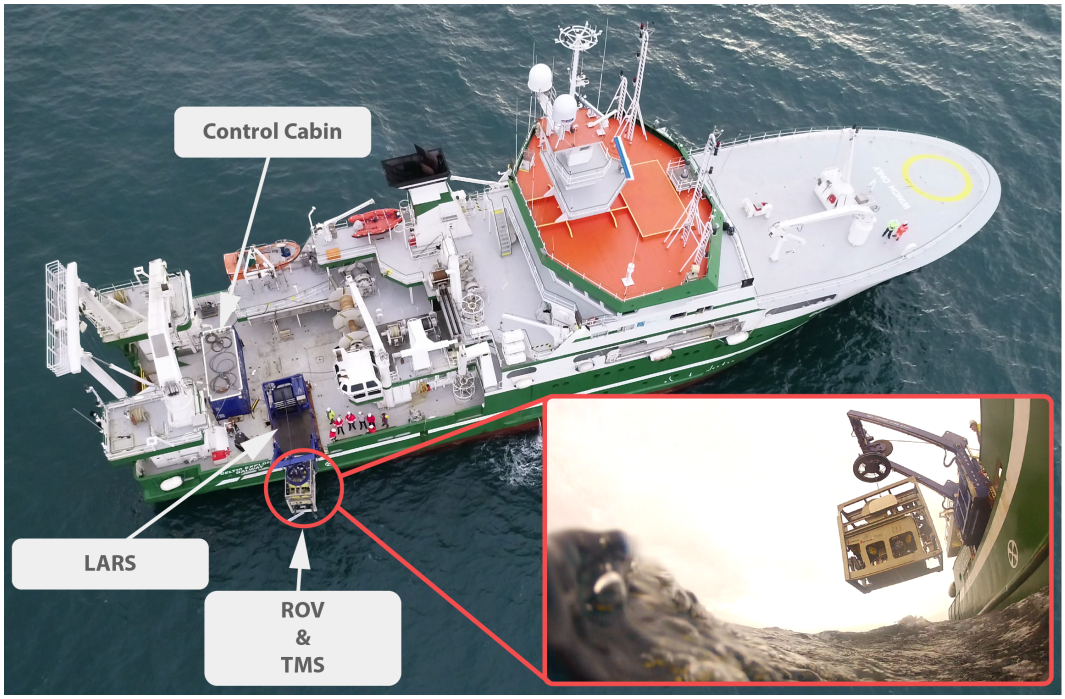

Fig. 3.1 Experimental setup overview of ROV Étaín aboard Research Vessel Celtic Explorer.

mapping, pipeline survey, and inspection of underwater structures. The survey mission is pre-planned and conducted generally without operator intervention, although acoustic modems are used for direct communication. After the end of a mission, the AUV returns to a pre-programmed location. The difference between the ROVs and the AUVs lies in the presence of a tether between the surface and the vehicle. While AUV is not physically connected with the operator, with ROVs a tether is used for communication and/or power delivery between the surface and the vehicle. A ROV can be controlled via remote operation or autonomously. The tether provides higher bandwidth than acoustic modems, thus real-time visual feedback is available. The vehicle can be battery-powered, powered through the tether, or using a combination of both approaches. ROVs can be equipped with robotic arms used in intervention tasks such as valve turning, taking physical samples, object retrieval/recovery, guiding large construction pieces into place underwater and for many other applications.

The ROV, acquired by CRIS in 2018 and named Étaín after a heroine of Irish mythology, is a state-of-the-art fully electric Comanche ROV produced by Forum Energy Technologies, with additional onboard hydraulic power used for manipulators

and tooling. The ROV is equipped with an inertial navigation system coupled with various aiding sensors such as: a Doppler Velocity Log (DVL), an Ultra Short Baseline (USBL) system to eliminate navigation drift solution underwater, a depth sensor, and a DGPS system which operates when the ROV is on the sea surface. The vehicle is equipped with four horizontal and three vertical thrusters and can achieve a maximum speed of 2.5 knots. The ROV buoyancy was trimmed to be slightly positive, which in case of severe damage would bring the ROV to the surface. The ROV weights approximately 1650 kg in the air, and is docked to a cage type, side entry TMS, which is used as a docking station. More detailed technical specification of the ROV is given in Appendix B.

3.2.2 Tether management system and Launch and recovery system (LARS)

There are two main types of tether management systems (TMS), top-hat TMS and cage-type (garage-type) TMS. While using a top-hat TMS the ROV is placed under the TMS structure. Since a top-hat TMS in general has a smaller footprint than a cage-type TMS, there have been versions of the top-hat assisted with thrusters for station holding and manoeuvring capabilities, which is useful when the ROV deployment vessel is following the ROV during pipeline surveying for example. A cage-type TMS provides more protection to the ROV since the ROV is parked inside the TMS. This allows for a faster descent, safer transition through the splash zone and allows for the system deployment to the seabed.

Fig. 3.2 shows an overview of the cage-type TMS and ROV system used during the offshore trials, with the overall dimensions relevant for docking. The TMS is a conventional Comanche ROV TMS and is not designed to operate as an auto-docking station. The ROV fits tightly within the TMS. The red shaded area in the figure shows the funnel-shaped TMS entrance which helps to physically guide the vehicle. In comparison to the funnel-shaped AUV receptacle (Allen et al., 2006; Park et al., 2009; Vallicrosa et al., 2016), a significant difference lies in the vehicle to DS entrance size ratio. The entrance nozzle of AUV docking stations is typically

4 to 5 vehicle diameters, as presented in Allen et al. (2006) and Palomeras et al. (2018), whereas the entrance of the TMS used as a docking station in this chapter is approximately 1.3 times the vehicle size as shown in Fig. 3.2. The entrance allows only for a small misalignment during the docking procedure, which makes the autonomous-docking task presented in detail in Chapter 5 more challenging.

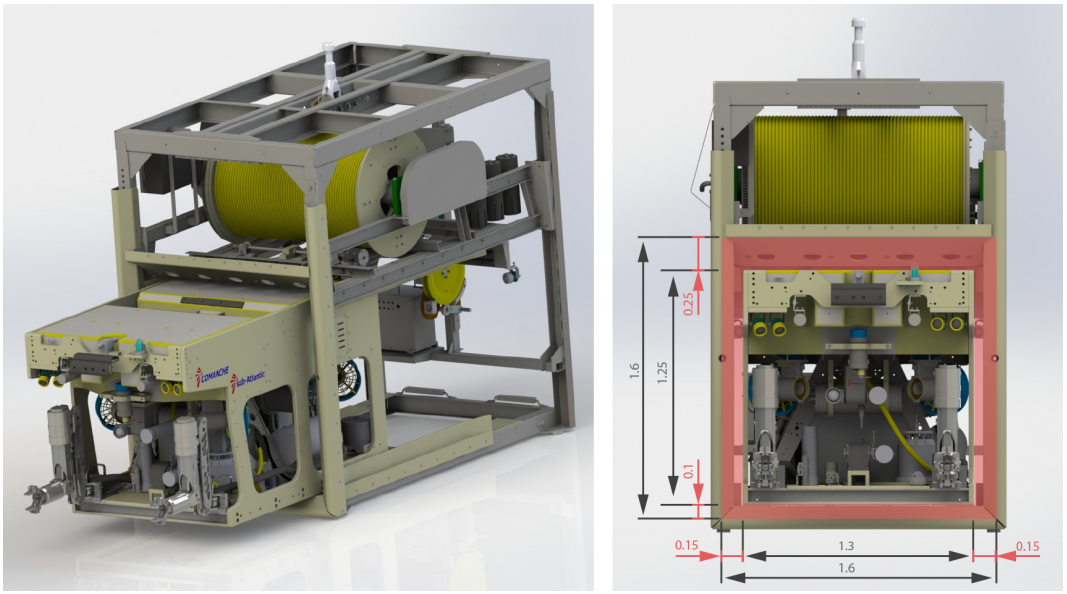

Fig. 3.2 The TMS and ROV system overview with overall dimensions [m]. The funnel shaped entrance allows small ROV-TMS misalignment (red shaded area).

To accommodate one of the planned tests, that of docking to a static docking station presented in Section 5.3.1, the TMS has been slightly modified. Fig. 3.3 shows four legs mounted on each corner of the TMS to create clearance of the TMS from the seabed and thus allow static docking manoeuvres. The legs are 0.8 m long, which is enough to safely operate the ROV without disturbing the stability of the TMS.

The LARS system is used as the over boarding equipment, and its primary role is to move the ROV from the deck and deploy it safely. The most typically used LARS in industry is the A-frame type, such as the one used during the trials. On one side the LARS is connected to the control cabin and power supply, and on the other side to the TMS through the umbilical. The umbilical used for TMS deployment is steel reinforced for lifting to/from the water, and it provides the power and communication

Fig. 3.3 The ROV within the TMS with four legs retrofitted for the static docking experiment prior to launch.

link between the ROV and the control cabin. Vessels that are specially designed for ROV operations may include the moonpool or Cage & Rail LARS system (Fahrni et al., 2018) for deployment. However, such equipment is more complicated, thus more expensive, and generally is used as a permanent feature on the vessel.

3.2.3 The navigation system

The heart of the ROV navigation system is a state-of-the-art inertial navigational system PHINS 6000. The system is coupled with a DVL Nortek 500, a depth sensor, an ultra-short baseline system Teledyne Ranger 2, and a differential GPS unit Okeanus GPSR-3015G. The technical specifications of the navigational system components are given in Table 3.2. Detailed technical specification of each sensor is given in Appendix C. The navigation filter within the commercial INS unit is an Extended Kalman Filter (EKF). The EKF is used to combine and fuse all PHINS

Table 3.2 The DVL, USBL, and GPS system technical specification.

Nortek 500 DVL - Bottom velocity	
Single ping std @ 3m/s	5 mm/s
Long term accuracy	$\pm 0.2\% / \pm 1$ mm/s
Minimum altitude	0.3 m
Maximum altitude	200 m
Velocity resolution	0.01 mm/s
Teledyne Ranger 2 USBL	
Operating range	> 6000 m
System accuracy	0.2% of Slant range
Position update rate	1 s
Okeanus DGPS	
Position accuracy GPS	< 15 m
Position accuracy DGPS (WAAS)	< 3 m
PPS Time	± 1 us

internal and external aiding sensor data. The GPS unit and the USBL are used for the absolute navigation measurements and position drift corrections. Additionally, the GPS unit is used for initial alignment of the fibre optic gyroscope (FOG) within the INS unit, and for navigation aiding when the vehicle is on the surface, while USBL provides absolute position underwater. Without USBL the ROV position underwater drifts over time.

Inertial navigation system PHINS 6000

Commercial inertial navigation system PHINS 6000 was used during the trials. The system presents a gold standard within marine robotics navigation and consists of three major components:

- Inertial measurement unit (IMU) which consists of three fibre optic gyroscopes and three accelerometers,
- Inertial navigation system resolving inertial measurements and updating position, velocity, and attitude,

- Extended Kalman filter for optimal integration of external and internal sensor measurements.

Fig. 3.4. shows a functional block diagram of the PHINS Kalman filter. If no external sensors data is fed in, the output of the INS unit is based purely on the IMU measurements. This data is used to update coefficients of the error equations. The error equations are used to update the covariance matrix. The INS estimates are compared with the observed external sensor measurements and used as feedback to the INS. In case no external sensor measurement was received, the Kalman filter provides error bound estimates. A software switch separates the external sensors and the EKF. Thus, it is possible to operate the system in different operation modes with various combinations of external aiding sensors connected.

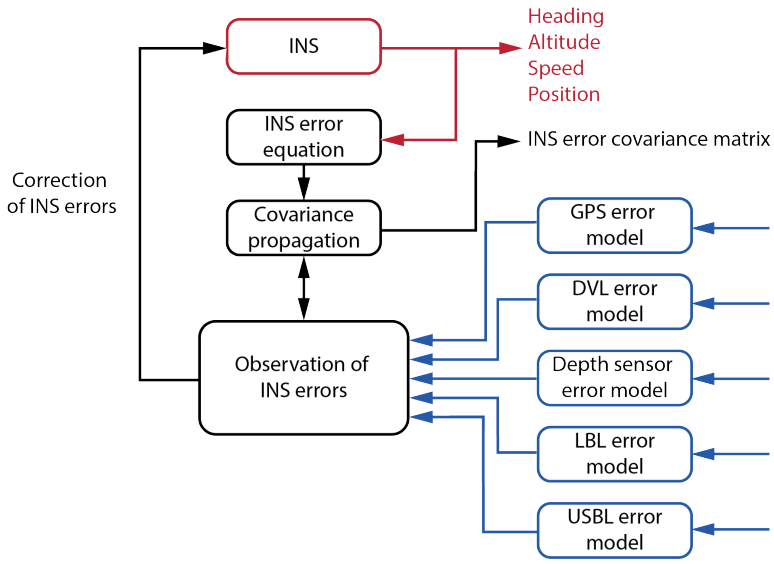

Fig. 3.4 Function block diagram of Kalman filer (IxSea, 2007).

PHINS operating modes

The navigation system PHINS 6000 operates with various external sensors such as GPS, USBL/LBL, depth sensor, and DVL. The system operates in various modes depending on the combination of external sensors used. The GPS is usually used

for initial heading alignment process while on the ship's deck, and to acquire an absolute, geo-referenced position while ROV is on the surface.

While operating underwater, there are three PHINS operating modes based on the external sensors used:

- INS + USBL/LBL + (DVL) + Depth
- INS + DVL + Depth
- INS (Pure inertial) + Depth

The best pose estimation performance is achieved with all aiding sensors, in USBL + INS mode with DVL in bottom lock and precise depth measurements. The USBL providing link through ship to GPS provides an absolute position while INS/Kalman filter reduces the noise on the USBL position measurements. As shown in Table 3.3, PHINS position accuracy in this mode is three times better than the accuracy of the standalone USBL system. Throughout the trials the recorded standard deviation of the ROV position, in this mode, was between 0.25 m and 0.3 m at all times.

Without USBL/LBL absolute position fix, the position measurements drift over time. The DVL + INS operating mode minimises the drift due to speed over ground measurements. In this mode, the position drift of PHINS 6000 is approximately 0.1% of the travelled distance. Pure inertial mode without external sensor aiding is considered a worst-case scenario. The position error is estimated based on the integration of the IMU data within the PHINS, thus it depends on the quality of the FOG and accelerometers.

Table 3.3 The PHINS 6000 INS system technical specification.

Position accuracy with USBL/LBL	Three times better than USBL/LBL accuracy
Position accuracy with DVL	0.1% of travelled distance
Position accuracy with no aiding for 1min/ 2min	0.8 m/ 3.2 m
Heading accuracy with GPS	0.01 deg secant latitude
Heading accuracy with DVL/USBL/LBL	0.02 deg secant latitude
Roll and Pitch accuracy	0.01 deg
Heave accuracy	5 cm or 5% (Whichever is greater)

3.3 The TMS motion analysis

The TMS with the ROV is usually deployed from a surface vessel or floating platform which is exposed to various disturbances such as waves, currents, wind, tides and others. Since the surface vessel for TMS deployment is the main source of the TMS motion, it is necessary to understand all the disturbances introduced to the surface vessel and how they map to the TMS. Since the disturbances act on all 6 degrees of freedom (DOF) of the surface vessel and considering the TMS is connected to the vessel through the non-elastic umbilical in longitudinal direction but free to surge, sway and yaw, some surface vessel motions couple to the TMS directly, while others result in a gravity/pendulum coupling with in-water damping. Therefore, the primary goal during the TMS deployment is to minimise the impact of these disturbances of a surface vessel on the TMS.

Fig. 3.5. a) shows a vessel's six degrees of freedom. Work-class ROV operations generally imply use of a deployment vessel with dynamic positioning (DP) capabilities. A DP vessel is capable of holding position and heading, thus sea current and wind-related disturbances are bounded by vessel's surge, sway and yaw control. However, the sea-wave height and period have a direct impact on vessel's roll, pitch, and heave, which cannot be directly compensated for, thus these remaining three DOF translate to TMS principally as a heave motion. Fig. 3.5. b) shows the ship motion translated to the TMS.

Given the ship heave, roll, and pitch, a total TMS heave displacement z_{TMS} is calculated as:

$$z_{\mathrm{TMS}} = z_{\mathrm{h}} + z_{\mathrm{r}} + z_{\mathrm{p}} \tag{3.1}$$

where z_{h} is heave of the TMS directly proportional to the heave of the ship, z_{r} is heave of TMS due to the ship roll motion, and z_{p} is the heave of the TMS due to the ship pitch. As shown in the figure, to reduce the TMS heave, the suspension point SP should ideally be placed close to the ship pitch and roll axis. The vessels designed specifically for ROV operations exploit this with integrated, moonpool

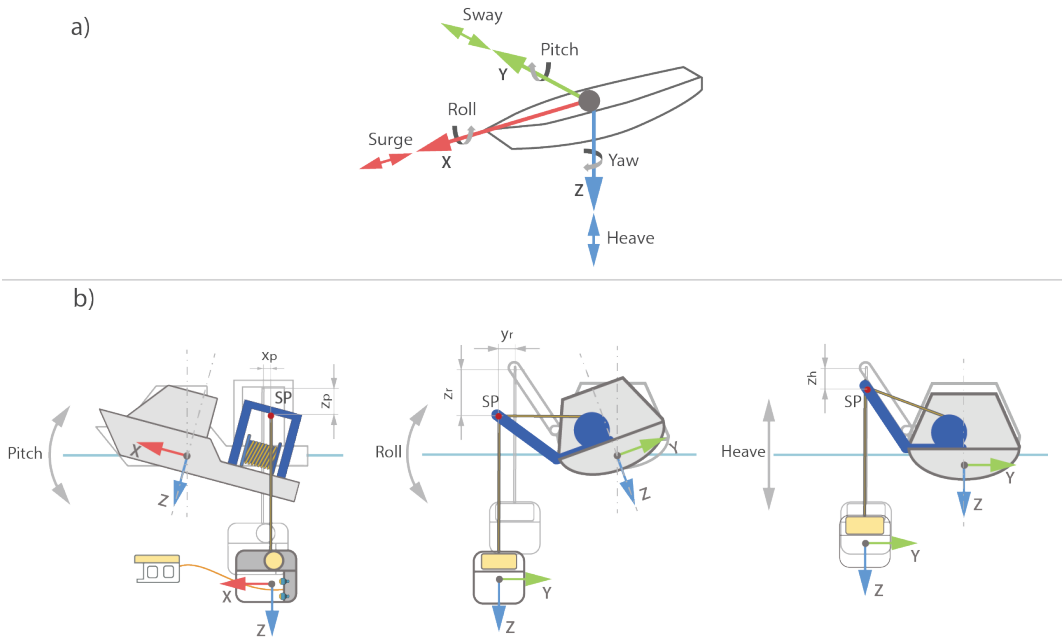

Fig. 3.5 Ship motion mapped to the TMS heave motion. a) Vessel's six degrees of freedom; b) Deployment vessel pitch, roll, and heave mapped in TMS coordinate frame.

LARS or ship door LARS (Barnatt, 2013; Christ and Sr, 2013) systems. However, the most typical LARS is the A-frame type, as shown in Fig. 3.3.

The docking station is relatively stable on the roll and pitch axis since the TMS centre of gravity is below the point where TMS is attached to the umbilical, thus positive longitudinal and lateral stability is achieved. Sea current generally rotates the TMS around the yaw axis, until TMS reaches the orientation that creates the least amount of drag. There are two sources of TMS surge and sway: (1) surface vessel surge and sway which depends on DP capability, and (2) the TMS surge and sway caused by displacement of suspension point y_r and x_p due to vessel's roll and pitch, which, for relatively small angles can be neglected. In addition, the TMS inertia, length of the deployed umbilical, and water act together as a damper, thus they reduce surge and sway oscillations.

In summary, the suspended TMS heave displacement z_{TMS} depends on the surface vessel motion, which depends on various parameters, such as vessel's size and type, the weather conditions, the location of the LARS on vessel's deck, the size of the LARS, etc. Although it is not possible to measure all the variables, as

explained in the next section, given suitable conditions and telemetry the ROV pilot is able to perform the docking manoeuvre successfully based solely on the visual estimation and prediction of TMS heave displacement. In practice, during manual docking the ROV pilot estimates the displacement by observing the video feed either from the ROV or the TMS camera to estimate relative motion between the two. A similar approach is presented in this thesis in Chapter 4, with an ANFIS based TMS heave displacement prediction z_{TMS} up to t seconds in the future, based on previous z_{TMS} measurements. There are various ways to measure TMS heave displacement, such as using depth sensor, altimeter, acoustic positioning system, vision system etc. Since the dataset acquired during the trials consists of TMS depth measurements, and the ROV uses depth control, ANFIS is trained to predict TMS depth. In the next section a manual ROV docking is presented, and the importance of TMS heave prediction for the docking is discussed.

3.4 Standard operating procedures

3.4.1 Manual ROV docking procedure

Docking of a ROV system is one of the most critical tasks dictated by operation weather windows. It introduces a high risk of ROV damage, and it can be a highly stressful operation for a ROV pilot in challenging sea conditions. Manual docking into a cage type TMS starts with the ROV stern facing the entrance of the TMS as illustrated in Fig. 3.8. During the docking procedure a pilot first matches heading, depth, and lateral alignment of the vehicle relative to the TMS. In general, the TMS mechanically allows for certain vertical and horizontal misalignment due to the funnel-shaped entrance. Therefore, for relatively small TMS heave amplitudes, approximately $heave_{max} \leq 1$ m peak-to-peak for the system presented in this thesis, the ROV is able to dock while holding mean TMS depth.

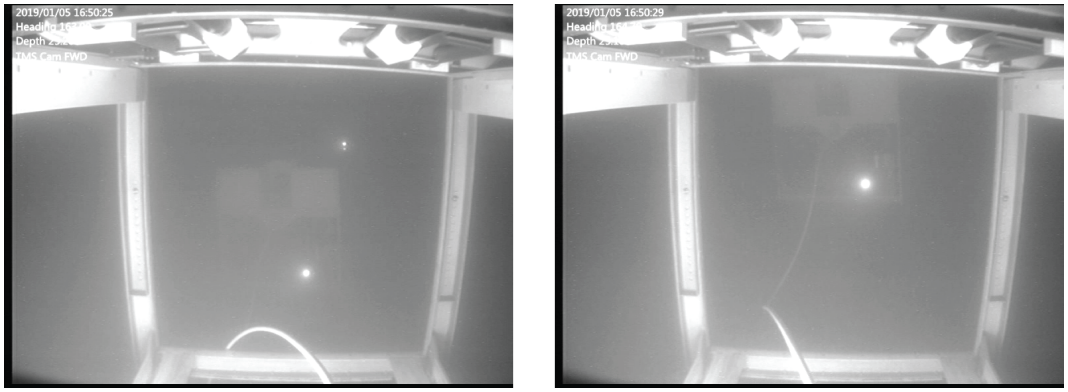

Fig. 3.6 The TMS heaving while ROV holds constant depth. Photo taken during the trials.

Fig. 3.6 shows the TMS heaving prior to a manual docking manoeuvre, while the ROV holds constant depth. However, $heave_{max}$ is often exceeded, thus the vehicle approaches the TMS entrance slowly, while the ROV pilot estimates the amount of TMS heave amplitude and frequency. At this moment there is a low amount of tension present in the tether connecting the TMS and ROV. Generally, the work-class ROVs are not agile enough to match the TMS heave motion due to the weight, and high drag forces associated with the ROV's large cross-section area. To overcome the problem, the pilot positions the ROV to the docking depth that covers either the top or the bottom half of the TMS heave range, as shown in Fig. 3.7.

As the TMS reaches the minimum or the maximum heave value, it slows down, until it entirely stops and reverses direction. The pilot exploits this knowledge and positions the ROV at a corresponding depth, as the shaded area in Fig. 3.7 shows. Although the TMS heave amplitude and frequency are not fixed, once the ROV is in the desired area, the ROV depth can be fine adjusted quickly. To allow for large ROV inertia, the docking manoeuvre typically starts before the TMS reaches the optimal position for docking. Therefore, the pilot must predict the TMS position based on experience, and current and previous observations, and undertake a decision in a fraction of second while controlling the ROV. At the appropriate moment, a light forward thrust is applied to the ROV while a 'tether in' command is given. The light ROV forward thrust keeps the tether under tension as the ROV is docked. With taut tether the ROV moves backwards as we start tethering in due to the tether tension. It

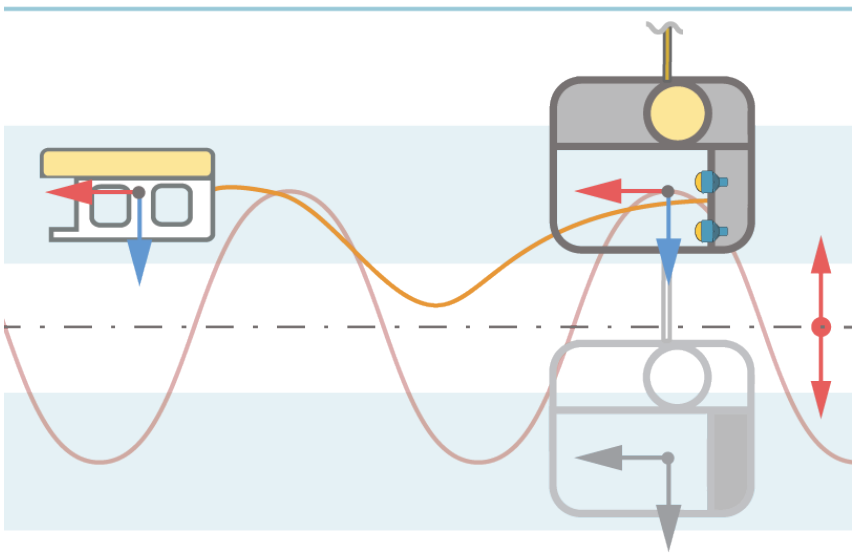

Fig. 3.7 The ROV docking procedure. Red line presents the TMS heave motion, while blue shaded area shows optimal docking position with minimal TMS heave speed.

may seem counterintuitive, but the forward thrust is applied to maintain a constant tension on the tether which allows for best spooling performance and lowers the risk of tangling the tether.

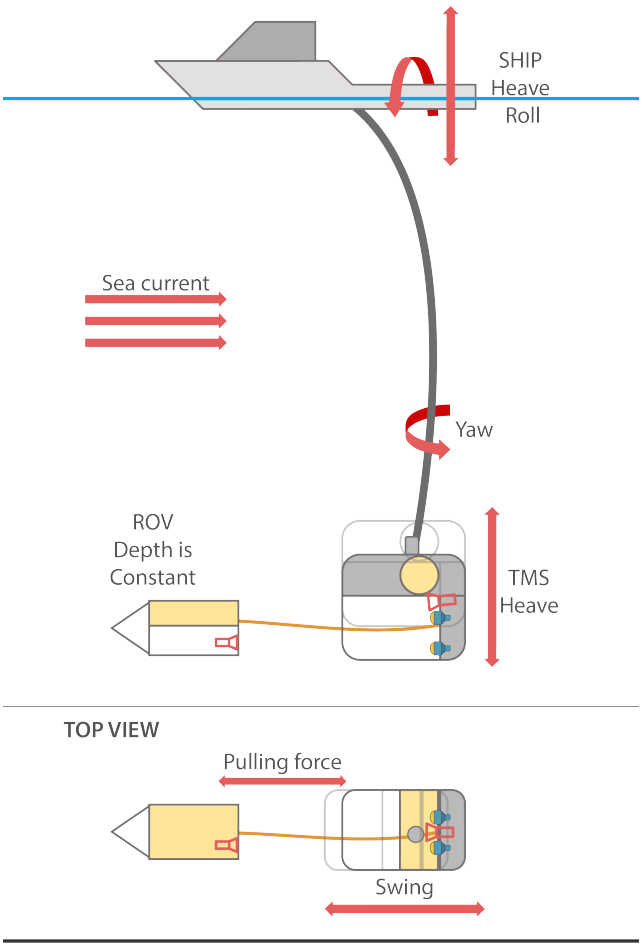

Fig. 3.8 Major disturbances acting on TMS.

As discussed, the major disturbances potentially acting upon a TMS during such a docking include:

- The sea current/wave motion
- The tether pulling force between the ROV and the TMS
- Rolling and heaving motion of the surface ship, translated to the TMS through the Launch and Recovery System (LARS) as a heaving motion

The sea current is a disturbance, usually in a horizontal direction, that acts upon the tether, TMS and the ROV. Since the TMS acts as a clump weight as well, it absorbs the cross-section drag. Thus, the ROV is relieved of the umbilical drag from the surface to the working depth. Therefore, the ROV needs to compensate only

for vehicle drag and tether drag introduced on the soft tether between TMS and the vehicle. However, since the TMS is suspended from umbilical in a single point, the sea current generally rotates the TMS around the yaw axis to an orientation that creates the least amount of drag. The TMS stays in such yaw orientation as long as tension in the tether connecting the ROV and the TMS do not cause a rotating moment. The tension in tether can produce a swinging pendulum motion of the TMS in the direction of the ROV. There are two sources of TMS heave motion. Since the TMS is suspended from a ship, the amount of heave introduced to a ship through waves directly translates to the TMS. As shown in Fig. 3.8, the TMS was deployed from the starboard side of the ship. Therefore, a roll motion of the ship generates a TMS heave motion through the LARS acting as a lever arm. A TMS heave motion can be reduced if a heave compensating winch is employed, however this is costly and was not available within the CRIS system. One of the main objectives of the LARS is to move the ROV and TMS through the splash zone safely to the working depth. Close to the surface, the ROV could easily be overpowered by the waves. This would lead to possible contact between the ROV, TMS, and the ship hull. To avoid direct impact of waves on the TMS and the ROV, which could possibly lead to severe damage, the docking is generally performed below the splash zone at depths of 20 metres or more.

In summary, the relative motion of the ROV and TMS may have a combination of heave, yaw, and pendulum swing motion. It is generally not possible to compensate for all the motion, thus docking regularly involves a rough contact bump between the ROV and TMS, which are designed for such.

3.4.2 The TMS deployment process to the seabed

To test docking to a static target, the TMS was deployed to the seabed. Although static docking is less complicated in terms of control of the vehicle, the risk of damaging equipment was significantly higher since the TMS and the LARS used for the experiment are not designed for such operation. Deployment of assets is a complicated procedure and many factors should be taken into account. Waves, sea

currents, and tides act upon the TMS during the deployment process. The TMS used during the trials was not designed for deployment to the seabed thus additional precaution had to be taken.

The deployment of the TMS to the seabed was a challenging task because of the numerous problems that can occur and cause severe damage to the system. The main challenges were:

- Heaving and rolling motion of the ship, transferred through the LARS can cause a heavy impact between the TMS and the seabed in the last few metres before touchdown, thus causing damage
- The umbilical connecting the LARS and the TMS should not be loose because its armour can unwind
- The horizontal movement of the ship must be minimized in order to avoid flipping and damaging the TMS
- Operating from a station-keeping vessel introduces the risk of umbilical and ship thruster entanglement

When deploying assets to the seabed in high sea states different techniques can be used to compensate for heave motion. There are 'Active' and 'Passive' heave compensation systems (Christ and Sr, 2013). In Active systems, the amount of heave is measured with motion sensors. Depending on the measurement the winch pays out or takes in the umbilical. In passive systems, the umbilical tension is held constant.

Since the LARS used in this case did not have automatic heave compensation, the TMS was deployed in sheltered location during a window of relatively good weather conditions. A few metres of umbilical slack was allowed to compensate for the heaving motion of the ship once the TMS was on the seabed. Attention had to be paid not to release too much umbilical in order to avoid entanglement with the TMS and interference with the ROV operation. The slack also had to be continuously trimmed over time for tidal change.

The umbilical connecting the LARS and the TMS is armoured, and it is designed for a constant tension load (suspended TMS). If a long part of the umbilical gets

loose, there is a possibility of armour unwinding which could cause severe damage to the LARS, TMS, and the ROV. Therefore, static docking operations were limited to shallow waters.

With a few metres of slack and a relatively short distance between the ship and the TMS, horizontal movement of the ship should not exceed a few metres to avoid flipping the TMS over or dragging it on the seabed. To compensate for that the ship was using its station-keeping system in the highest precision mode. While using station-keeping the ship's thrusters are active, thus additional caution should be taken to avoid contact between loose umbilical and the thrusters. The motion of the ship was within the radius of five metres which allowed us to successfully perform the static docking experiment.

To deploy the TMS on the seabed, the TMS with the ROV inside it was lowered down to 20 metres of depth. Altitude was approximately 10 metres. The pilot then flew the ROV out of the TMS, which was slowly lowered down while a continuous general visual inspection of the umbilical, seabed, and the TMS was being carried out. Once the TMS was safe on the seabed, experiment was ready to proceed.

3.4.3 Closing remarks

In this chapter the overview of the hardware used during the offshore trials has been presented. The motion analysis of the TMS suspended from the floating platform has been described and the standard operating procedures such as manual ROV docking, and the TMS deployment process to the seabed have been presented. In addition, the chapter provides the necessary information about challenges associated with ROV operations.

Chapter 4

Visual pose estimation

4.1 Introduction

This chapter describes a developed visual pose estimation solution based on active light marker. The system has been developed around industry standard equipment and thus has the potential to easily retrofit to the existing ROV fleet, or subsea station. The system consists of four conventional underwater light beacons, used as a light marker, and a machine vision camera, with image processing and position estimation is done on a dedicated PC. For underwater experiments the light marker was mounted on the tether management system presented in Section 3.2.2, while image acquisition camera was mounted on the ROV stern. The developed system is demonstrated for use as both autonomous ROV docking and as a navigation tool for subsea vehicles and this chapter is considered as the foundation for Chapters 5 and 7.

Section 4.2 describes a hardware implementation of the system, while image processing method is presented in 4.3. The pose estimation method details are given in Section 4.4. The experimental results of the developed system on dry and real-world experiments in the Atlantic ocean are presented in Section 4.6, while additional considerations and limitations of the system are presented in Section 4.7. The chapter concludes with summaries in Section 4.8.

4.2 Hardware

4.2.1 Navigational lights

The initial pose estimation tests in laboratory included the use of a chequerboard pattern marker such as the one used for camera calibration shown in Fig. 4.3. Although this type of marker showed great performance, it could be only used for short range position estimation, as estimation based on passive markers relies completely on good visibility and low water turbidity. In addition the pose estimation based on the chequerboard and similar augmented reality (AR) markers relies heavily on camera resolution when marker is tracked from a longer distance. Considering expenses related to offshore operations making them more efficient is of great value, thus an active marker based on conventional subsea lights is developed.

However, to complete testing of algorithms for lights recognition and pose estimation, prior to any mobilisation for offshore missions, a simple rig to quantify the developed system was built. A plywood board was used as the test rig body with 100x100 mm inscribed squares, which form a raster for the different light patterns and configurations that were tested. The rig is shown in Fig. 4.1 a). For laboratory tests conventional, off the shelf LED light bulbs were used as light beacons. An optimal light beacons arrangement has been achieved taking into account the camera Field of View (FOV), robustness to light saturation, possible light mounting positions on the TMS, and possible camera mounting positions on the ROV. The light beacons have been arranged asymmetrically to uniquely define the orientation of the light marker. Fig. 4.1 b) shows the developed underwater marker rig with asymmetrically arranged light beacons attached to the tether management system used during the trials.

The lights used for the visual pose estimation underwater are conventional, off the shelf Teledyne Bowtech LED-K-3200-DC underwater lights, rated to 3000 m, with 80 deg beam angle. This type of lights is typically used on the TMS systems, ROVs, trenchers and other subsea structures for better visibility in a dark or turbid environment. Therefore, the existing TMS lights were remounted to form

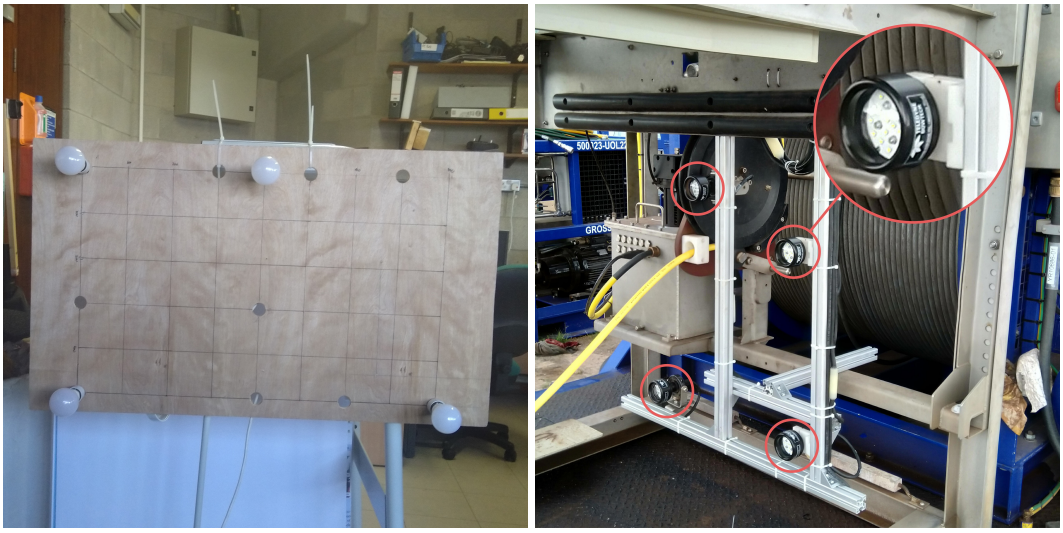

(a) (b)

Fig. 4.1 Navigational lights (a) test rig; (b) on the TMS.

an asymmetrical pattern, which is to be recognised by the camera. The lights were mounted at the back of the TMS, using aluminium profiles.

4.2.2 Camera

The machine vision camera used for testing and trials is a Power over Ethernet (PoE), IDS uEye (UI527xCP-C) GigE with Sony 1/1.8" CMOS (IMX265) sensor, and with diagonal field of view of 90 deg. The maximum resolution of the camera is 2056 x 1542 pixels. Horizontal and vertical subsampling is used to reduce network overload, image processing time, and to achieve a higher sample rate. Therefore the chosen camera frame resolution is 1028 x 770 pixels. The camera is enclosed in a subsea housing rated to 2000 m, as shown in Fig. 4.2 .

A Lensagon BM4518S lens with fixed focus is used. The camera housing has a flat port and the narrow angle lens has been used, thus the FOV is reduced significantly due to light refraction in water. To achieve the widest possible FOV, dome ports and wide-angle lenses should be utilised. The advantages of dome ports are further discussed in Section 4.7.4. Due to the ROV design, which requires reversing into the TMS while docking, the camera is mounted at the stern of the ROV facing backwards.

Fig. 4.2 IDS uEye camera used for the experiment.

4.3 Image acquisition and processing

4.3.1 Camera calibration

To achieve highest pose estimation precision, the camera was calibrated before the beginning of the experiment. Although methods to pre-calibrate in air exist (Łuczyński, Pfingsthorn and Birk, 2017) the best practice is to acquire calibration parameters on site. The calibration panel used for the calibration process is a 7 x 10 chessboard pattern printed on an A4 sized PVC board. The panel was mounted on the port side of the TMS and deployed in water. The ROV was manually manoeuvred around the TMS while images of the panel were acquired from different angles. Approximately 50 images were taken from different angle and distance combinations. The images were processed, and intrinsic camera parameters derived. The calibration algorithm assumes a pinhole camera model (Hartley and Zisserman, 2004). Fig. 4.3 shows images with a chessboard pattern attached to the TMS. Acquired lens distortion and intrinsic parameters of the camera are used to correct image distortion, thus providing better pose estimation.

4.3.2 Image processing

The relative position between the ROV and the docking station (DS) is estimated using a single camera and a light marker of known size and layout. The underwater

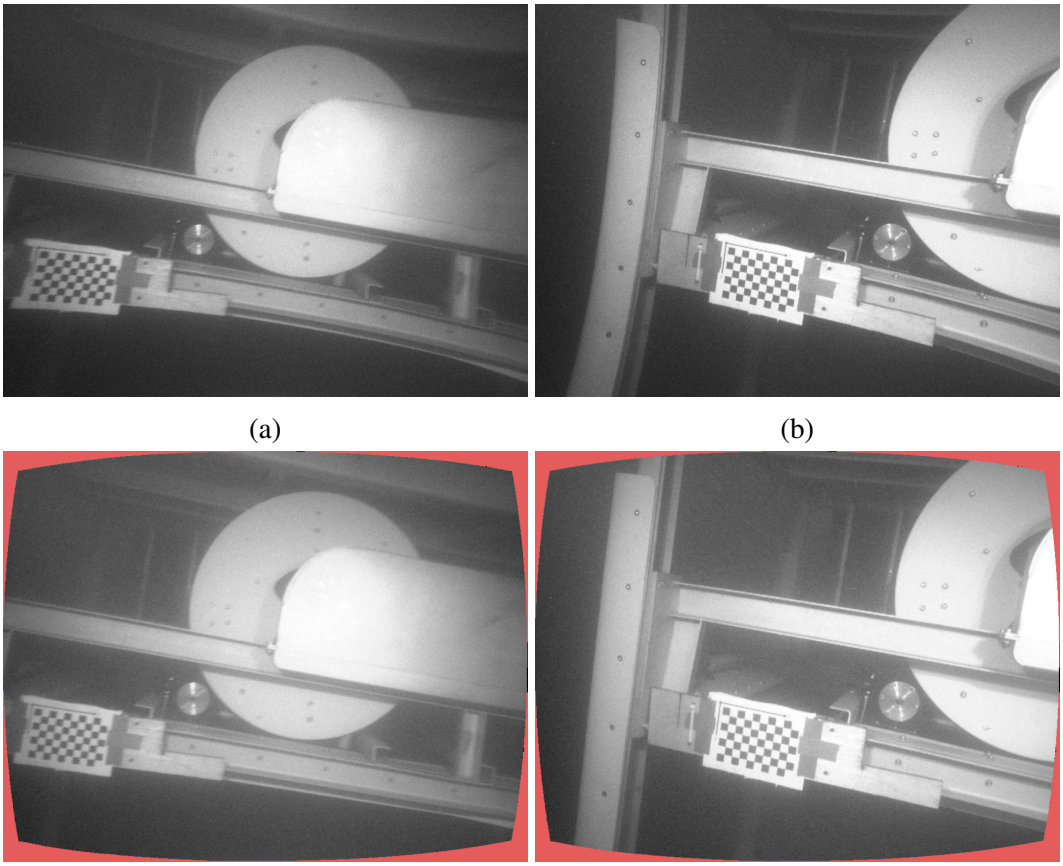

(a) (b)

(c) (d)

Fig. 4.3 Comparison between images before and after the calibration process. (a)(b) original images with distortion; (c)(d) undistorted images.

light marker consists of four light beacons mounted on the aluminium frame. The frame with the marker is mounted on the DS as shown previously in Fig. 4.1. As mentioned before, to avoid ambiguity, the light beacons were mounted asymmetrically, thus creating a unique light marker. The marker ambiguity is discussed in more detail in Section 4.8.

The image processing steps are shown in Fig. 4.4. The process starts with image acquisition (a). Distortion is then removed based on known camera intrinsic parameters obtained through the camera calibration (b). To avoid problems related to light scatter, as mentioned in Park et al. (2009), camera exposure is set to a value where only strong sources of light (relative to surroundings) can be detected. A Gaussian filter is used to blur the image in the next step (c). Image blur is used as a low pass filter which averages out the pixel intensities. Although by adding

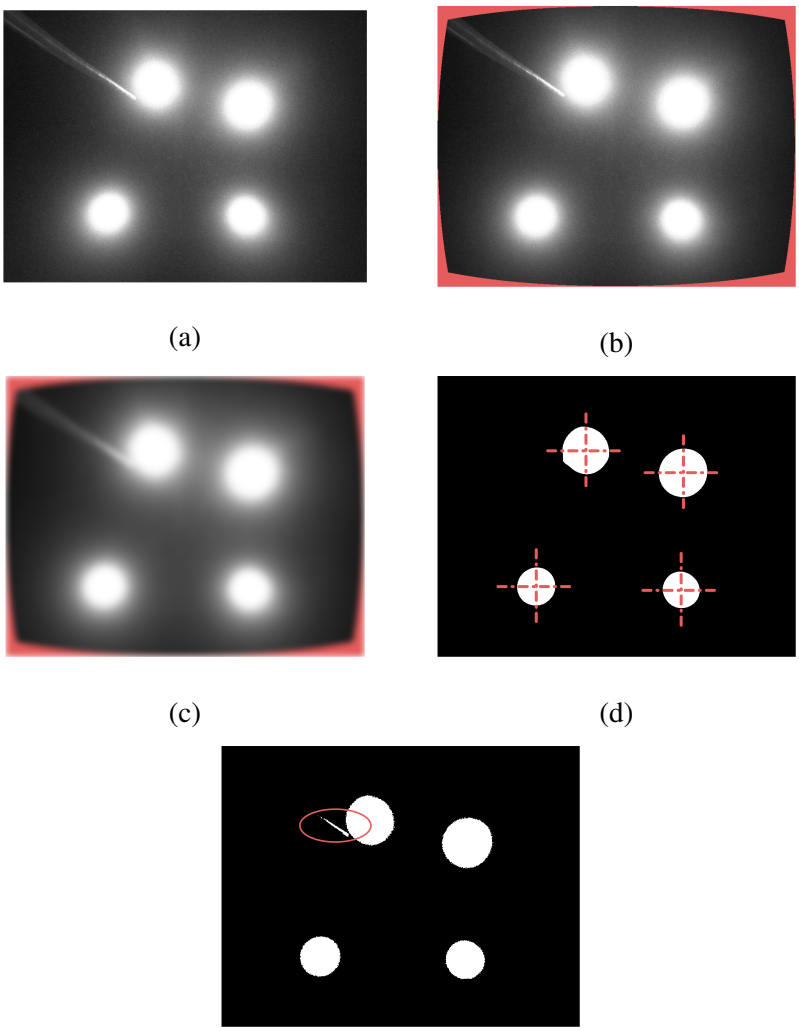

Fig. 4.4 Image processing stages - frames recorded underwater. (a) captured frame; (b) image distortion removed; (c) Gaussian filter applied to average out pixel intensities; (d) blurred binarized image with calculated centres of the light markers; (e) non blurred binarized image, reflection from tether present (circled).

blur more detail is being removed, the position of the brightest objects in the image (light beacons) is not changed, thus the precision is not reduced while robustness is achieved. Additionally, salt and pepper noise could occur during the image acquisition and transmission and affect the binarization of the image in the last step. In that case a non-linear filter from the group of Median filters should be used (Chan et al., 2005; Esakkirajan et al., 2011). In the last step, the image is thresholded and the centres of the four detected disk-shaped objects are calculated (d). The image

threshold function returns a binary image from a grayscale image by replacing all values that are above a globally determined threshold with the value 1, while setting all other values to 0. If the image is not blurred, small reflections from metal objects or the ROV tether can be detected, as shown in Fig. 4.4 e).

4.3.3 Enhanced image processing

Although the developed image processing algorithm performed well during the autonomous ROV docking trials discussed in Chapter 5, the algorithm showed a lower level of robustness when operating close to the sea surface. At depths greater than 30 m the algorithm performed well since sunlight reflections off the metal TMS parts were weak, however, close to the surface the reflections caused multiple pose estimation failures. Therefore, the author looked to development of a new image processing algorithm in an effort to increase robustness of the vision system.

Fig. 4.5 Light conditions for image processing algorithm testing.

Fig. 4.5. shows an image captured during the algorithm testing in the laboratory. As shown in the figure the light conditions in the laboratory during this algorithm testing are highly complex. The light marker with four light beacons is in the

centre of the frame. The marker lights reflections are visible on the floor and on the cabinet on the right next to the marker. The marker light is slightly scattered, and multiple sources of the light are visible on the ceiling of the room. The image is first undistorted and blurred to partially soften reflections and scattered light, as explained in the previous section.

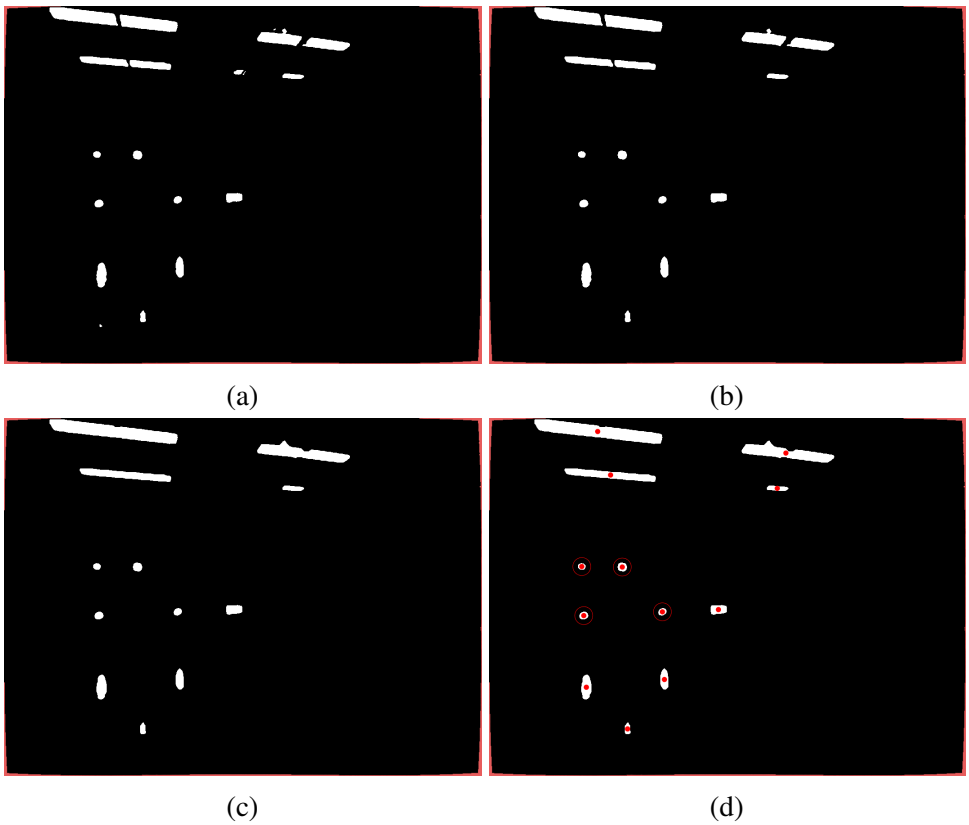

Fig. 4.6 Image processing stages after image is undistorted and blurred. (a) image binarized; (b) objects with less than P pixels removed; (c) image morphologically closed; (d) final step with four roundest objects detected.

The image is then binarized as shown in 4.6 a), and objects that have fewer than P pixels are removed (b). The size of P is determined experimentally. In the next step the image is morphologically closed (c) which fills the gaps between two objects separated by less than N pixels. However, by moving the marker further away from the camera, the distance between the light beacons mapped in the camera frame is reduced. Therefore, the N value must be less than the distance between the two closest light beacons in the camera frame at any time. In the last step the centres of

the objects' mass are calculated, the roundness of the objects is checked, and four roundest objects are then detected and chosen as candidates for pose estimation (d).

4.4 Position estimation

Ideally, the processed binary image returns four perfectly disk-shaped objects with calculated centres of these objects matching the centres of the real light beacons. Based on the known distance between the centres of the four light beacons and known camera parameters, a transformation matrix between two planes can be computed, providing information about all six degrees of freedom.

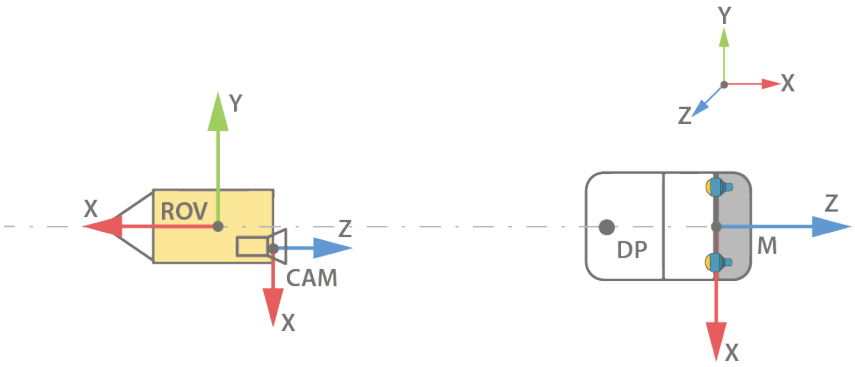

Fig. 4.7 Coordinate systems - top view.

The coordinate systems used in this section are shown in Fig. 4.7. The light marker *M* reference frame is considered the fixed world frame and it is defined by the four light beacons, with the *XY*- plane being coplanar with the plane passing through the centres of the light beacons. The origin of the *M* frame can be an arbitrary point in that plane. Once the origin of the frame is chosen, the relative distance between the light beacons and the origin is measured as shown in Fig. 4.8, which also shows the orientation of the *X* and *Y* axes.

The measured distances yield the world coordinates of the light beacons $\boldsymbol{B}^{\mathrm{M}}$. In practice the origin of the *M* frame is chosen to align with the camera frame when the ROV is docked and latched. However, since the image acquisition camera is mounted on the ROV stern, the light marker is out of the camera FOV when the ROV is completely docked. Therefore, the docking point *DP* is introduced as shown in

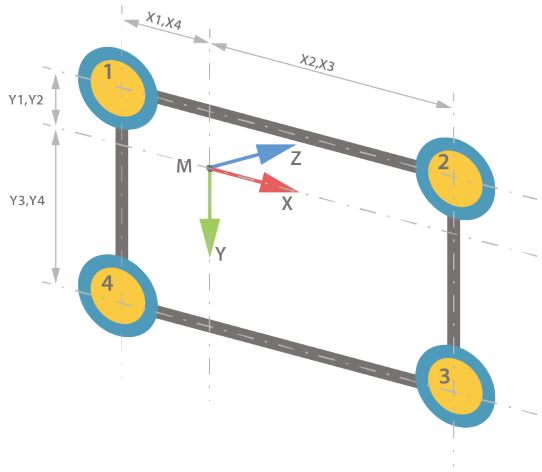

Fig. 4.8 Origin of *M* reference frame is coplanar with the plane passing through the centres of the light beacons. The relative distance between centres of light beacons and the origin of the frame yield the world coordinates of the lights.

Fig. 4.7. When the docking point is aligned with the origin of the *ROV* coordinate frame, the ROV stern is already inside the TMS, while the light marker is still in the camera FOV. Since reversing the ROV completely into the TMS at this point is straightforward, the ROV is considered already docked.

The *ROV* frame is defined as the intersection of lines connecting the centres of diagonally placed ROV thrusters. Since the vehicle control system is designed to operate in the *ROV* coordinate frame, the position error between the docking point *DP* and the origin of the *ROV* frame is used to calculate setpoints for position and speed controllers.

Given the world coordinates of light beacons $\boldsymbol{B}^{\mathrm{M}}$, their corresponding image coordinates $\boldsymbol{I}_{\mathrm{B}}$, and intrinsic camera parameters $\boldsymbol{K}$, the extrinsic camera parameters are calculated as:

$$\boldsymbol{H}^{\mathrm{M}}_{\mathrm{CAM}} = [\boldsymbol{R}^{\mathrm{M}}_{\mathrm{CAM}}, \boldsymbol{t}^{\mathrm{M}}_{\mathrm{CAM}}] = E(\boldsymbol{B}^{\mathrm{M}}, \boldsymbol{I}_{\mathrm{B}}, \boldsymbol{K}), \tag{4.1}$$

where $\boldsymbol{B}^{\mathrm{M}}$ is an $\mathrm{M} \times 3$ matrix with at least $\mathrm{M} = 4$ coplanar points, $\boldsymbol{I}_{\mathrm{B}}$ is a corresponding $\mathrm{M} \times 3$ matrix, $\boldsymbol{H}^{\mathrm{M}}_{\mathrm{CAM}}$ is a homogenous transformation matrix consisting of a 3-D rotation matrix $\boldsymbol{R}^{\mathrm{M}}_{\mathrm{CAM}}$, and a 3-D translation vector $\boldsymbol{t}^{\mathrm{M}}_{\mathrm{CAM}}$.

The transformation of an arbitrary point *N* from the light marker frame to the camera frame therefore is:

$$\boldsymbol{p}^{\mathbf{N}}_{\mathbf{CAM}} = \boldsymbol{p}^{\mathbf{N}}_{\mathbf{M}} \boldsymbol{R}^{\mathbf{M}}_{\mathbf{CAM}} + \boldsymbol{t}^{\mathbf{M}}_{\mathbf{CAM}}, \tag{4.2}$$

where $\boldsymbol{p}^{\mathbf{N}}_{\mathbf{CAM}}$ is the position vector of point *N* in the camera frame with coordinates $[x^{\mathrm{N}}_{\mathrm{CAM}}, y^{\mathrm{N}}_{\mathrm{CAM}}, z^{\mathrm{N}}_{\mathrm{CAM}}]$ and $\boldsymbol{p}^{\mathbf{N}}_{\mathbf{M}}$ is the position vector of point *N* in the *M* frame. The transformation of an arbitrary point N from *CAM* frame to *ROV* frame is defined as:

$$\boldsymbol{p}^{\mathbf{N}}_{\mathbf{ROV}} = \boldsymbol{p}^{\mathbf{N}}_{\mathbf{CAM}} \boldsymbol{R}^{\mathbf{CAM}}_{\mathbf{ROV}} + \boldsymbol{t}^{\mathbf{CAM}}_{\mathbf{ROV}}, \tag{4.3}$$

therefore, given the docking point *DP* in the *M* frame, the position error vector $\boldsymbol{e}$ in the *ROV* frame, used as feedback for the vehicle position/velocity control loop, is calculated as:

$$\begin{aligned} \boldsymbol{p}^{\mathbf{DP}}_{\mathbf{CAM}} &= \boldsymbol{p}^{\mathbf{DP}}_{\mathbf{M}} \boldsymbol{R}^{\mathbf{M}}_{\mathbf{CAM}} + \boldsymbol{t}^{\mathbf{M}}_{\mathbf{CAM}}, \\ \boldsymbol{e} &= \boldsymbol{p}^{\mathbf{DP}}_{\mathbf{CAM}} \boldsymbol{R}^{\mathbf{CAM}}_{\mathbf{ROV}} + \boldsymbol{t}^{\mathbf{CAM}}_{\mathbf{ROV}}, \end{aligned} \tag{4.4}$$

where $\boldsymbol{e} = [x_{\mathrm{e}}, y_{\mathrm{e}}, z_{\mathrm{e}}]$.

4.4.1 Enhanced position estimation

The fact that resident vehicles will operate in partially structured environments consisting of known subsea structures (docking stations, subsea interconnection stations, oil wells, etc.), can be utilised and can offer a means of facilitating a low cost, low maintenance, navigational marker that can eliminate drift in INS estimated pose solution when the vehicle is close to the IMR target.

Although the discussed pose estimation method provides information on the marker relative orientation and position, initial tests presented in Results section of this chapter, showed low sensitivity to angle measurements at larger ranges from the marker, therefore provide lower accuracy at range. As shown in Fig. 4.9, during the visual pose estimation process a relative heading between the marker and the

camera, maps as a perspective distortion of the marker in the camera projection plane. If the distortion is not detected correctly, the rotation matrix $\boldsymbol{R}_{\mathbf{Cam}}^{\mathbf{M}}$ contains angle measurement errors. From a longer distance those relatively small angle measurement errors can produce a significant error in the pose estimation. Since during the autonomous ROV docking approach the ROV is getting closer to the light marker in every image processing loop iteration, sufficient pose estimation accuracy for docking is achieved by the time the vehicle is close to the docking station. Therefore, within the close range to the docking station these errors can be neglected and do not influence the docking manoeuvre. However, to improve longer range pose estimation and to enable use of the developed low cost, low maintenance LED based marker for elimination of navigational drift in INS estimated ROV pose solution as presented in Chapter 7, the pose estimation method has been improved.

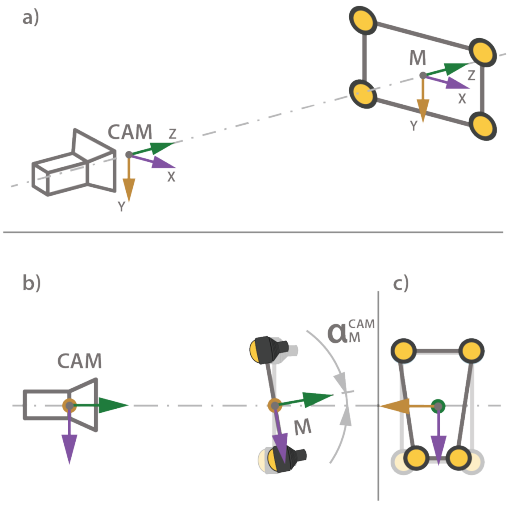

Fig. 4.9 The camera and light marker coordinate systems (a). Relative heading $\boldsymbol{\alpha}_{\mathbf{M}}^{\mathbf{Cam}}$ between the image acquisition camera and light marker(b), maps as a perspective distortion of light beacons in the camera projection plane (c).

As mentioned in Section 4.4., the output of the visual pose estimation is the homogeneous transformation between the light marker and camera $\boldsymbol{H}_{\mathbf{Cam}}^{\mathbf{M}}$ which consists of relative position vector $\boldsymbol{t}_{\mathbf{Cam}}^{\mathbf{M}}$ and orientation matrix $\boldsymbol{R}_{\mathbf{Cam}}^{\mathbf{M}}$. Fig. 4.10, represents the relevant homogeneous transformations between the ROV, the navigational marker attached to the permanently deployed subsea structure, and the world frame.

The position of the ROV in the world frame is calculated as:

$$\boldsymbol{H}_{\mathbf{world}}^{\mathbf{ROV}} = \boldsymbol{H}_{\mathbf{Cam}}^{\mathbf{ROV}} \boldsymbol{H}_{\mathbf{M}}^{\mathbf{Cam}} \boldsymbol{H}_{\mathbf{world}}^{\mathbf{M}}, \tag{4.5}$$

where the transformation matrix $\boldsymbol{H}_{\mathbf{Cam}}^{\mathbf{ROV}}$ describes the relative position and the orientation between the ROV, and the camera frame. The transformation matrix between the camera and the light marker $\boldsymbol{H}_{\mathbf{M}}^{\mathbf{Cam}}$ is acquired using a visual pose estimation. Since the light marker is to be attached to a permanently deployed subsea structure, the position and orientation of the marker in the world frame $\boldsymbol{H}_{\mathbf{world}}^{\mathbf{M}}$ is known.

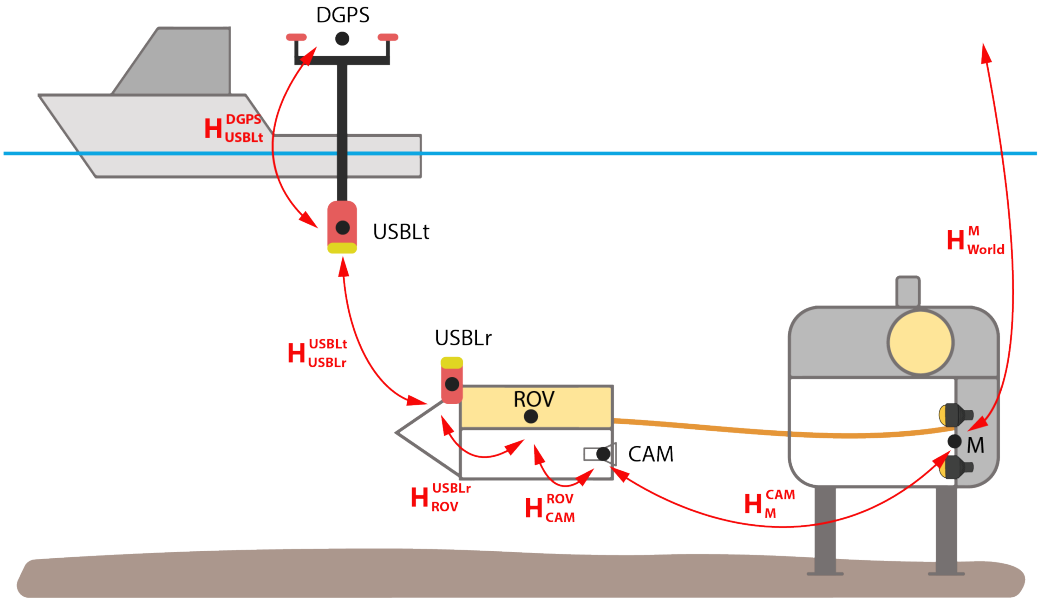

Fig. 4.10 Homogeneous transformations between ship, ROV, TMS and world coordinate frames.

With known orientation of the marker in the world frame, and the ROV attitude measured with high precision IMU, to compensate for the angle measurement error, the relative orientation between the camera and marker $\boldsymbol{R}_{r}{}_{\mathbf{Cam}}^{\mathbf{M}}$ can be derived, and the corrected position of the marker in the camera coordinate frame is calculated as:

$$\boldsymbol{p}_{\mathbf{Cam}}^{\mathbf{M}} = \boldsymbol{t}_{\mathbf{M}}^{\mathbf{Cam}} \boldsymbol{R}_{r}{}_{\mathbf{Cam}}^{\mathbf{M}}. \tag{4.6}$$

4.5 Implementation

Image acquisition and processing software has been implemented in MATLAB on a dedicated computer located in the ROV control cabin. An interface between the machine vision camera and MATLAB has been developed based on the (*uEye Camera Interface in Matlab*, 2016) in order to use the C++ SDK provided by the camera manufacturer. The term MEX stands for 'MATLAB executable'. The camera acquired image is sent via the ROV Gigabit network to a dedicated topside PC where image processing is done. The network uses the TCP/IP protocol. The physical network layer consists of a dedicated optical fibre enclosed in 2.2 km steel reinforced umbilical connecting the ROV topside control cabin and LARS with the TMS, and a 400 m soft tether connecting the TMS and the ROV.

4.6 Results

This section presents experimental results achieved by testing the developed visual pose estimation system. The section consists of two subsections each reporting two experiments. The first subsection presents laboratory experiments performed in air. The dry test provides a comparison between pose estimation based on the passive, chequerboard pattern marker, and the active, light-beacons based marker. Since the chequerboard marker can be considered as an augmented reality (AR) marker, in the remainder of this thesis the term AR marker is used. Therefore, the main scope of the dry tests is to evaluate the pose estimation quality and performance, and to determine the limitations of the developed vision system using the AR marker and the light based marker.

The second subsection presents the experiments performed in the North Atlantic Ocean during January 2019. The scope of the wet tests is to evaluate the developed visual pose estimation system in a real-world environment. The results show the original camera estimated position during the trials and a ground truth position measured with the state-of-the-art navigation system, compared to the corrected

camera position after the enhanced pose estimation algorithm discussed in Section 4.4.1. was applied to the recorded dataset.

4.6.1 Laboratory test

The hardware set-up for the dry tests is shown in Fig. 4.11 with corresponding coordinate systems. The set-up consists of the camera attached to the camera stand with adjustable yaw angle, and both, the light and AR marker have been attached to a trolley which can move only in the camera's Z direction. The position, roll, and pitch angle of the camera are all fixed while it can be rotated around the yaw axis freely between ± 20 deg relative to the markers. The goal of the laboratory tests is to compare results between visually estimated pose using light beacons and using AR marker.

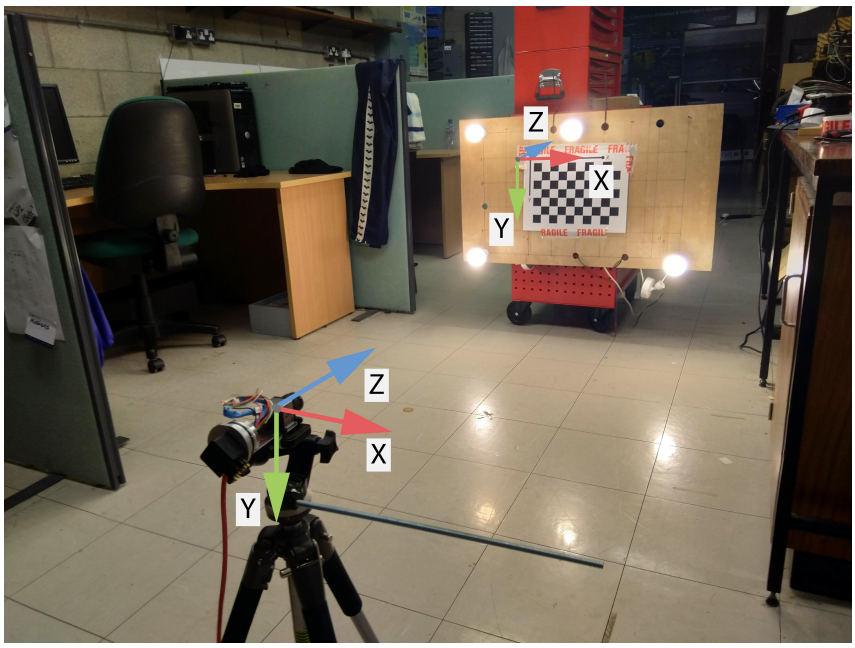

Fig. 4.11 Hardware set-up consisting of a camera attached to a camera stand, a light marker, an AR marker and a trolley.

The test started with the relative yaw angle between the camera and the markers fixed at approximately 0 deg, thus the camera is looking straight towards the markers placed approximately 1.5 m from the camera. The marker is then slowly moved away only in Z-axis from the camera up to distance of 9 m while keeping the same

orientation. The goal of the experiment has been to approximately evaluate the limitations of the system, thus the ground truth distance and orientation between the markers and the camera has not been specifically measured. Therefore, the results showed in Fig. 4.12 are presented as a function of the time, rather than the distance between the marker and the camera.

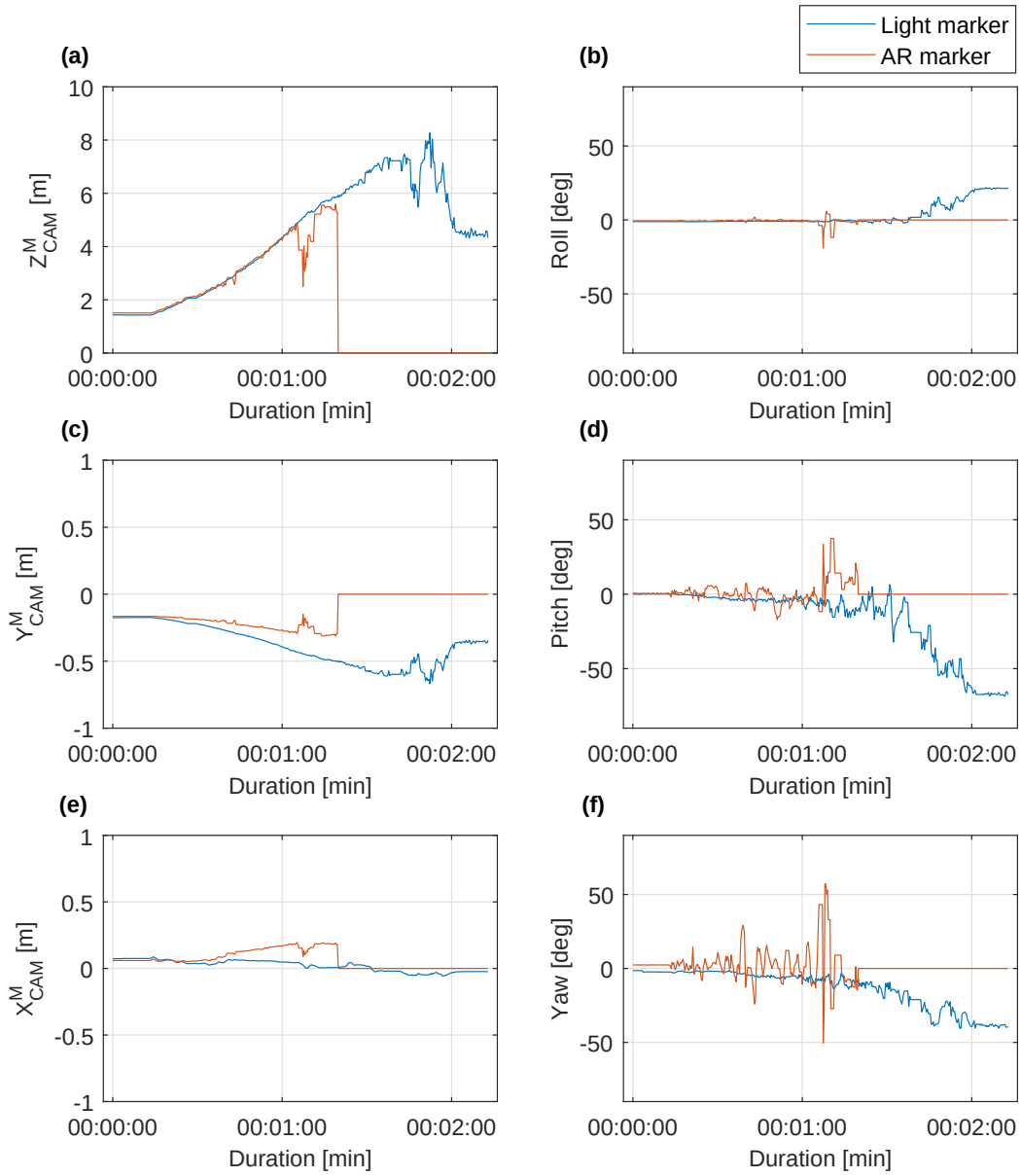

Fig. 4.12 Distance between the camera and the light marker (blue), and the camera and the AR marker (orange), measured in the camera coordinate frame.

The left column shows the position of the marker in the camera frame, thus presents elements $[X^{\mathrm{M}}_{\mathrm{CAM}}, Y^{\mathrm{M}}_{\mathrm{CAM}}, Z^{\mathrm{M}}_{\mathrm{CAM}}]$ of the transformation matrix $\boldsymbol{t}^{\mathbf{M}}_{\mathbf{CAM}}$, while

the right column presents relative Euler angles between the camera and the marker derived from the rotation matrix $\boldsymbol{R}^{\mathbf{M}}_{\mathbf{CAM}}$. Fig. 4.12 a) shows the distance Z^{M}_{CAM} between the camera and markers in the camera coordinate frame. The orange line presents estimated pose using the AR marker, while the blue line presents the light marker pose. Both pose estimation methods showed great results when the distance between the marker and the camera is less than 5 metres. As the markers reached a distance of 5 m and greater the AR marker tracking became intermittent and noisy due to constant change in lighting conditions (marker passing multiple room lights) and due to issues of camera resolution (marker becomes pixelated). At the time approximately 1:20 min, at distance Z^{M}_{CAM} = 6m, the AR marker tracking stopped since the marker is not recognised by the vision system. The light marker performed well up to a distance of 7.5 m from the camera. Although the markers have been moved only in Z direction, Fig. 4.12 (c) and (e) showed a deviation in measurement. However the error in both $X^{\mathrm{M}}_{\mathrm{CAM}}$, and $Y^{\mathrm{M}}_{\mathrm{CAM}}$ is less than 0.5 m at marker distance 7.5 m from the camera. Fig. 4.12 (b), (d), and (f) show relative roll, pitch, and yaw angle between the camera and the markers. As expected the angle measurements are getting noisier as the marker is moved away from the camera, however, the angles estimated using the light marker deviate significantly, due to low angle measurement sensitivity at larger ranges as discussed in Section 4.4.1. The experiment also showed that the angle measurements using the AR marker have been much noisier than the one estimated using the light marker.

4.6.2 Real-world environment experiments

This section presents results of the position estimation method and the enhanced position estimation method, presented in Section 4.4 and Section 4.4.1, as used underwater in the real-world environment. Prior to the test, the TMS system with the light-based marker was deployed to the seabed as described in Section 3.4.2 and shown in Fig. 4.10. The USBL underwater acoustic positioning system was used for qualitative comparison and monitoring. Such a system consists of an inertial navigational system , coupled with a DVL and USBL transponder, all mounted on

the ROV, and a USBL transceiver mounted on the ship. The ROV position measured with the USBL + INS is considered as the ground truth.

Since the INS operates in the world frame, it was necessary to determine the marker position in the world frame. The position and the orientation of the light marker in the TMS frame was measured prior to the deployment. After the TMS deployment, the ROV was docked and latched into the TMS. Based on the known ROV position within the TMS when docked and latched, the ROV navigation system was used to measure the TMS position and the orientation in the world frame. Thus, with the known position of the marker within the TMS frame and the position of the TMS in the world frame, the position of the light marker in the world frame was derived.

Visual pose estimation - static test

Fig. 4.13 shows the ROV position estimation in the $X_{\mathrm{M}}^{\mathrm{ROV}}$, $Y_{\mathrm{M}}^{\mathrm{ROV}}$, $Z_{\mathrm{M}}^{\mathrm{ROV}}$ axis, and relative heading $\alpha_{\mathrm{M}}^{\mathrm{ROV}}$ in the marker reference frame. The coordinate frames were shown previously in Fig. 4.7. During the test, the ROV was approximately 7.1 m from the light marker. The ROV was holding position while heading was changed in increments of 5 degrees, for a total change of 20 degrees, as shown in Fig. 4.13, while the depth of the vehicle was constant. The continuous line presents PHINS measurements of the position and angles. The INS operated in the highest precision mode with all external aiding sensors used (USBL, DVL, depth sensor). The PHINS measurements are considered the ground truth with position standard deviation during the test between 0.2 m and 0.3 m. The heading standard deviation was 0.04 deg, while roll and pitch standard deviation was 0.001 deg. The dotted line shows visual pose estimation measurements. As shown, the visually estimated pose data is noisy and contains significant errors within $\boldsymbol{R}_{\mathbf{Cam}}^{\mathbf{M}}$. After the rotation matrix is replaced with $\boldsymbol{R}_{r\,\mathbf{Cam}}^{\mathrm{M}}$, the new position is calculated. The dashed line presents the updated and corrected ROV position based on the fusion of PHINS relative angle measurements and camera estimated position.

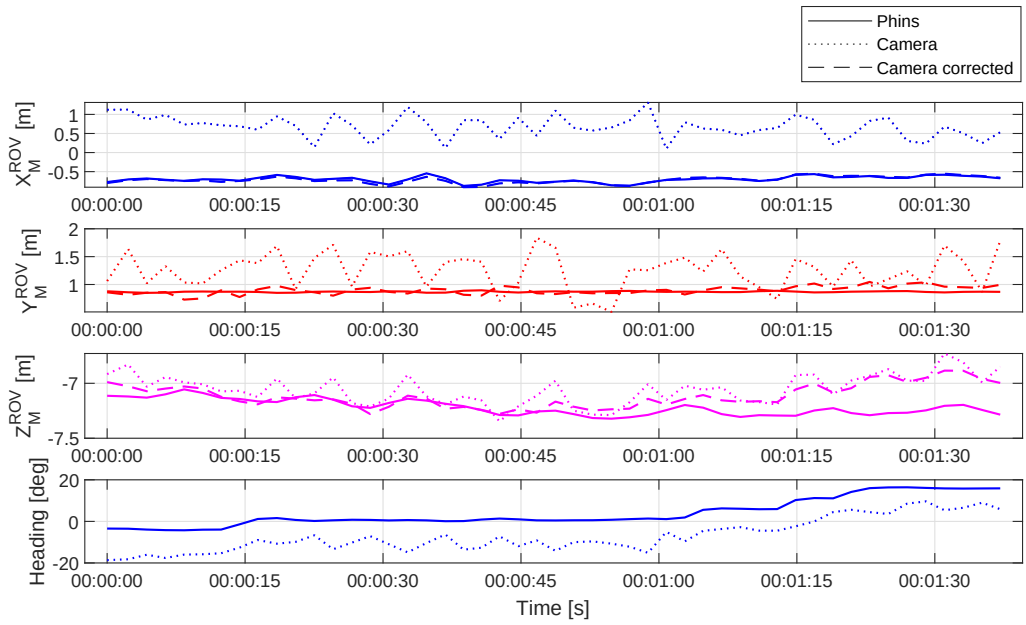

Fig. 4.13 Position estimation of the camera in the marker coordinate frame.

Fig. 4.14 shows relative position error between camera estimated position and PHINS position (dotted line), and corrected camera position and PHINS position (continuous line), previously shown in Fig. 4.13. As shown in the figure, the position error is significantly reduced. As expected, the INS angle measurements outperform the visually estimated relative orientation. The measurements contain less noise, and the updated position is more accurate. Fig. 4.15 shows position error distribution and mean values in the XYZ axes with a normal distribution curve fitted. The graphs in the left column present the distribution of the visually estimated relative pose error before the position correction. The right column shows the error distribution after the INS angle measurements were used for a position correction. As shown the mean error value and standard deviation are significantly reduced. The biggest improvement is achieved in $X_{\mathrm{M}}^{\mathrm{ROV}}$ and $Y_{\mathrm{M}}^{\mathrm{ROV}}$, since those estimations mostly depend on the perspective distortion of the light marker in the camera frame, thus relative angle measurements.

The experiment showed that visual pose estimated data is comparable with data acquired by PHINS operating in highest precision mode with all aiding sensors active. The vision system performed well in good visibility up to 10 m from the

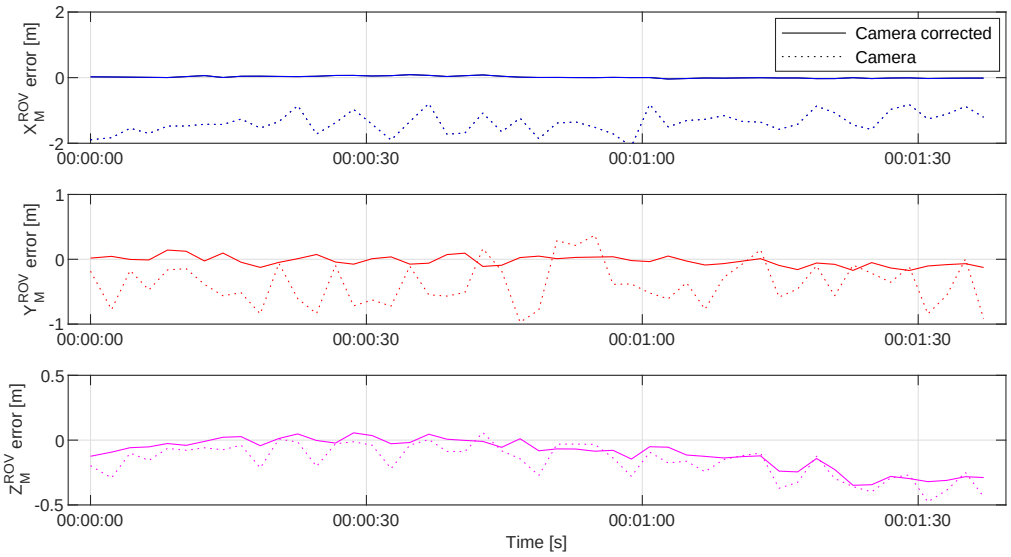

Fig. 4.14 Relative position error of visually estimated pose before and after correction.

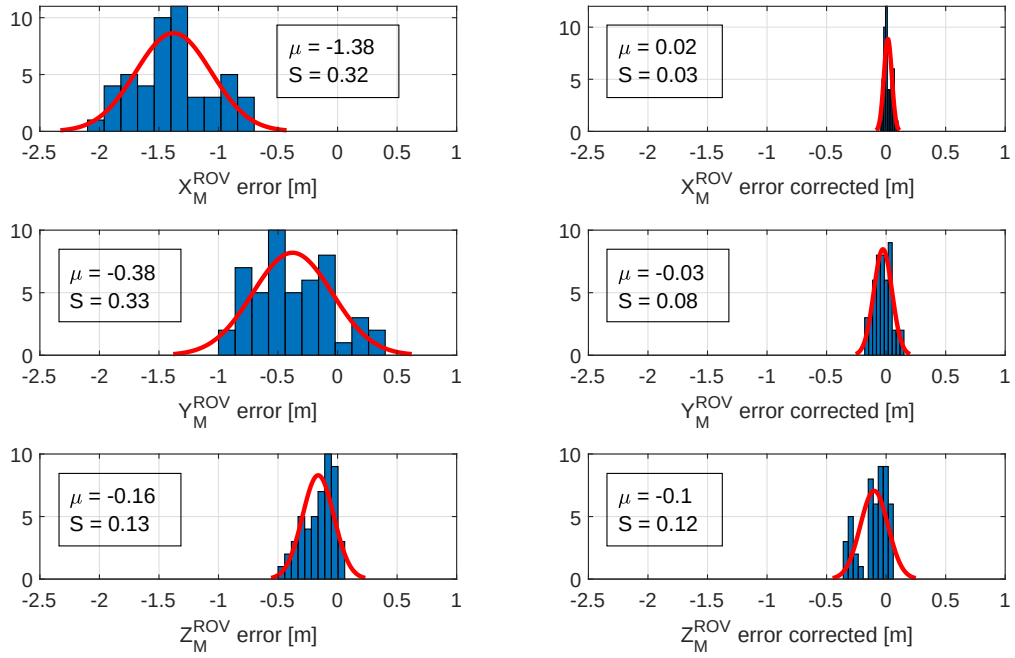

Fig. 4.15 Position error distribution in marker frame before (left column) and after correction (right column).

target using the light beacon-based position marker and with a standard deviation less than 0.5 m.

Visual pose estimation - dynamic test

The ROV position and relative heading in the *M* frame during a dynamic test are shown in Fig. 4.16, while Fig. 4.18 shows a series of images during the dynamic test as seen from the image acquisition camera. The test begins with the ROV placed approximately 6 m from the light marker in $Z_{\mathrm{M}}^{\mathrm{ROV}}$ axis, and approximately 2 m in the $X_{\mathrm{M}}^{\mathrm{ROV}}$ axis. After the initial ROV position is measured, the vehicle is sent to a position $Z_{\mathrm{M}}^{\mathrm{ROV}} = 2$ m from the marker, and aligned with the marker frame in $X_{\mathrm{M}}^{\mathrm{ROV}}$ axis. The ROV depth has been constant throughout the experiment. As the vehicle approaches the marker, at the time around 25 s and distance $Z_{\mathrm{M}}^{\mathrm{ROV}} \approx 3.5$ m from the marker, the camera estimated position and heading (dotted line) starts to overlap with the PHINS position (continuous line). While from the static test shown in Fig. 4.13 it may seem that the camera estimated relative heading has a constant offset from the PHINS heading, Fig. 4.16 shows that the offset changes with the distance from the marker, and as the ROV gets closer to the marker the camera-based pose estimation becomes more accurate.

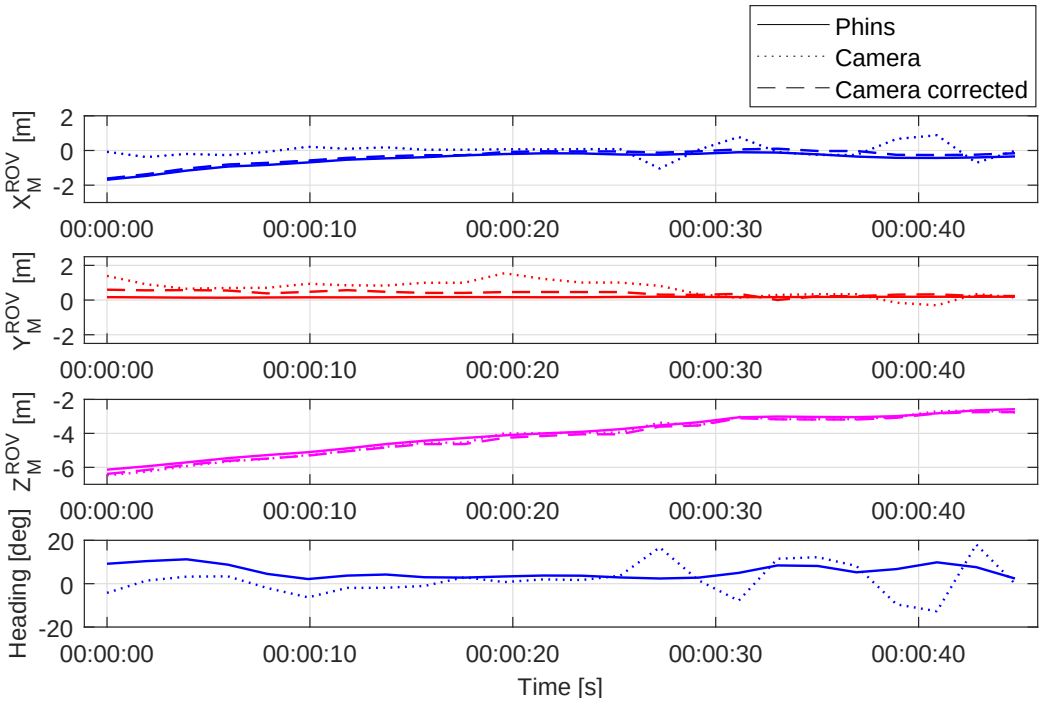

Fig. 4.16 Position estimation of the camera in the marker coordinate frame during the dynamic test.

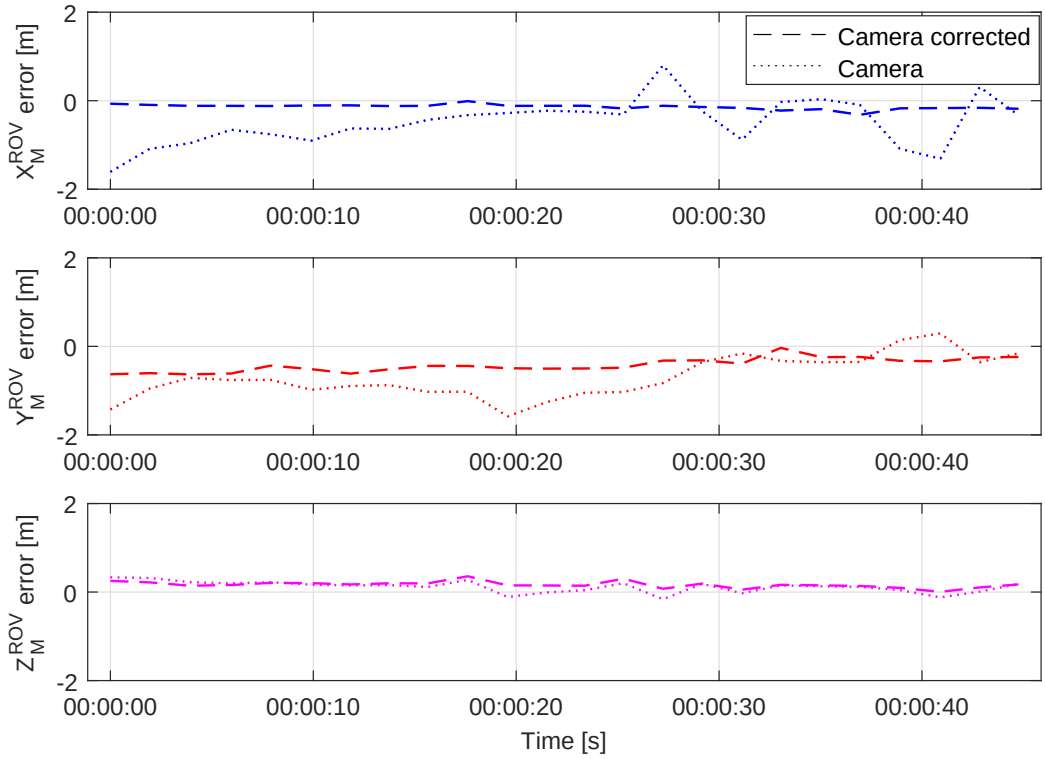

Fig. 4.17 Relative position error of visually estimated pose before and after correction during the dynamic test.

However, to achieve more accurate camera pose estimation throughout the whole distance range, the IMU angle measurements have to be used. As shown in Fig. 4.17, the position error has been reduced and improved in all axes, with the significant improvement achieved in $X_{\mathrm{M}}^{\mathrm{ROV}}$ and $Y_{\mathrm{M}}^{\mathrm{ROV}}$ as expected. The measurement noise caused by partial light marker occlusion, most visible in the heading measurement in Fig. 4.16, has been significantly reduced after the camera pose estimation correction using the INS angle measurements. The problems associated with the light marker occlusion have been addressed and discussed in more detail in the next section. However, partial light marker occlusion due to the ROV tether is shown in Fig. 4.18, at time T = 42 seconds.

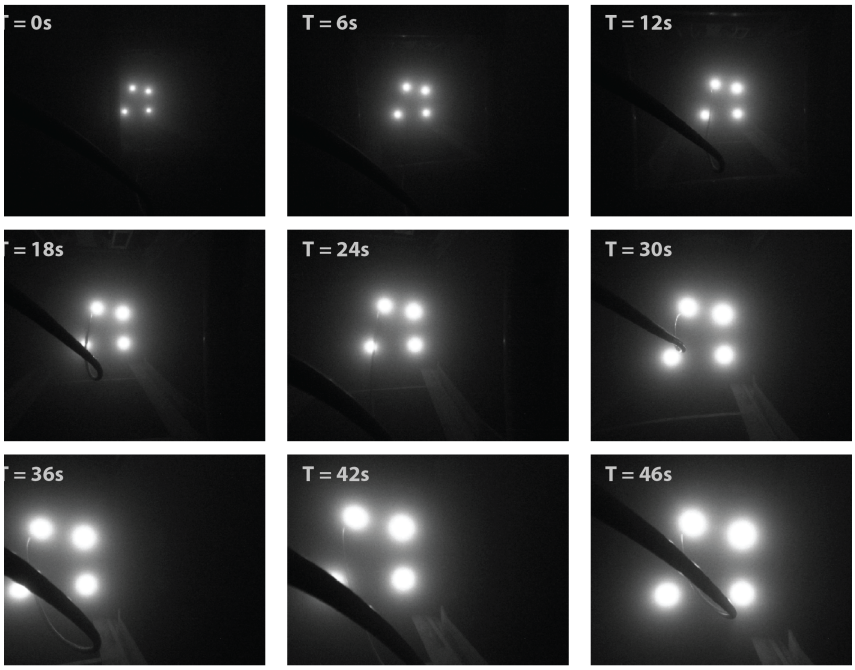

Fig. 4.18 The dynamic test. The ROV position is estimated and corrected while the ROV is approaching the light marker.

4.7 Additional considerations and limitations

4.7.1 A light marker ambiguity

To avoid an active light marker ambiguity, different methods can be used. Pose estimation presented in this thesis relies on asymmetrically arranged light beacons, while active light beacons with known blinking patterns were used by Palomeras et al. (2018), and colour coding was used by Lwin et al. (2018).

However, a vision system does not necessarily require the overall marker to provide a unique position and orientation solution. In that case the orientation of the vehicle has to be assumed or measured with an additional sensor. For example, if a rectangular marker is used, the vehicle orientation is not uniquely defined, and there are two possible solutions. The ROV is either oriented normally or it is rotated 180 deg about the roll axis. To determine the ROV orientation, a measurement from the onboard INS system can be used. Otherwise, the orientation can be assumed based on the mechanical properties and the design of the ROV. Since the ROV centre of buoyancy is above the centre of gravity, positive longitudinal and lateral

stability is achieved. Therefore, the vehicle is stable on the pitch and roll axis, and the orientation of the vehicle can be assumed with a certain probability, yielding a unique solution. However, to achieve additional redundancy and robustness, the use of a marker providing a unique solution is recommended.

4.7.2 Light propagation in water

The analysis of the propagation of the light through seawater is a well-established area of research (Duntley, 1963; Haltrin, 1999). The research shows that the red end of the spectrum of light is highly attenuated in deep ocean water while the blue light attenuates to a much lower degree. This low attenuation property can be shifted towards green light in coastal areas with yellow solutes, which result from plant and animal material decomposition. Therefore, the property of blue light penetration in sea water is often used in the subsea wireless optical communications field (Caiti et al., 2016*a*; Pontbriand et al., 2008), for AUV visual based docking as in Cowen et al. (1997) and Liu et al. (2018), and underwater object detection and tracking (Lee et al., 2012). However, within the scope of the research presented in this thesis, use of existing industry-standard technology is chosen, thus conventional underwater lights have been used.

4.7.3 Water turbidity

The performance of an underwater vision system depends on water turbidity. For pose estimation with a vision system in clear water, providing up to 10 m range capability is easily achievable. A solution that results in a low cost and stable platform for localization can be realized whilst avoiding the common pitfalls of acoustic navigation/positioning systems such as noise pollution.

Although turbid water does limit the system's operation range, precision for the system is not affected significantly due to position estimation method based around the calculating centre points of the light beacons. Since the brightest object of the light beacon is always the centre of the beacon itself, in turbid water the intensity of the light is reduced, however the position of the brightest objects in the image

(light marker beacons) is not changed. Therefore, as long as four light beacons are visible in the acquired image, the visual pose estimation is viable. In highly turbid water, where visual pose estimation is unavailable, the use of acoustic based position estimation technology should be considered.

4.7.4 Camera lens port shape

The machine vision camera available for the autonomous docking trials was enclosed in a housing with a flat port and relatively small 90 deg diagonal FOV. However, this lens and port are not the best choice for such a task. A flat port is a good choice for a close-up photography, and in general, flat port housings are much smaller and compact than the dome port camera housings. However, using a flat port introduces multiple aberrations when used underwater such as: light refraction, radial distortion, and chromatic aberration. Due to the light passing through mediums of different optical density the focal length of the lens increases by between 25 and 30 percent. In addition, flat ports introduce the same amount of magnification effect, thus reducing the field of view. Since the light entering a flat port is not distorted equally, and it is separated into the colour spectrum, a radial distortion and chromatic aberration occurs, however, this is more noticeable with wider lenses. Fig. 4.19 shows a sample level of magnification introduced when using flat port lens underwater. The photos are taken using GoPro Hero2 camera enclosed in a flat port housing.

The dome port significantly reduces the mentioned problems since the light enters the dome ideally under 90 deg angle, thus refraction is minimal. For the tasks where wide FOV is needed, such as autonomous docking, it is therefore recommended to use wide-angle lenses and camera housings with dome ports. A detailed comparison between flat and hemispherical lens ports is presented in Menna et al. (2016).

4.8 Closing remarks

The system presented in this chapter has been developed around a standard camera and light systems found commonly throughout the underwater sector, and serves as

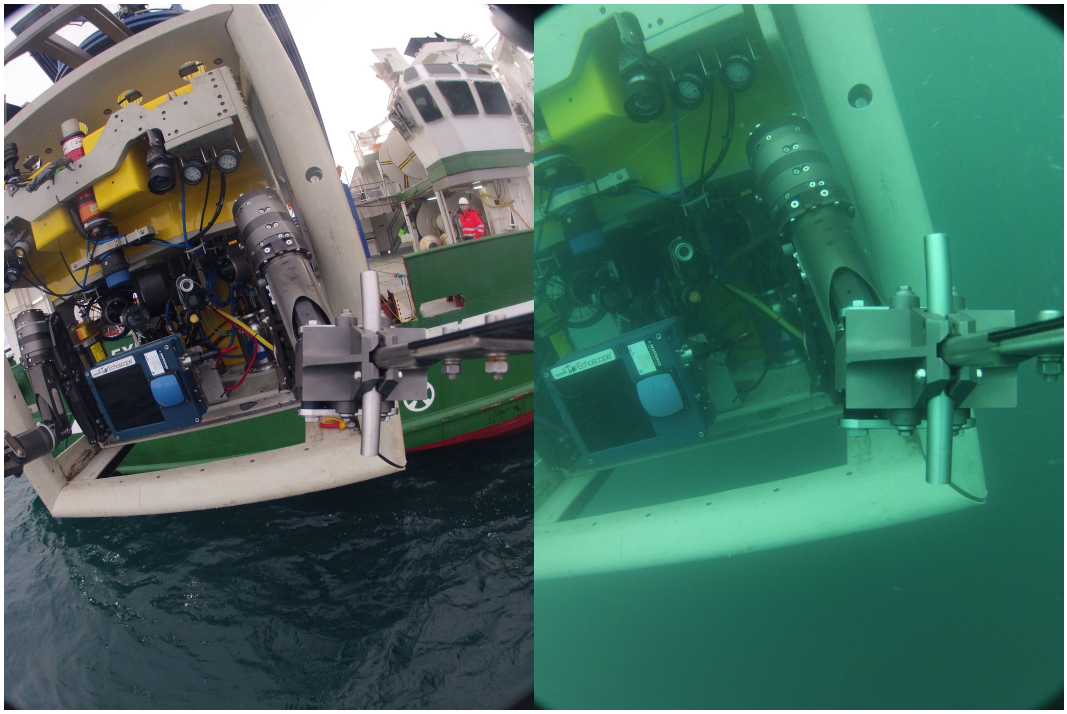

Fig. 4.19 Flat port magnification effect due to light refraction. Difference between photo taken from the same position in air(left), and underwater (right).

a foundation for the autonomous ROV docking experiments presented in Chapter 5. The relative position between the camera and the light marker has been estimated using a single camera and a known light marker pattern. A multi-step pipeline of image acquisition, distortion removal, exposure estimation, Gaussian filter blur and image thresholding allows for the centres of each light beacon within the light marker to be estimated with a high level of precision. The centre points and distances between each beacon then allow for pose estimation of the ROV to the docking station.

The accuracy of the developed pose sensor has been shown to be a function of distance from the navigational marker. It has been shown to be capable of accurately measuring the pose distances and angle up to distances of 4 metres. In close proximity within 3 metres, during the real-world environment experiments, the differences between camera system estimates and the INS solution IXBLUE unit were minimal. Fusing data from the onboard inertial navigation system with vision-based navigation contributes to system robustness and accuracy. This enables the high precision vision-

based localization system suited to resident underwater vehicles presented in Chapter 7. Moreover, the system has been developed around industry standard equipment with the main objective being to create a solution suitable for deployment on the global fleet of work-class ROVs or subsea stations.

Chapter 5

Autonomous docking

5.1 Introduction

This chapter presents autonomous docking of an industry standard work-class ROV to both (a) static and (b) a suspended TMS using a visual based pose estimation approach. Evaluation of the system has been demonstrated through completion of offshore trials in the North Atlantic Ocean in January 2019. Through comprehensive literature review and to the best of the author's knowledge, this is the first autonomous docking of an work-class ROV system to a suspended TMS within the water column. Furthermore, the approach taken does not require specific narrowing entry/funnel shape designs on the docking station. This approach has the dual benefit of minimising mechanical complexity and footprint needed and enabling the possibility to retrofit to the existing ROV fleet. As discussed previously in Section 3.2.2, the entrance of the TMS used as a docking station is only 1.3 times the vehicle size, which makes autonomous docking task more challenging. Accurate position sensing and advanced ROV control described herein allows for this docking manoeuvre.

5.2 ROV control system

The robust ROV control system is essential for autonomous ROV docking. A suite of smart technologies for ROV control and subsea operations called $\mathrm{OceanRINGS}^{+}$,

has been continuously being developed in house at the Centre for Robotics and Intelligent Systems (CRIS).

OceanRINGS$^+$ consists of speed, depth, and heading controllers for subsea navigation and dynamic positioning, and various pilot interfaces with visualisation and situation awareness (Omerdic and Toal, 2012; Toal et al., 2012). The system is designed as a 3-layer ROV control system as presented in Omerdic et al. (2013). Low-level controllers with fault-tolerant control allocation algorithms are part of the bottom layer, an interface between an ROV and other supporting platforms is part of the middle layer (e.g. supporting vessels, TMS, image acquisition PC), while supervision, monitoring, and mission planning tools are part of the top layer (Capocci et al., 2018). Based on the camera pose estimation presented in Chapter 4, control parameters are sent to the ROV low-level controllers. Six low-level controllers (LLCs) control the ROV, each for one degree of freedom (DOF). Surge and Sway controllers are velocity controllers while Heave, Roll, Pitch, and Yaw are position controllers. The internal structure of an LLC loop is shown in Fig. 5.1.

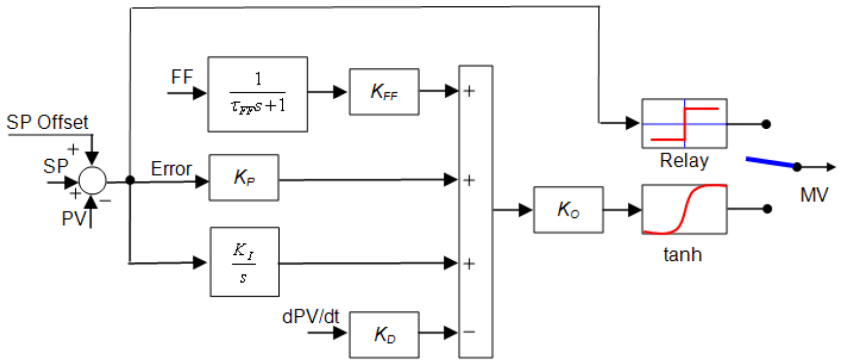

Fig. 5.1 Internal structure of a LLC loop.

Modified PID controllers with normalized outputs were used to control the ROV. The difference between setpoints *SPs*, acquired from the image acquisition PC, and process variables *PVs* are used to generate a manipulated variable *MV*. The manipulated variable is applied to drive the actuators, thrusters. If a controller is disabled, the corresponding *MV* is set to zero. In the case of a time-varying *SP*, feed-forward (*FF*) input is used to improve tracking performance. To avoid problems related to integrator saturation, a vector SP_{Offset} is used. Individual controller

outputs are bundled into a vector of normalized forces and moments τ_{LLC}. Since the instruments and equipment onboard are likely to be removed, added or replaced during the trials, the dynamic properties of the ROV change. Therefore, for the optimal controller performance, autotuning of the low-level controllers is necessary. The relay output is used for the LLC autotuning with two developed autotuning algorithms. The recorded force-speed static characteristic is utilised for tuning the velocity controllers tuning, while position controllers use a self-oscillations approach. The control architecture of the ROV, presented in more detail can be found in Appendix A.

5.3 Results

This section presents the results of offshore docking experiments. Video material of the trials is available on the CRIS YouTube channel (CRIS UL, 2019). Results indicated that visual pose estimation based autonomous docking of a work-class ROV and TMS, in a real-world environment is possible. Both static and dynamic docking experiments were performed during the trials. Although initial camera pose estimation tests were performed earlier, the camera pose estimation for ROV control and autonomous docking has never been tested before, thus it was necessary to determine the system performance first.

To validate the performance of the system, the ROV position was measured simultaneously using two different techniques. Camera pose estimation was used for the ROV control as described in Section 4.4. The PHINS INS with depth, DVL and USBL underwater acoustic positioning system aiding was used for qualitative comparison and monitoring in a similar way as discussed in Section 4.6.2.

5.3.1 Static docking

To be able to measure the performance of camera estimated relative distance between the ROV and the docking station with the INS and USBL, the position of both must be known. The DS position was recorded prior to the static docking experiment, with

the ROV with INS and navigational sensors docked, since only one USBL beacon, attached to the vehicle for continuous monitoring, was provided during the trials, as shown in Fig. 5.2. It is assumed that the DS position did not change over time.

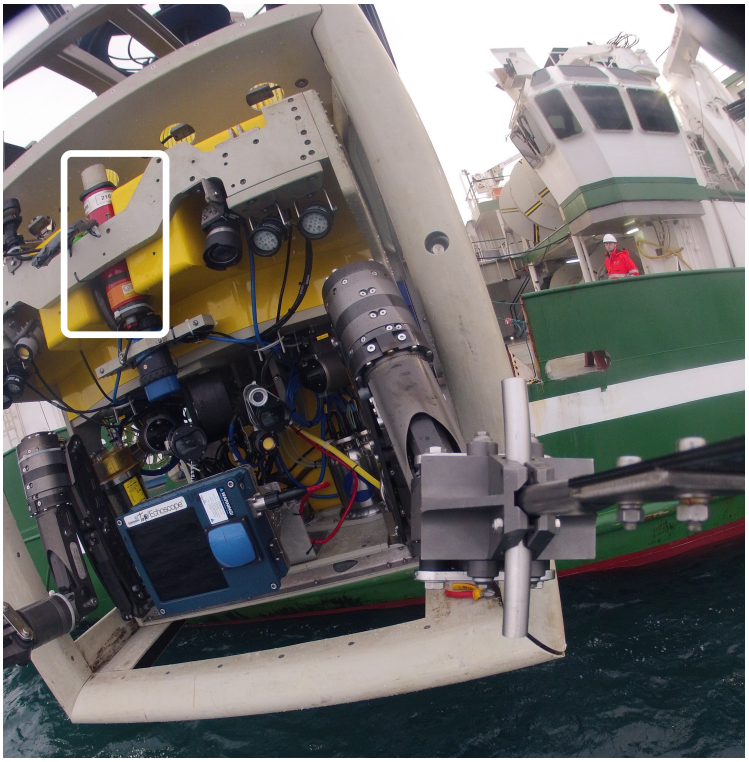

Fig. 5.2 The USBL transponder mounted on the front of the ROV.

The experiment started with the ROV placed 4-5 metres in front of the DS entrance. The start position was randomly chosen while the light beacons were kept in the camera's FOV. The maximum ROV speed during the experiment was limited to 0.4 knots. The docking station was placed on a rocky seabed at a water depth of approximately 25 m.

Fig. 5.3 shows the distance $X_{\mathrm{DP}}^{\mathrm{ROV}}$ and $Z_{\mathrm{DP}}^{\mathrm{ROV}}$, and the relative heading α_{DS}, between the origin of the ROV frame and the docking point DP during the docking experiment. The orientation of coordinate frames is shown in Fig. 4.7. Fig. 5.3(a) shows the distance between the ROV and docking point in *XZ*-plane. The red line with triangles represents the camera pose estimation while the blue line with circles represents the pose measured with USBL and INS systems. The position standard deviation of the USBL + INS system is illustrated by the blue shaded area.

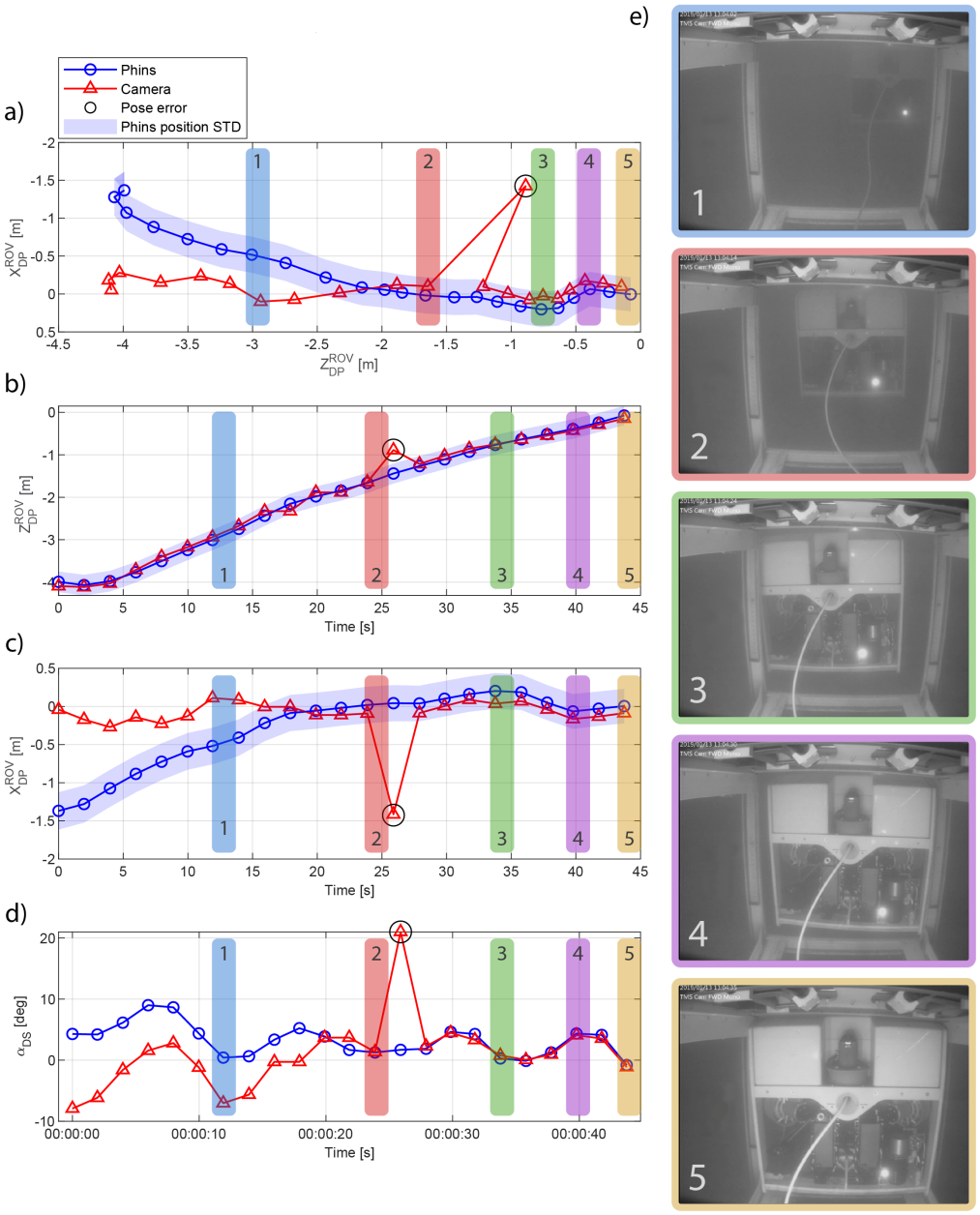

Fig. 5.3 The distance $X_{\mathrm{DP}}^{\mathrm{ROV}}$ and $Z_{\mathrm{DP}}^{\mathrm{ROV}}$ between the ROV position and the docking point in the DM frame during static docking. a) The distance in the *XZ*-plane; b) The ROV distance $Z_{\mathrm{DP}}^{\mathrm{ROV}}$ in the M frame; c) The ROV distance $X_{\mathrm{DP}}^{\mathrm{ROV}}$ in the M frame; d) Relative heading α_{DS} between the ROV and the DS; e)A series of images during autonomous docking.

Throughout the experiment the deviation was between 0.22 and 0.25 m. A disparity between the estimated and the true position is present at greater distances, but as the ROV gets closer to the docking station, the estimated and true positions converge.

The disparity is due to the low angle measurement sensitivity, as explained in Section 4.4.1, which is reflected as a pose estimation error, particularly in the x_{d} axis. The distance $Z_{\mathrm{DP}}^{\mathrm{ROV}}$ and $X_{\mathrm{DP}}^{\mathrm{ROV}}$ plotted against time are shown in (b) and (c). Estimation of $Z_{\mathrm{DP}}^{\mathrm{ROV}}$ shows good performance during the experiment with the estimated position within 0.2 m from the ground truth position at all times. Due to the partial light beacon coverage discussed in Section 5.4.2, pose estimation errors were present and are shown as spikes in the graphs. In the case of a 'not feasible' estimated pose or velocity in step n, the measurement is neglected, and the pose estimated in step n_{-1} is used for ROV control as explained in Fig.5.10. Estimated and true relative heading α_{DS} between the ROV and the docking station, is shown in (d).

Images $(\mathrm{e})_{1-3}$ show the ROV approaching the DS entrance. The images were acquired with the camera mounted on the DS, at different times during the experiment. The ROV heading is aligned with the DS heading during the approach. The relative heading α_{DS} should be ± 5 deg before the ROV enters the DS $(\mathrm{e})_4$ in order to dock successfully. Once the ROV stern entered the DS entirely $(\mathrm{e})_5$, there is only one DOF between the ROV and the DS left. Since the narrow camera FOV does not allow for pose estimation from a closer distance, and moving the ROV along the z-axis in this position is trivial, the docking experiment is considered successful.

Multiple successful dockings were performed during the trials. Fig. 5.4 shows the ROV distance from the *DP* in the *XZ*-plane during five different dockings. Each docking experiment started from a different position and with a different orientation. The red rectangle shows a region within ± 0.2 m from the centre of the DP frame. When the centre of the ROV coordinate frame is within this region the docking is considered successful. During Docking 1 and Docking 2, approximately 1 metre from the target there is an overshoot in the ROV position measurement. This error is due to partial marker occlusion caused by the ROV tether. As explained in more details in Section 5.4.2, partial coverage of navigational light beacon causes significant pose error. Therefore, the change in the position between two consecutive steps is monitored. If an unrealistic change in position is detected the algorithm shown in

Fig. 5.10 assumes inadequate pose and the previous known position measurement is used instead.

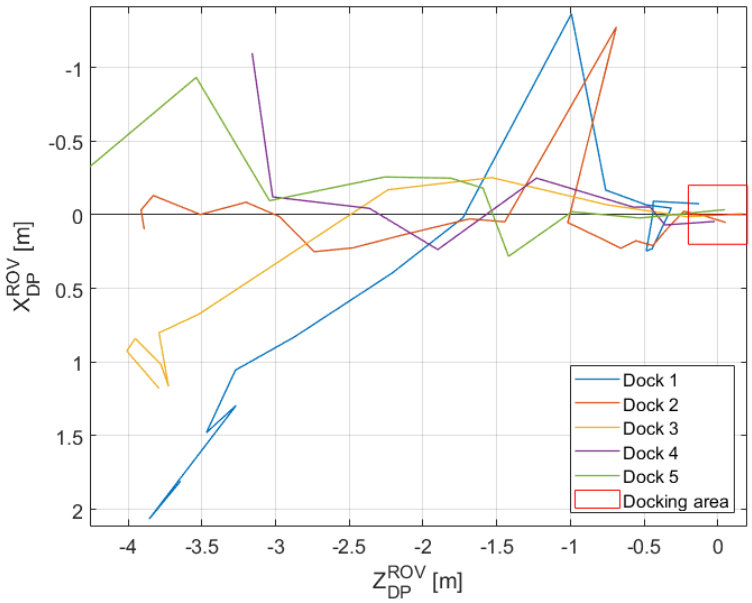

Fig. 5.4 The estimated ROV position in the M frame during multiple static dockings.

As mentioned previously, low angle measurement sensitivity at bigger distances from the light marker can present as a position error, particularly in the X-axis. Fig. 5.5(a) shows the visual pose estimation error distribution of $X_{\mathrm{DP}}^{\mathrm{ROV}}$ depending on the relative heading α_{DS} and distance from the docking station $Z_{\mathrm{DP}}^{\mathrm{ROV}}$. While the position error is minimal at the closer distances up to 3 m (light green dots), and it does not depend on the relative heading, at longer distances the $Z_{\mathrm{DP}}^{\mathrm{ROV}}$ error grows significantly. Fig. 5.5(b) shows a folded normal distribution of position error $|X_{\mathrm{DP}}^{\mathrm{ROV}}\mathrm{err}|$ for range of $Z_{\mathrm{DP}}^{\mathrm{ROV}}$ between 0 and 1.5 m with corresponding mean and standard deviation value. The position error for the range between 1.5 and 3 m is shown in (b) while the distribution of position error in the range between 3 and 4.5 m is shown in (c).

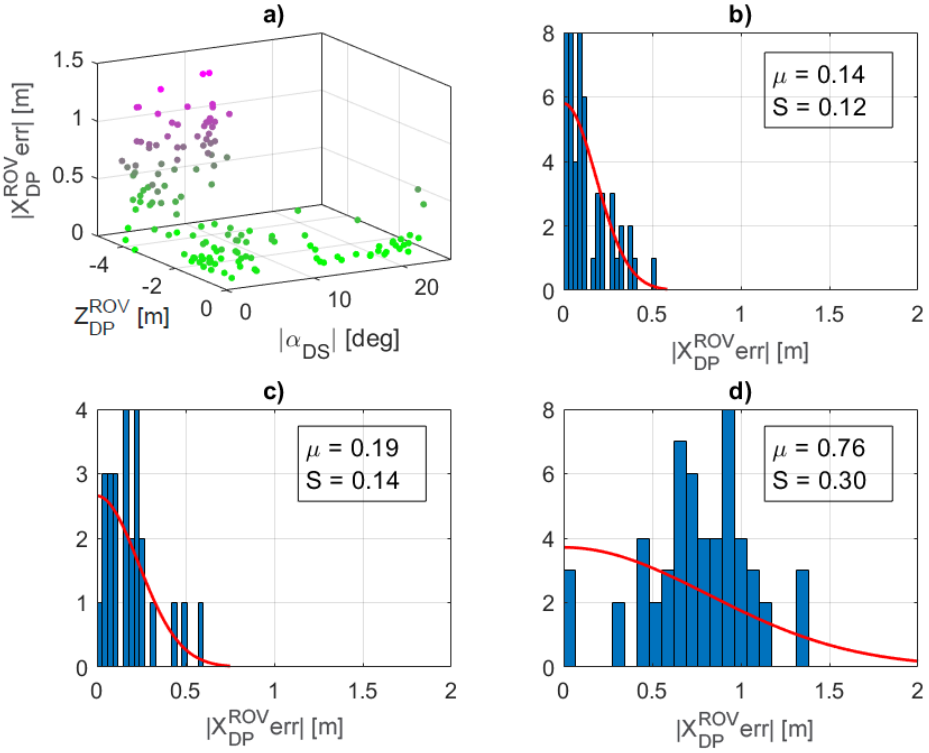

Fig. 5.5 Folded normal distribution of the position error $|X_{\mathrm{DP}}^{\mathrm{ROV}}\mathrm{err}|$ during multiple static dockings. a) Influence of distance and relative heading between ROV and docking point on pose estimation error of $X_{\mathrm{DP}}^{\mathrm{ROV}}$; b) Distribution of error at distance 0 to 1.5 m from the docking point; c) Distribution of error at distance 1.5 to 3 m from the docking point; d) Distribution of error at distance 3 to 4.5 m from the docking point.

5.3.2 Dynamic docking

The ROV position and relative heading in the DP frame during a dynamic docking experiment are shown in Fig. 5.6. The operating depth was approximately 20 metres throughout the experiment. Since one USBL beacon was provided, the comparison between camera pose estimation and INS/USBL position was not viable because of the inability to measure the DS position continuously.

The docking procedure started approximately 2.5 m from the DS entrance $(e)_1$. Partial light beacon occlusion caused an error which was detected, and the vehicle continued moving towards the DS entrance. The contact between the vehicle and the DS was established $(e)_2$. The ROV position was aligned with the docking station $(e)_3$, and the ROV was docked successfully $(e)_4$. During the experiment the DS was

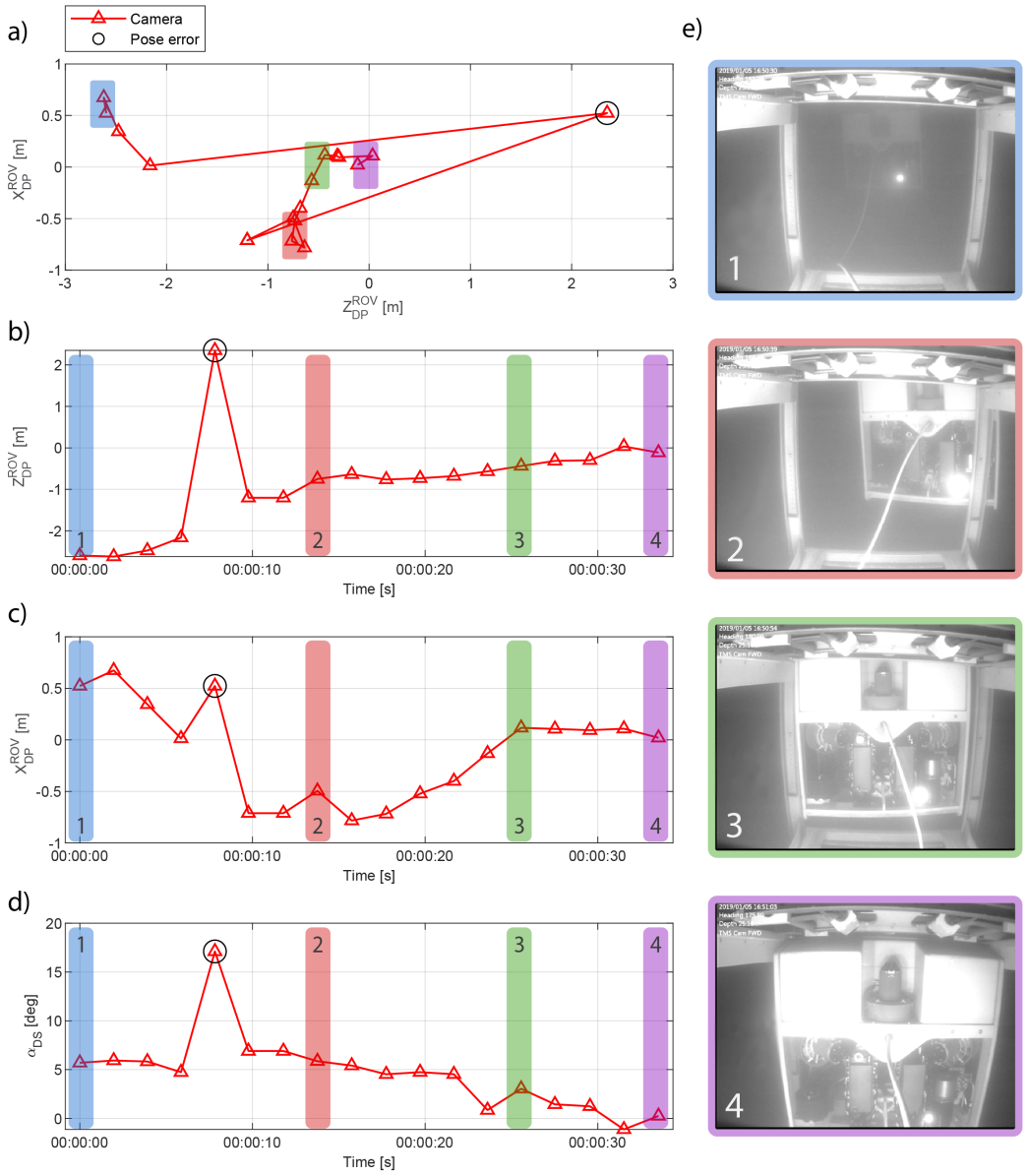

Fig. 5.6 The distance $X_{\mathrm{DP}}^{\mathrm{ROV}}$ and $Z_{\mathrm{DP}}^{\mathrm{ROV}}$ between the ROV position and the docking point in the M frame during dynamic docking. a) The distance in the *XZ*-plane; b) The ROV distance $Z_{\mathrm{DP}}^{\mathrm{ROV}}$ in the M frame; c) The ROV distance $X_{\mathrm{DP}}^{\mathrm{ROV}}$ in the M frame; d) Relative heading α_{DS} between ROV and the DS; e) A series of images during autonomous docking.

suspended and exposed to the disturbances previously shown in Fig. 3.8, thus the docking approach was changed compared to that used in static docking. Due to inertia, larger mass vehicles react slowly to thruster output, thus it was not feasible to compensate fully for the DS heave motion. Therefore, while static docking was performed with minimal contact between the vehicle and the docking station, during

dynamic docking, contact is inevitable. Fig. 5.7 shows the DS heave motion during the experiment.

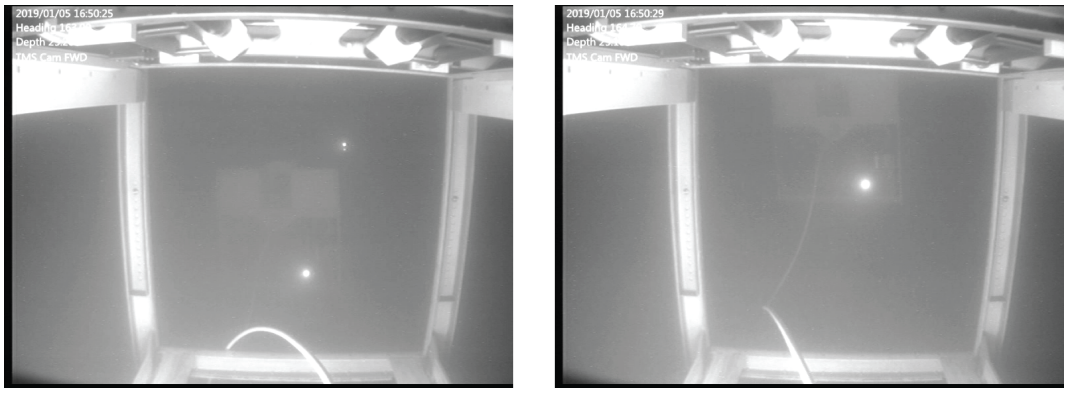

Fig. 5.7 The DS heaving while the ROV holds constant depth.

The peak-to-peak amplitude was approximately 1.1 m with a period of 8.5 seconds. To dock the vehicle successfully, an average DS depth was calculated and used as the setpoint for ROV depth. There is a limit using this approach. For the DS system used during the trials, the maximum peak-to-peak amplitude must be lower than the DS entrance height to avoid tether damage. ROVs are designed for harsh environments and able to handle mechanical stress, but it is crucial not to damage the tether.

Fig. 5.8 shows a series of images during the docking manoeuvre. The ROV in initial docking position starts with the docking manoeuvre (1) and approaches the DS (2)(3). The DS heading has the tendency to change if an external force acts upon it (e.g. contact between the ROV and the DS). After the contact (4) it is important to maintain reverse thrust on the vehicle. The reverse thrust creates momentum around the DS yaw axis and helps with the ROV heading alignment (5)(6)(7). The ROV position is thus aligned in (8)(9). While the vehicle was still reversing back completely aligned, the DS depth changed due to the heave motion and the ROV docked in (10)(11)(12).

The presented docking manoeuvre is the worst-case docking scenario since the DS used in these experiments does not have thrusters (the DS position and orientation are not controllable). While DS pitch and roll are stable, the DS has a tendency to yaw. Since the DS is equipped with an onboard magnetic compass, by adding two

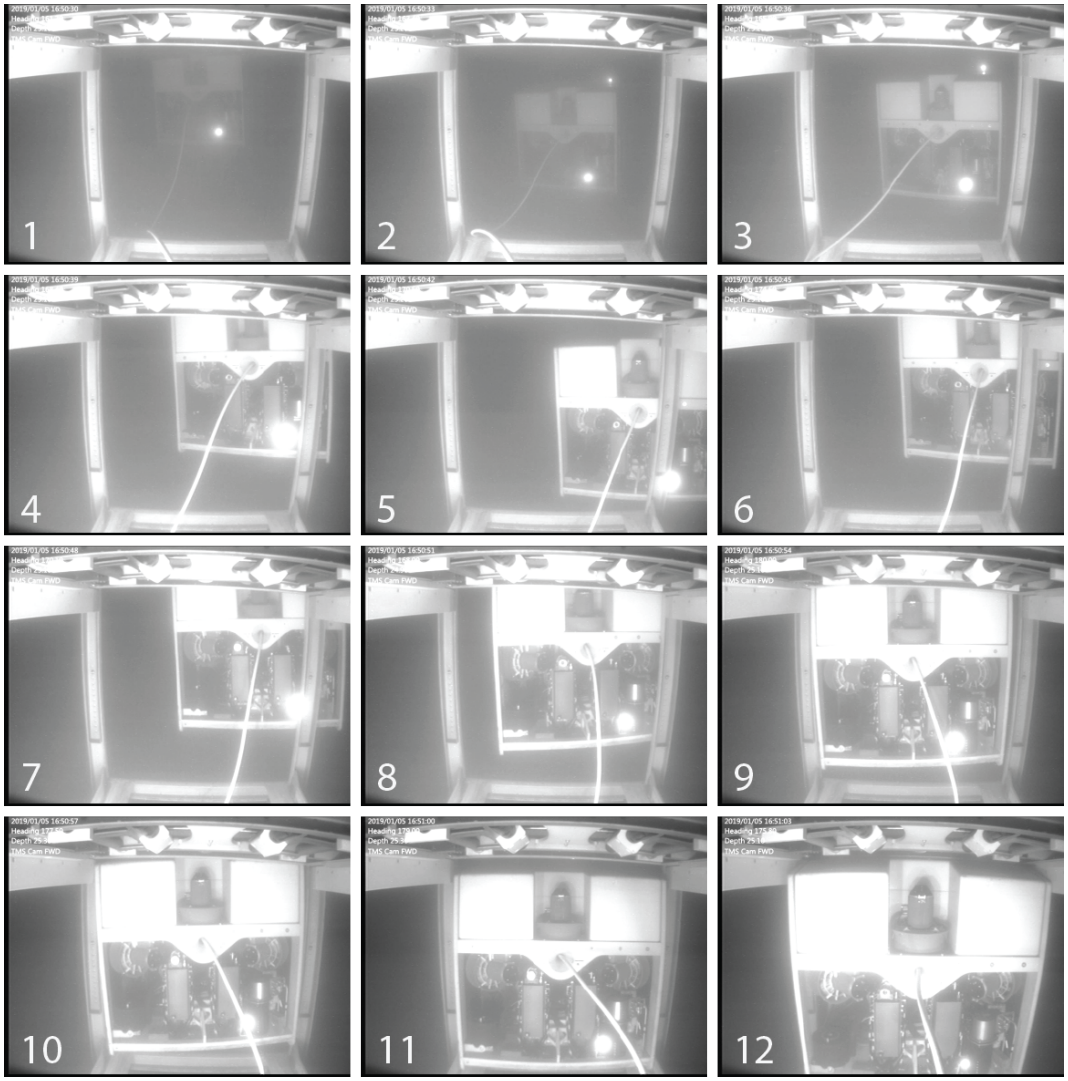

Fig. 5.8 Dynamic docking to suspended DS.

thrusters it would be possible to control the DS yaw motion and hence its heading. If the DS heading is controlled and an active heave compensation LARS system is used to compensate for heave motion, the dynamic docking practically reverts to a static docking problem.

5.4 Additional considerations and limitations

This chapter has presented a visual pose estimation for autonomous docking to a static, and to a suspended docking station. While visual pose estimation performed well during the trials in a low to medium water turbidity, with higher water turbid-

ity, the operation range of the optical sensing is reduced. In highly turbid water, where a visual pose estimation is unavailable, the acoustic pose estimation based on USBL/LBL technology should be used. Since the precision of acoustic-based positioning systems is lower than vision-based systems, the docking station entrance should be modified. The extended, funnel-shaped entrance allows for a larger position error and helps to physically guide the vehicle.

5.4.1 TMS heave motion

The major limitation of the autonomous ROV docking to the suspended docking station is the docking station heave motion. During the trials the ROV has been successfully docked multiple times with TMS heave motion up to 1.1 metres, while the ROV operated at constant depth matching the average TMS depth. However, with the increase in TMS heave motion during the docking manoeuvre the risk of damaging the ROV system inevitably rises due to increased vertical misalignment. To reduce the misalignment and to allow for faster and smoother docking the ROV should compensate for the TMS heave motion, which is the main motivation for Chapter 6.

5.4.2 Light marker occlusion

In the instance of full or partial occlusion of one or more light beacons, pose estimation is not viable. Such a situation is shown in Fig. 5.9 with the light beacons fully covered by the ROV tether and the TMS frame. Such a situation can also occur due to other factors, such as fish or the approach of curious mammals (e.g. seals, dolphins).

During the docking procedure, the ROV trajectory is always towards the entrance of the TMS, thus it always moves towards the area with better optical marker visibility. As shown in Fig. 5.10 the algorithms have been implemented to filter pose estimation errors and to protect the system in case such errors become too large.

In case of full coverage of one of the light beacons Fig. 5.9, the pose cannot be estimated, thus the last known pose is used to align and guide the ROV towards the

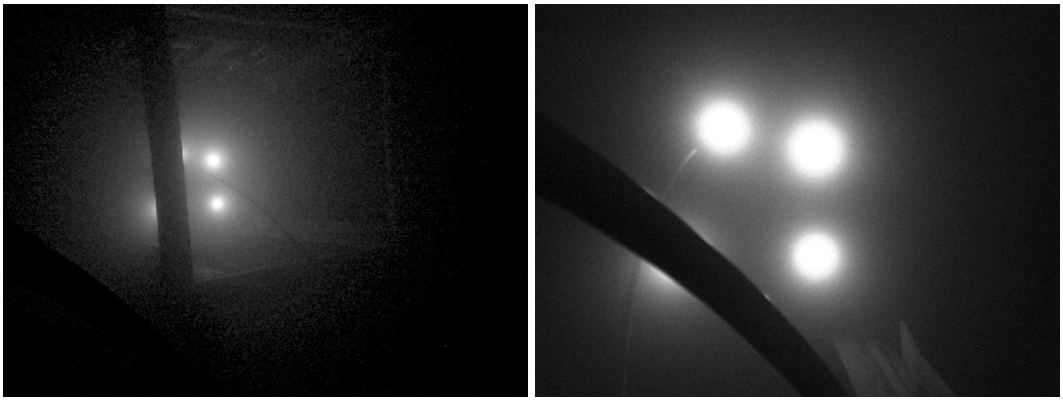

(a) (b)

Fig. 5.9 The light markers fully covered (a) by the TMS frame; (b) by the tether.

entrance of the DS. Therefore, by increasing the proximity to the DS, the probability to acquire an image with all markers rises in the next iteration. If the pose cannot be estimated after multiple iterations, the ROV docking manoeuvre is aborted. Due to the slow dynamics of the ROV and low speeds (<0.4 knots) the motion between two consecutive iteration is small, making the described algorithm suitable for this application.

Partial light beacon coverage causes significant pose error, thus every calculated position in step n is compared with the position calculated in step $n-1$. If an unrealistic change in position between two iterations is detected, the algorithm assumes inadequate pose estimation, in which case the last known position is used. An additional light search algorithm is recommended to be implemented for future operations beyond the scope and time frame of this project/thesis.

5.5 Closing remarks

Subsea navigation currently employed in residential ROVs is manual control from the support vessel or from shore-based control centres. With an existing fleet of vehicles and experienced ROV pilots as an in-field proven solution, the offshore industry is still highly dependent on manual pilot skill. However, a transition towards automation in the resident ROV field can provide significant advantages and can specifically increase operational weather windows for the marine IMR sectors.

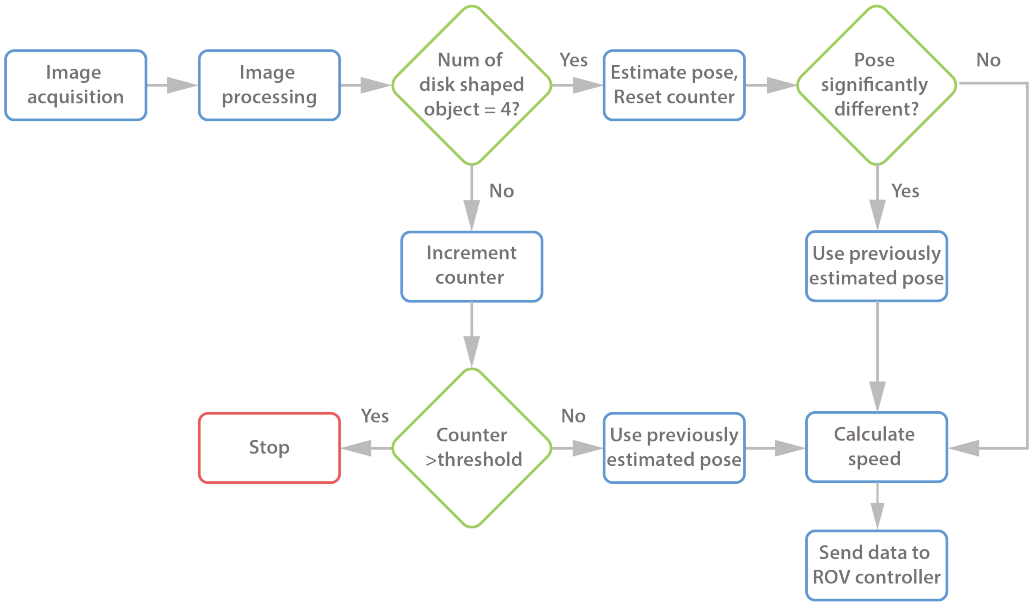

Fig. 5.10 Flowchart of safety checks.

One of the most critical operations is the docking of the ROV at the end of a mission, which was the targeted operation for automation in this thesis. The results showed that the ROV speed and position controllers, coupled with camera pose estimation, provided a strong platform for such operations. A machine vision based docking system has been developed around the subsea camera pose estimation presented in Chapter 4. The position error between docking point DP and the origin of the ROV frame is used to calculate setpoints for position and speed controllers which are fed into ROV low-level controllers (LLC). The reference system used for comparison is a commercial state of the art underwater navigation system based on the IXBLUE PHINS INS coupled with Nortek 500 DVL and Teledyne Ranger 2 USBL, and ROV and DS pose estimation results have shown to be comparable for the vision based system and INS solutions.

The full system including the ROV automated navigational control was trialled first using a static docking station and the results were within tolerances to allow multiple successful dockings. This system was further tested using a dynamic docking station suspended from surface vessel and the results achieved were sufficient to dock multiple times in heave disturbances due to wave motion of 1.1 metres. Such

suspended DS is proposed as an analogue for docking stations on floating production platforms, which have not yet been trialled or implemented within the offshore sector. To dock the vehicle successfully, the maximum peak-to-peak amplitude for the trialled ROV and DS was found must be lower than 2 metres to avoid damaging the ROV tether. The system has been tested and demonstrated in a real-world environment during January 2019 in the North Atlantic Ocean. To the author's knowledge, this is the first autonomous docking of an ROV system to a dynamic docking station and represents a significant contribution towards robustness and viability of the use of resident ROVs in offshore operations including floating platform based ROVs and docking stations.

Chapter 6

TMS position prediction based on ANFIS

6.1 Introduction

One of the major limitations of the autonomous ROV docking to a suspended TMS is the TMS heave motion, which can exceed amplitudes of 3 m. Those limits were recognised during the autonomous docking trials presented in the previous chapter. Findings acquired during those trials investigating TMS behaviour in a real-world environment and associated docking limitations, have served as the motivation for this chapter.

This chapter presents development and evaluation of the method for suspended TMS heave motion prediction, based on an adaptive neuro-fuzzy inference system (ANFIS). The prediction of TMS heave motion has the potential benefits of allowing autonomous docking in higher sea states, extending the ROV operational weather windows, and reducing the misalignment between the ROV and TMS during the docking process, thus reducing the impact on the ROV system and extending the ROV operational life. Furthermore, the method has a dual benefit of being applicable to autonomous docking or as an aiding tool for pilot flight control of the ROV.

Various authors reported use of ANFIS for modelling nonlinear functions such as: motion prediction of moving targets (de Costa Sousa and Setnes, 1999; Rajpurohit

and Pai, 2011; Sivcev et al., 2019), predicting stock market return (Boyacioglu and Avci, 2010), electricity price forecasting (Yaser and Allah, 2019), and various other publications. In addition, ANFIS performs exceptionally well when predicting chaotic time series. This is demonstrated by Jang (1993), where comparison is given between use of ANFIS, cascaded-correlation neural networks, backpropagation MLPs, autoregressive models, and others have been given. Since the position prediction of the TMS belongs to the same class of problems, the use of ANFIS has been selected for evaluation in the ROV docking to a heaving DS experiments of this thesis.

The ANFIS performance is evaluated on a real-world dataset recorded using a work-class ROV with corresponding cage type TMS, deployed during offshore trials in the North Atlantic Ocean. The hardware used for dataset acquisition has been has been presented in Section 3.3 together with the TMS motion analysis.

6.2 Adaptive neuro-fuzzy inference system - ANFIS

This section describes the implementation of the adaptive neuro-fuzzy inference system for TMS motion prediction. ANFIS is an adaptive neural network which is equivalent to a fuzzy inference system (FIS) that was first introduced by Jang (1993). With ANFIS, a set of fuzzy if-then rules is identified, with membership function parameters tuned through a hybrid learning algorithm.

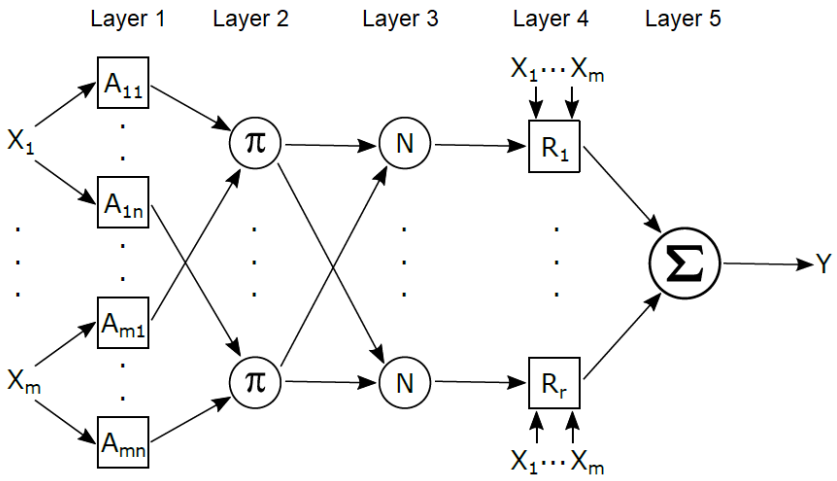

Fig. 6.1 ANFIS network framework architecture.

Fig. 6.1 shows the ANFIS network architecture that consists of five layers. Each of *m* inputs (X) is assigned with *n* fuzzy membership functions described with linguistic labels (A), constituting *r* rules (R). Each node in the first layer is adaptive and specifies the degree to which a given input satisfies the fuzzy membership function related with that node. The first layer is called the "fuzzification" layer, while parameters in this layer are called *premise parameters*. In the second layer a firing strength for each rule is determined. Every node in this layer is fixed and labelled π, while the node performs multiplication of the incoming signals. Every node in the third layer is fixed and normalizes the firing strengths of the previous layer. The fourth layer is called the "defuzzification" layer. This layer consists of adaptive nodes and it involves computing the weighted consequent values for each given rule. Parameters in this layer are called *consequent parameters*. The node in the last layer performs summation of all incoming signals.

The tuning of the network is done using an existing dataset consisting of input-output pairs, while the network tries to model the function which relates input to output. By using past values of the heave displacement z_{TMS} up to time t, ANFIS is used to predict the future value of the $z_{TMS}(t+P)$. Since z_{TMS} is measured using a depth sensor, this is achieved by mapping a dataset of known TMS depth values using D points of the time series spaced Δ apart as:

$$[z_{TMS}(t-(D-1)\Delta), ..., z_{TMS}(t-\Delta), z_{TMS}(t)], \tag{6.1}$$

to a predicted value in future $z_{TMS}(t+P)$. Therefore, for parameters $D = 3$, $\Delta = 1.5$, $P = 2$, one input-output ANFIS pair is given by:

$$[z_{TMS}(t-3), z_{TMS}(t-1.5), z_{TMS}(t)], [z_{TMS}(t+2)] \tag{6.2}$$

where $[z_{TMS}(t-3), z_{TMS}(t-1.5), z_{TMS}(t)]$ is the input which consists of the last $D = 3$ depth measurements, spaced $\Delta = 1.5$ s apart, mapped to the output $[z_{TMS}(t+2)]$, which presents predicted TMS depth value $P = 2$ s into the future.

The ANFIS training and evaluation has been carried out on a pre-recorded dataset. The data used for the ANFIS training and evaluation was recorded during the offshore trials that took place in the North Atlantic Ocean during January 2019. The TMS depth was recorded using a depth sensor attached to the TMS frame. The sensor used during the trials was a UV-SVP by Valeport. It is a conventional commercial unit that offers pressure, sound velocity and temperature measurements in one housing. Technical specification of the unit is given in Table 6.1.

Table 6.1 The Valeport UV-SVP sensor technical specifications.

	Pressure [bar]	**Temperature [deg]**	**Sound Velocity [m/s]**
Operating range	300	-5 to +35	1375 to 1900
System resolution	0.001% of range	0.001	0.001
System accuracy	$\pm$ 0.01% of range	$\pm$ 0.01	$\pm$ 0.02

For the given task, different process values are involved in constructing an efficient and reliable ANFIS network. These variables include: the size of the input-output dataset pairs (training dataset length), the number of membership functions per input MF, the number of training epochs NE, the number of training points D, how far in the future TMS position is to be predicted P, the spacing between the points Δ, the sensor sampling frequency f_s, etc.

While there are guidelines about the ANFIS training process (Jang, 1993; Karaboga and Kaya, 2019), as with other neural networks, there are still no specific

rules to estimate the optimal parameters for the network training. The parameters can vary greatly and depend on the quality of the data and the complexity of the problem, thus it relies on trial and error experiments. If such an approach is not possible, various techniques for estimating optimal ANFIS tuning parameters have been presented before in Buragohain and Mahanta (2008); Shoorehdeli et al. (2007). Although extensive trial and error experiments have been performed to investigate the effect of various network parameters, the focus of this section is to:

- Evaluate ANFIS performance for TMS position prediction,
- Analyse the network training time, and consider real-time ANFIS training,
- Investigate the influence of the depth sensor sample rate on ANFIS performance.

Therefore, in the next section an overview of the best network configuration is given at the start, followed by an ANFIS overall performance evaluation.

6.3 Results

The scope of this section is to investigate and evaluate the usage of an ANFIS network for the prediction of TMS heave motion. Prior to the evaluation, an optimal network configuration and training parameters should be explored. The optimal ANFIS for the given problem achieves minimum error $RMSE$ with a minimum network training duration. The $RMSE$ is a root mean square error between the predicted future TMS depth value and the measured value at that time, and it is considered as one of network performance measures. As explained in Section 3.3, the TMS heave motion depends on the LARS type and the deployment vessel type. Once the network is trained, the performance is reduced if LARS, TMS and deployment vessel combination is changed. Since the goal is to enable the possibility to retrofit the solution to the existing ROV fleet, network training on-site is necessary to accommodate individual ROVs. In addition, constantly changing sea conditions should be considered. Although the trained network can perform well for a certain

amount of time after training, a change in sea condition influences the network performance, thus an online ANFIS training is considered and tested.

6.3.1 Optimal ANFIS configuration for TMS heave prediction

To find the optimal ANFIS training parameters experiments included varying the following parameters:

- The dataset length in the range 50 s to 600 s,
- The number of the membership functions MF per input in the range 2 to 5,
- The number of previous measurements D in the range 1 to 12,
- The spacing between previous measurements Δ in the range 0.5 s to 5 s,
- The number of training epochs NE in the range 1 to 250.
- The prediction time P in the range 0.5 s to 5 s.

The effect of each parameter on ANFIS performance and training duration is shown in Table 6.2. In general, the input selection criteria are based on Jang (1996), which is based on the assumption that the ANFIS network with the smallest RMSE after one epoch of training has a better potential to achieve a lower RMSE given more training epochs.

Table 6.2 The relationship between different parameters, ANFIS training duration and performance.

Parameter		**Training duration**	$RMSE_{CHK}$	$RMSE_{TRN}$	**Generates overfitting**
Dataset length	$\uparrow$	$\uparrow$	$\downarrow$	$\downarrow$	No
Number of MF	$\uparrow$	$\uparrow$	$\downarrow$	$\downarrow$	Yes
Number of D	$\uparrow$	$\uparrow$	$\downarrow$	$\downarrow$	Yes
Prediction time P	$\uparrow$	-	$\uparrow$	-	No
Number of Epochs	$\uparrow$	$\uparrow$	$\downarrow$	$\downarrow$	Yes

The relationship between the number of training points D and the number of epochs, and the $RMSE$ and the duration of the training process, is shown in Table 6.3. The data in the table is divided in two major columns by the number of epochs

used for training. The left column provides results after only one epoch of training, while the right column shows the RMS errors and training duration at the epoch with the minimum $RMSE_{CHK}$. As shown in the table both, training $RMSE_{TRN}$ and checking $RMSE_{CHK}$ error are decreasing until D = 4. For D = 5, the training error keeps decreasing, while the checking error grows. In addition, the difference between the two grows significantly at D = 5, which is the sign of network overfitting and this must be avoided. Although in general the network performed better after more than 1 epochs, the difference in the $RMSE_{CHK}$ is not significant. For example, at D = 4, after one epoch the checking error is $RMSE_{CHK} = 0.0422624$ m, while the minimum error is achieved at epoch 63 with $RMSE_{CHK} = 0.0421802$ m. The difference between the two is negligible, while the duration of the training extended ten times from 0.053 s to 0.53 s. The number of membership functions is $MF = 2$ since the increase in MF leads to exponential growth of fuzzy rules, thus the training time grows exponentially. In addition, no reduction in $RMSE_{CHK}$ has been achieved.

Table 6.3 The relationship between training points D, the number of training epochs, the $RMSE$, and the duration of the training process.

D	**Epoch 1**			**Epoch with minimal check error**			
	$RMSE_{TRN}[m]$	$RMSE_{CHK}[m]$	$Duration[s]$	$Epoch$	$RMSE_{TRN}[m]$	$RMSE_{TRN}[m]$	$Duration[s]$
2	0.103221	0.0864964	0.03305	1	0.103221	0.0864964	0.03305
3	0.0613137	0.0577967	0.050134	189	0.0569494	0.0560394	0.370561
4	**0.0374812**	**0.0422624**	**0.052966**	63	0.0337162	0.0421802	0.526817
5	0.0296526	0.0973706	0.102934	42	0.0276815	0.0861169	1.863842

From extensive experiments, the optimal ANFIS input parameters for the given task are found as: $D = 4$, $\Delta = 1$, $NE = 1$, $MF = 2$ per input. Therefore, the best network performance is achieved by using the last four consecutive measurements ($D = 4$), spaced one second apart ($\Delta = 1$), using only one training epoch, with two membership functions per input $MF = 2$. The same network configuration performed best for various values of prediction time P.

The amount of data used for online training should be taken into consideration as well since a larger training dataset increases the ANFIS training duration. The effect of the training dataset length on the ANFIS training cycle duration, the training

$RMSE_{TRN}$, and the checking $RMSE_{CHK}$ error is shown in Fig. 6.2. Multiple experiments have been conducted with the training dataset increased from 50 s to 600 s. As shown in Fig. 6.2 (a), for 50 s of the training data, the $RMSE_{TRN}$ is relatively low while the $RMSE_{CHK}$ is high, which is a sign of the network overfitting the training data, and this should be avoided. The overfitting is caused by a small amount of training datapoints compared to the number of ANFIS modifiable parameters. For up to 200 s of training dataset, most of the $RMSE_{CHK}$ is reduced. After that point, the training duration grows with little improvement in the $RMSE_{CHK}$ as shown in Fig. 6.2 (b).

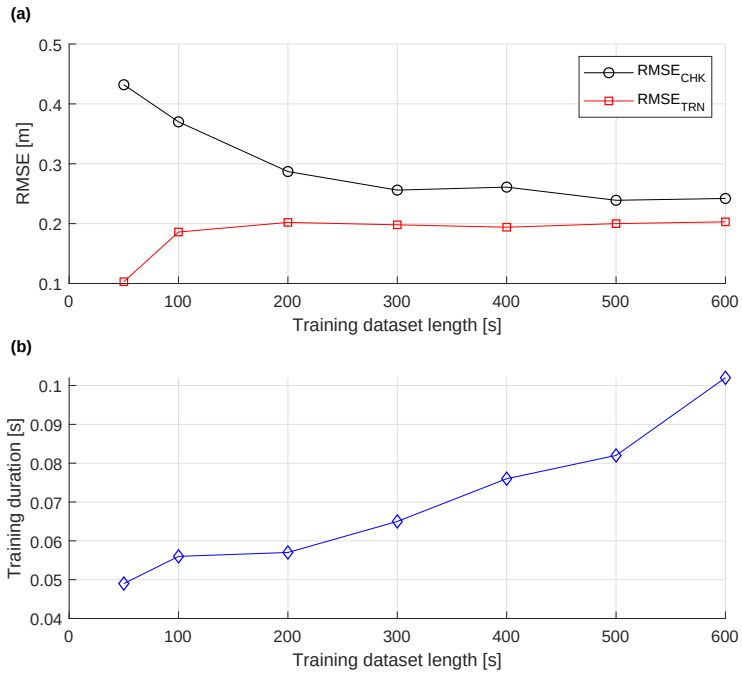

Fig. 6.2 The relationship between the length of the training dataset: and the checking error $RMSE_{CHK}$ and training error $RMSE_{TRN}$ (a); and training duration (b).

6.3.2 ANFIS based TMS heave prediction

After network parameters (D, Δ, EN, MF, dataset length) were evaluated as in subsection 6.3.1 above, multiple tests have been performed to evaluate the ANFIS performance for the TMS heave prediction. Prior to the ANFIS performance test, it is necessary to establish the evaluation criteria. While hard contact between

the ROV and the TMS is expected during the docking in a harsh environment, the main objective is to reduce rough contact to a minimum. This is achieved by reducing the misalignment between the ROV and the TMS at the moment of contact during docking. In general, the TMS and the ROV are designed in such a way as to allow a certain amount of misalignment for easier docking. However, this should be minimised to reduce the risk of ROV damage, which leads to increased operational expenditure (OPEX) costs. The amount of allowed misalignment is determined experimentally. As reported in Chapter 5.3.2, the work-class ROV was autonomously docked multiple times with the TMS peak-to-peak heave amplitude of 1.1 m, while the ROV operated at mean TMS depth. Therefore, the particular ROV-TMS configuration shown in Fig. 3.3., and Fig. 3.6. tolerates vertical misalignment of ± 0.55 metres. Thus, the ANFIS is considered as performing well when the difference between predicted and measured value is:

$$err_{TMS} = |z_{TMS}p(t+P) - z_{TMS}m(t+P)| \leq 0.55 \text{ m}, \tag{6.3}$$

where $z_{TMS}p(t+P)$ is the predicted TMS depth, and $z_{TMS}m(t+P)$ is the measured TMS depth at the same time. However, sometimes during manual docking the TMS heaves more than the pilot predicts, thus the misalignment between the TMS and the ROV is larger than $err_{TMS} > 0.55$ m, and the manoeuvre has to be aborted. Therefore, as an additional ANFIS performance indicator a mean absolute error (MAE) is calculated as:

$$MAE = \frac{\sum_{i+1}^{N} a_i}{N}, \tag{6.4}$$

for $a_i = 1$ if $err_{TMS_i} \leq 0.55$ m, and $a_i = 0$ for $err_{TMS_i} > 0.55$ m, which essentially shows the percentage of time the error between the predicted and the measured TMS depth was $err_{TMS} \leq 0.55$ m. Due to the equipment involved in offshore operations being particularly expensive, the network is considered performing well when $MAE \geq 95\%$.

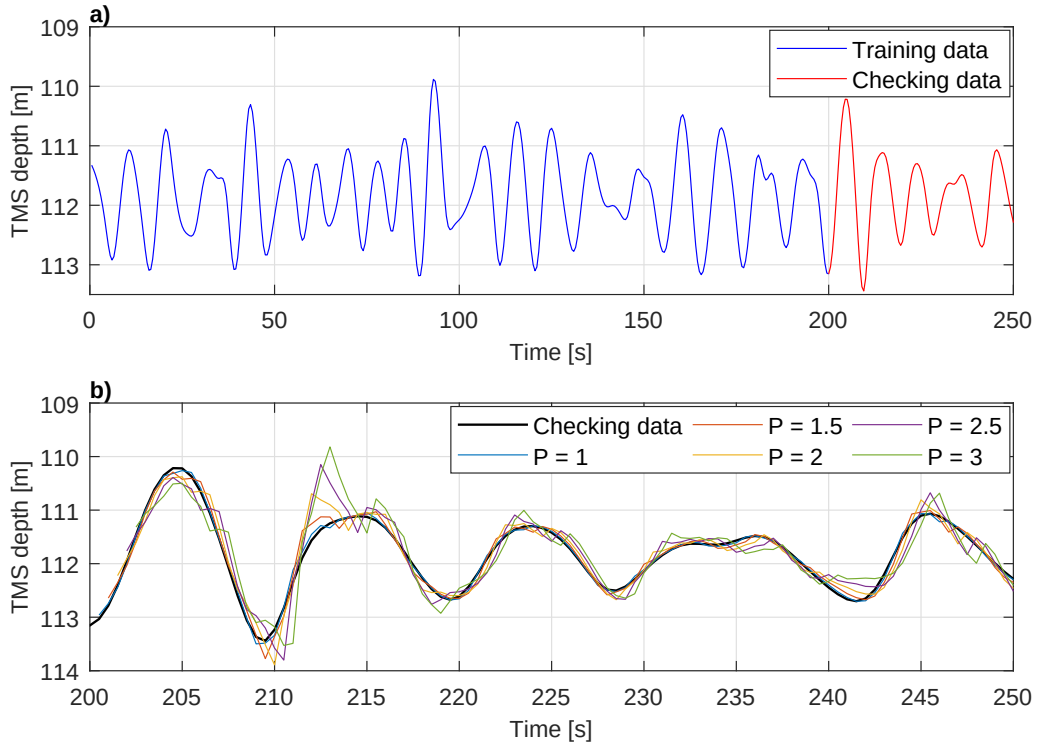

Fig. 6.3 Dataset used for ANFIS evaluation. a) the first 200 s of data is used for training, while 50 s of data is used for checking; b) the performance of the ANFIS prediction of the TMS depth between 1 s and 3 s into the future compared to the checking data.

The depth measurements of the cage type TMS suspended from the ship RV Celtic Explorer during the trials in the North Atlantic Ocean are shown in Fig. 6.3 a). The TMS depth recorded over 150 s period, ranges between 110 m and 113 m with the mean depth of approximately 112 m. The depth sensor sampling frequency was $f_s = 2$ Hz. While working with neural networks, it is common to use a fraction of the recorded data for the training, while the remaining fraction of the data is used for the network validation. The ANFIS training stage included the first 200 s of the data, while the next 50 s of data is used for the checking stage. The experimentally determined optimal ANFIS parameters are: $D = 4$, $\Delta = 1$ s, $NE = 1$, $MF = 2$ per input. Figure 6.3 b). above shows only checking data of the same dataset (the last 50 s) compared to the predicted TMS depth values. The TMS position prediction 1 s into the future $z_{TMS}(t+1)$ (continuous blue line) has the smallest deviation from

the measured value, while the difference between the checking data and the data predicted 3 s ahead is significant.

Table 6.4. and Fig. 6.4 show the ANFIS performance for TMS depth prediction up to $P = 3$ s into the future. ANFIS performs exceptionally well for predicting $z_{TMS}(t+1)$, with two standard deviations of the error only $2\sigma = 0.10$ m. For $P = 1.5$ s, 2σ reached the value of 0.23 m, and it continues to grow until it reaches the value $2\sigma = 0.55$ m for $P = 2.5$ s, with $MAE = 95.05\%$. By increasing the prediction time further to P = 3 s, the error grows further, and the criteria $MAE \geq 95\%$, is not satisfied. Therefore, the results of the experiment showed that ANFIS could be successfully used for the TMS heave position prediction z_{TMS} up to 2.5 s into the future for the particular TMS - ROV setup of the experiments while keeping the prediction error below 0.55 m for 95% of the time.

Table 6.4 ANFIS performance for predicting TMS depth up to $P = 3$s into the future.

P [s]	**MAE** [%]	$\boldsymbol{RMSE_{CHK}}$ [m]	$\boldsymbol{RMSE_{TRN}}$ [m]	$\boldsymbol{2\sigma}$ [m]
1	100	0.050	0.038	0.101
1.5	99.01	0.112	0.083	0.225
2	97.03	0.192	0.142	0.384
2.5	95.05	0.273	0.202	0.546
3	93.07	0.340	0.250	0.680

6.3.3 Online ANFIS training

The performance of the ANFIS network is further investigated to incorporate on-line training. As mentioned previously, the sea conditions continuously change, thus the performance of the network trained on one set of the data degrades with changes in TMS heave frequency and/or amplitude. Fig. 6.5. a) shows the TMS depth recorded over a 900 s period using the depth sensor sampling frequency $f_s = 2$ Hz. Three ANFIS networks, composing of the same structure ($D = 4$, $MF = 2$, $\Delta = 1$), are trained to predict the TMS depth 2.5 s in future ($P = 2.5$).

The first ANFIS network is trained using only the first 100 s of the data, which means that the prediction model of the TMS behaviour has been built based only

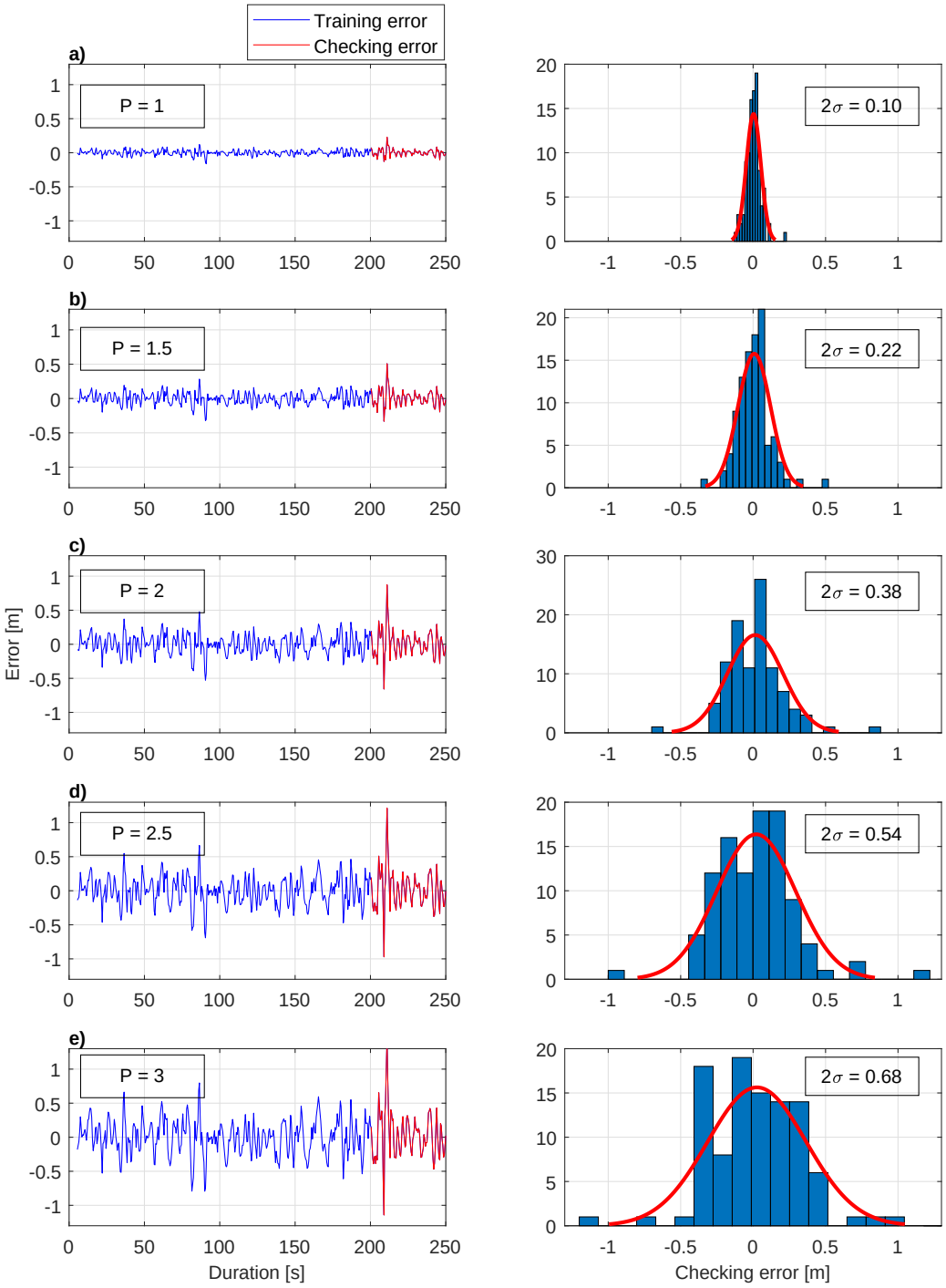

Fig. 6.4 The error between predicted and real TMS depth with corresponding checking error distributions. a) The TMS depth prediction 1 s into the future; b) The TMS depth prediction 1.5 s into the future; c) The TMS depth prediction 2 s into the future; d)The TMS depth prediction 2.5 s into the future; e) The TMS depth prediction 3 s into the future.

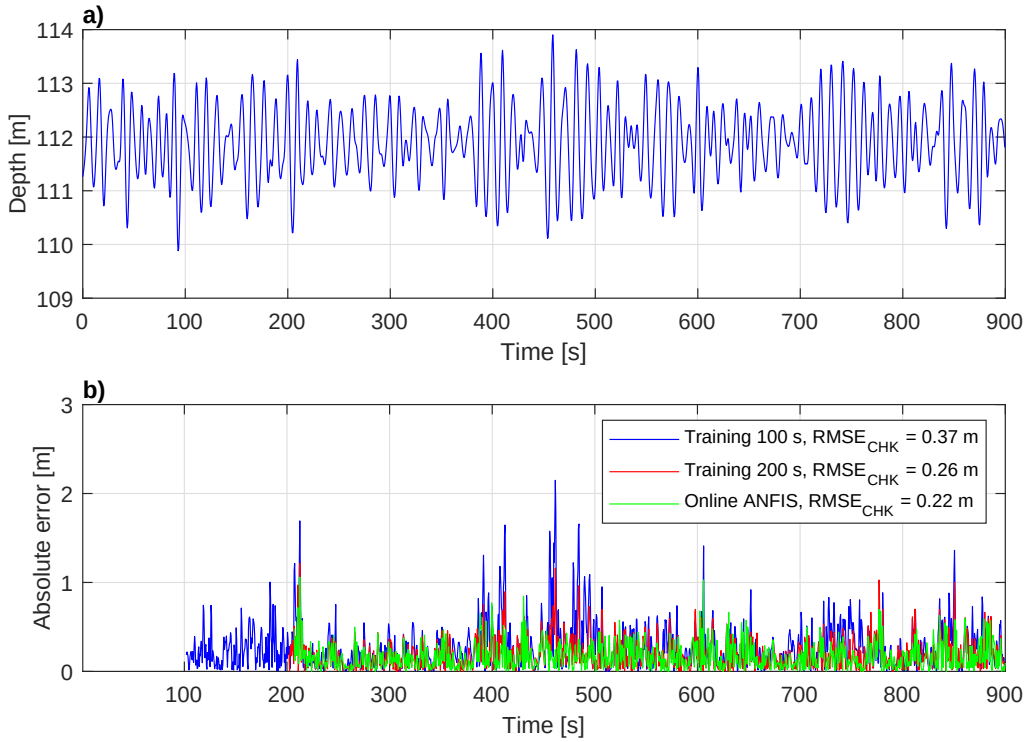

Fig. 6.5 Online trained ANFIS performance. a) The TMS depth dataset used for ANFIS training and evaluation; b)Comparison between ANFIS trained on first 100 s of data (blue), trained on first 200 s of data (red), and trained online using last 200 s of data before each prediction step (green).

on those measurements. Similar to other neural networks, once a new input data is out of the range the neural network has been trained for, big errors occur. Therefore, as shown in Fig. 6.5. b), at time 200 s, between 380 s - 420 s, and between 450 s - 500 s there is a significant error (blue line). For comparison, the second ANFIS network (red line) has been trained using the first 200 s of the data, therefore it is more "experienced", and has been able to predict the TMS behaviour better than the first one. However, a sudden change in TMS depth amplitude between 380 s - 420 s, and between 450 s - 500 s, still caused high prediction errors. To compensate for this, the ANFIS network should be trained considering the latest available data. With the online ANFIS (green line), the prediction model of the TMS behaviour has been recalculated and updated after each TMS depth measurement, using the latest 200 s of the data. For example, at the time 380 s the online ANFIS gives approximately the same error as the second ANFIS, however, at the time 420 s the prediction error

has been significantly reduced. Therefore, at time 450 s based on the last 200 s of "experience", which also includes the depth measurements between 380 s - 420 s, the ANFIS already "expects" sudden changes in the TMS depth, thus between 450 s-500 s the prediction error is reduced. In summary, with the online ANFIS training approach the network is trained continuously, while taking into account the latest acquired data from the TMS depth sensor. As the figure shows, the online ANFIS training further improved TMS depth prediction. While overall $RMSE_{CHK}$ is reduced (only 0.04 m), the error spikes are significantly reduced.

6.3.4 Depth sensor sample rate

In the previous subsection, the optimum training dataset duration is experimentally identified to be 200 s. However, the amount of data points recorded during the 200 s time period depends on the depth sensor sampling frequency f_s. Ideally, the sampling frequency of the sensor should be high enough to accurately capture relevant frequency spectra, but not so high as to cause long ANFIS training times.

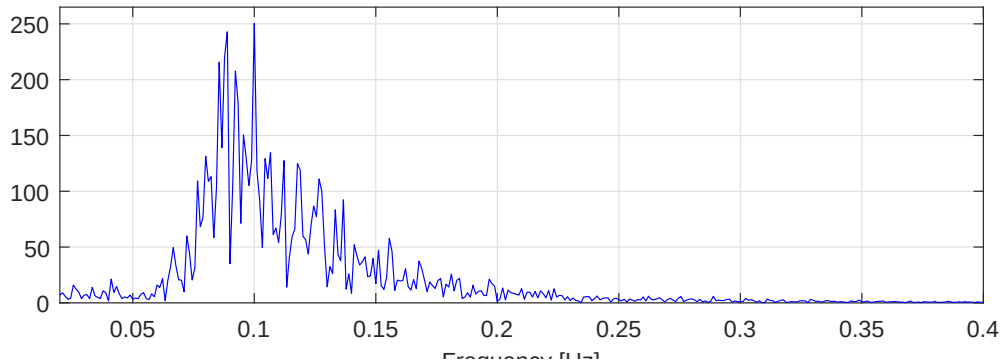

Fig. 6.6 The TMS heave frequency spectrum.

Fig. 6.6. shows a frequency spectrum of the dataset previously illustrated in Fig. 6.5 a). The frequency range of the TMS heave motion is between $f_{TMS} = 0.05$ Hz $-$ 0.25 Hz, with the most prominent frequencies between $f_{TMS} = 0.08$ Hz $- 0.1$ Hz. Therefore, the minimum sensor sampling frequency to cover the full TMS heave frequency spectrum, is by Shannon - Nyquist theorem $f_s min = f_{TMS} max * 2 = 0.5$ Hz . This was further inspected. Table 6.5. shows the relation between ANFIS performance and different sensor sampling frequencies. In each case the network

Table 6.5 The relationship between depth sensor sampling frequency and ANFIS performance.

Sampling frequency f_s [Hz]	**Number of datapoints** in 200 s	**Training duration** [s]	$\boldsymbol{RMSE_{TRN}}$ [m]	$\boldsymbol{RMSE_{CHK}}$ [m]
0.25	50	0.032	0.007	2.397
0.5	100	0.035	0.152	0.543
1	200	0.041	0.179	0.280
2	400	0.060	0.142	0.176
4	800	0.079	0.141	0.179
8	1600	0.144	0.158	0.156
16	3200	0.322	0.158	0.157

was trained with 200 s of data and evaluated on the remaining fraction using the same parameters as follows: $D = 4$, $\Delta = 1$, $NE = 1$, $MF = 2$, and $P = 2$.

With the sensor sampling frequency lower than f_smin, the actual TMS depth change is not recorded accurately. In addition, the low number of datapoints leads to overfitting, with $RMSE_{CHK}$ over 2 m at $f_s = 0.25$ Hz. With the increase of the sampling frequency to $f_s = f_smin = 0.5$ Hz, the number of datapoints doubled, and overfitting is avoided. By doubling f_s to 1 Hz, $RMSE_{CHK}$ is further reduced to 0.25 m, which is a big improvement over the previous case. The sensor sampling frequency $f_s = 2$ Hz provided best results with $RMSE_{CHK} = 0.179$ m, while the ANFIS training time cost is only 0.057 s and compared to the prediction time of 2.5 s this is negligible. Further increase in sensor sampling frequency leads to an increase in the ANFIS training duration, while the contribution to prediction performance is minimal.

6.4 Closing remarks

The docking of underpowered work-class ROVs to a heaving TMS relies entirely on the ROV pilot experience in estimating TMS heave motion, which is not available for autonomous and resident underwater vehicles. With large ROV inertia and drag forces acting against it, the ROV is not agile enough to match TMS heave motion, thus the docking manoeuvre starts before the ROV and the TMS align. The method presented in this chapter is used to extend the ROV operational weather windows,

reduce operational expenses, and reduce ROV damage due to the harsh conditions docking. The trained ANFIS network showed excellent performance when predicting the TMS depth up to 2.5 seconds into the future with the RMSE = 0.22 m, and with 97% of errors below the maximum allowed vertical misalignment between the ROV and the TMS, i.e. $err_{TMS_i} \leq 0.55m$. Further modification of the TMS entrance with a funnel-shaped receptacle would allow for larger misalignment, thus, extending the operational docking window.

The developed method presents an addition to the suite of technologies required for dynamic autonomous work-class ROV docking and is beyond the current state of the art in work-class ROV technology. In addition, the method has the potential for retrofitting to the existing ROV fleet, to be used as a ROV pilot aiding tool, and it does not require additional hardware.

Chapter 7

Vision based localization system suited to resident UUVs

7.1 Introduction

Traditionally, underwater navigation systems are solely based on or encompass acoustic systems, providing an absolute world coordinate frame position solution with technologies such as Long baseline (LBL) or Ultra-short baseline (USBL) systems (Paull et al., 2014). However, acoustic systems suffer from a number of disadvantages such as loss of accuracy in acoustic noise-polluted environments, due to poor calibration of the units, high system complexity/maintenance, and high error rates. This is far from an ideal solution for resident subsea field robotic systems where noise, maintenance and accuracy are key issues that need to be addressed in achieving cost effective IMR services.

Much research has been completed in the field of navigation sensor fusion (Majumder et al., 2001; Nicosevici et al., 2004), with modern commercial navigation systems exploiting a number of fused sensor types. A common practice in AUV navigation is to use onboard inertial navigation systems, coupled with a Doppler velocity log, and additional sensors such as depth sensor and sound velocity probe, ultimately providing a dead-reckoned relative based position solution. However, the concerning issue in this solution is drift over time which in a commercial state-of-

the-art system is 0.1% of distance travelled (iXblue, 2019; Sonardyne, 2019). This is not an acceptable error rate for subsea operations requiring close-quarter inspection, maintenance and repair activities. A solution that is widely used within bathymetric survey is the dual use of LBL/USBL acoustic positioning with INS. This eliminates a position drift and provides a greater level of accuracy in the solution. However, an acoustic system for elimination of the drift, does not address other issues in underwater resident robotics including noise-polluted environments and high system complexity / maintenance. Vision based navigation have also been recorded in the literature for use in underwater cable tracking (Balasuriya et al., 1997; Ortiz et al., 2002), localization in structured environment (Carreras et al., 2003), and various automation of intervention tasks (Cieslak et al., 2015; Sivčev et al., 2018). The field of underwater simultaneous localisation and mapping (SLAM) is very active (Hidalgo and Bräunl, 2015) and has allowed for vision and sonar-based navigation in unstructured environment (Ribas et al., 2010). However, the main concern is that most vision-based techniques require low water turbidity and a relatively close proximity to the target (Guth et al., 2014; Köser and Frese, 2020).

The fact that resident vehicles will operate in partially structured environments consisting of known subsea structures (docking stations, subsea interconnection stations, oil wells, etc.), these structures can be utilised and can offer a means of facilitating a low cost, low maintenance, navigational marker that can eliminate drift in INS estimated pose solution when a vehicle is close to an IMR target.

This chapter discusses the use of an LED based subsea location marker at known structure position and orientation for vehicle position update. The accurate visual pose estimation relies on a method discussed in Chapter 4.4.1. The localisation aid provides pose estimation based on active light marker beacons for intermittent resident ROV position update and intermittent drift elimination close to target, where accuracy is required. System performance and propagation of position error is inspected and estimated, and the effect of intermittent visual based position update is discussed in this chapter. The system is evaluated using experimental data acquired during the offshore trials in the Atlantic Ocean.

7.2 Propagation of errors in pure inertial mode

Since the proposed system is built around the commercial INS unit (IXBLUE PHINS), for which detail on the implementd INS Kalman filter, detail on the external sensor error models, and the raw IMU data are all unknown. Therefore, the system is treated as a "black-box". However, the position error propagation function of the system operating in the pure inertial mode can be modelled. This function is then used to simulate possible position trajectories in case of acquired vision-based position fix. Overview of the inertial navigation system PHINS 6000 used during the trials and its operating modes is given in Chapter 3.2.3.

Position estimation accuracy in the pure inertial mode depends on two factors: (1) the accuracy of the IMU acquired measurements, therefore the accuracy of the accelerometers and FOGs, and (2) an initial position, velocity, and attitude errors obtained after the alignment/position fix. Considering the IMU data is integrated over time, the position error contained within the INS covariance error matrix propagates with time as well. Therefore, assuming the same initial position, velocity, and attitude errors, in the pure inertial mode, the propagation of the position error is only a function of time. In practice, the initial position error varies mostly due to the quality of the position fix. During the few days of the ROV operations, the position error of PHINS system operating in INS + DVL + USBL mode was between 0.23 m and 0.57 m. Some of the factors that may influence the quality of the USBL position fix are the strength of the USBL signal, multipath errors, a partial USBL responder occlusion, subsea noise pollution, sound velocity profile, and distance between transponder and receiver.

The propagation of position error in the pure inertial mode was further studied. Figure 7.1. shows the propagation of the measured position error during three tests of various durations. The experiment was performed in the North Atlantic Ocean off the coast of Ireland. Each test started with PHINS operated in the INS + DVL + USBL mode. As shown in the magnified section, the initial position error was between 0.25 m and 0.33 m, depending on the test. After the initial position fix was acquired, the INS was set to operate in the pure inertial mode.

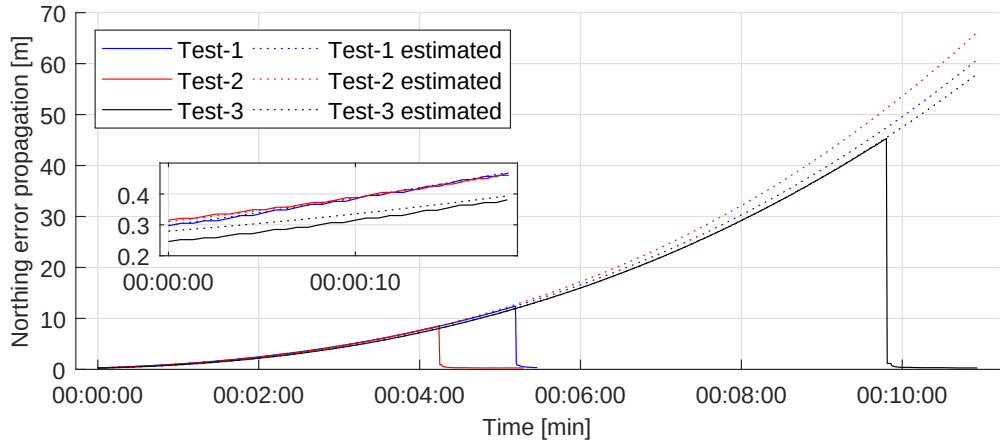

Fig. 7.1 The PHINS INS northing position error propagation in pure inertial mode.

The continuous line shows recorded position error propagation over time. During the tests, the ROV was manually piloted while performing a general visual inspection of the seabed. At the end of the test, PHINS was switched back to operate in INS + USBL mode. This reduced the position error to the initial values. Although the ROV paths during the tests were different, the propagation of the error behaves in nearly equal ways. As shown in the figure, the northing position error is approximately 2 m after 2 minutes, 12 metres after 5 minutes, and 40 metres after 9 minutes. Since PHINS is a commercial system, the error propagation model is not known, thus it was necessary to measure error propagation and model the error propagation function. The dashed lines in Fig. 7.1 present corresponding 3^{rd} order error propagation functions calculated using least-squares polynomial curve fitting. In case a vision based position fix is acquired at any time throughout the experiment, this function is to be used for the prediction of the position and position error estimates, assuming PHINS continues to operate in the pure inertial mode.

In the next section the performance of the vision-based pose estimation system used during the trials is compared with the USBL data. If comparable, the visually estimated pose data could be used for PHINS position update. Additionally, the estimated position error can be reduced using intermittent position fixes.

7.3 Results

The experiment simulates a hypothetical scenario of the autonomous vehicle completing a dock at docking station within a resident field. The initial conditions are as follows:

- The vehicle has no USBL onboard and is travelling at cruising speed with navigation system based solely on INS
- During the trial, the vehicle DVL system is disabled in order to effect a faster integration drift in INS system over time than just 10 minutes operation with DVL
- The vehicle operates in a structured environment
- Approximately halfway to the docking station there is a known landmark which can be recognized with the onboard vision system, and the position and orientation of the landmark is known in the world frame

The experiment starts at time T0 with the ROV docked and the navigational system running in USBL + INS mode. The INS position standard deviation is low. After the position STD reached a minimum value of 0.26 m, the PHINS was switched to operate in pure inertial mode, which simulates the USBL signal loss. The ROV was then piloted for approximately 10 minutes in the area around the TMS. Since the propagation of position error in pure inertial mode does not depend on travelled distance or speed, to reduce the risk of damaging the vehicle, the ROV was piloted in relatively close proximity to the deployed TMS. Fig. 7.2 shows relative northing and easting between the ROV and the light marker during the experiment.

The black dashed line shows PHINS estimated position throughout the experiment while the grey shaded area presents the corresponding position standard deviation (an output of the INS). During the experiment, the ROV position was simultaneously measured with the USBL system which was not set as aiding the INS but running independently. The blue continuous line shows the ground truth, USBL measured ROV position with corresponding position standard deviation. To

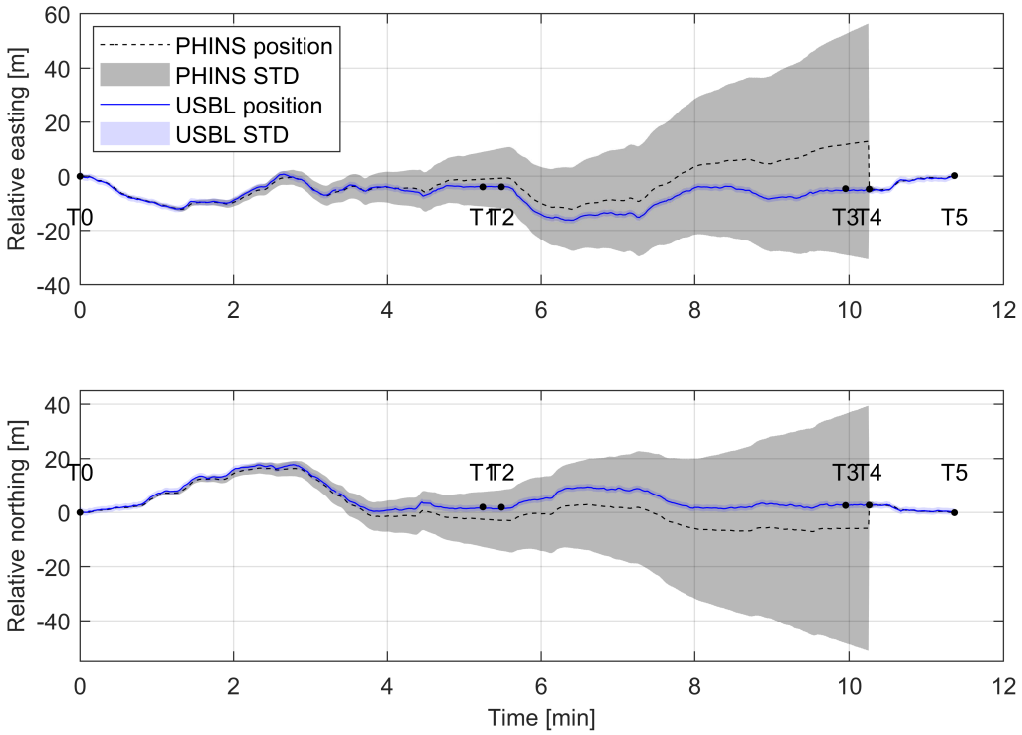

Fig. 7.2 Relative ROV position throughout the experiment simulating resident field hypothetical scenario. Blue continuous line presents the ROV ground truth USBL position. The PHINS estimated position, while operating in pure inertial mode is shown with black dashed line. At time T4, PHINS was switched to operate in INS + USBL mode, and the ROV was docked at T5.

avoid possible noisy measurements and achieve highest precision, the supporting vessel with the USBL transponder was positioned in direct ROV line of sight at all times. Due to the exponential nature of the position error propagation, the position error propagates slowly at the beginning. As shown in the figure, at time T1 after approximately 5 minutes, the PHINS position standard deviation is around 10 metres, reaching over 40 metres after 10 minutes at T4. At time T4 the PHINS system was switched to operate in INS + USBL mode, thus the position error standard deviation (gray shaded area) dropped to an initial value, and the ROV position was corrected. The ROV was then docked at T5, and the experiment finished.

Throughout the experiment the position of the ROV was visually estimated two times. Between time T1-T2, which presents ROV passing by known landmark, and between T3-T5, upon reaching the docking station. The magnified section of

Fig. 7.2 between time T3-T5 is shown in Fig. 7.3 and it shows the comparison between, PHINS data, USBL data, and visually estimated pose data. The figure shows that the visually estimated pose (red continuous line) is comparable with the USBL data (blue continuous line). Therefore, as alternative to USBL and while PHINS operates in pure inertial mode, the visual pose estimation data could be used as the intermittent INS position update to reduce the position error and to allow for transition of the subsea vehicle towards another known landmark or towards close quarter inspection/intervention.

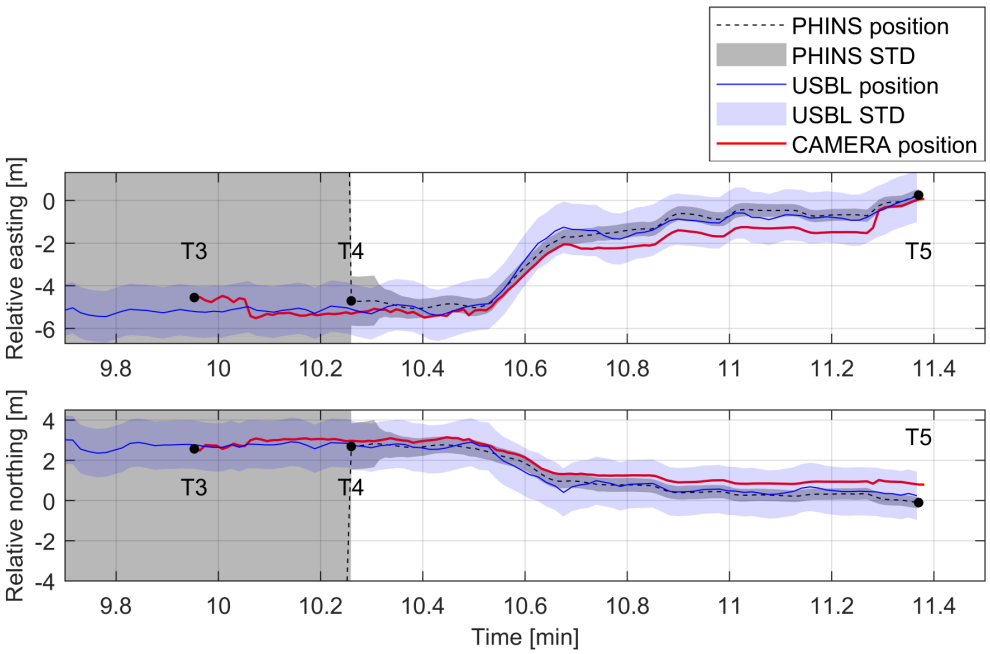

Fig. 7.3 The comparison between PHINS data, USBL data, and visually estimated pose acquired during the trials.

The influence of intermittent, vision-based position update on position error estimation was further investigated. Since PHINS 6000 does not provide a designated input for a visually acquired position update, the visually estimated ROV position between T1-T2 and T3-T5 could not be fed into the system Kalman filter. However, the known initial position, and the error propagation function modelled in Section 7.2, allows for estimates of a family of possible position trajectories and corresponding position errors to be developed.

Fig. 7.4 shows a family of possible position estimation trajectories between time T2 and T4 (continuous red lines) in the case where the ROV position was updated between T1-T2 and the ROV continued to operate from then in pure inertial mode until T4. A specific position trajectory could not be simulated since PHINS 6000 exact mathematical model of the EKF, sensor error models, and the raw IMU sensor data are not available. A red shaded area presents the estimated position STD between T2 and T4, in the case of position update at T2, for the trajectory which aligns with the USBL line (ground truth data).

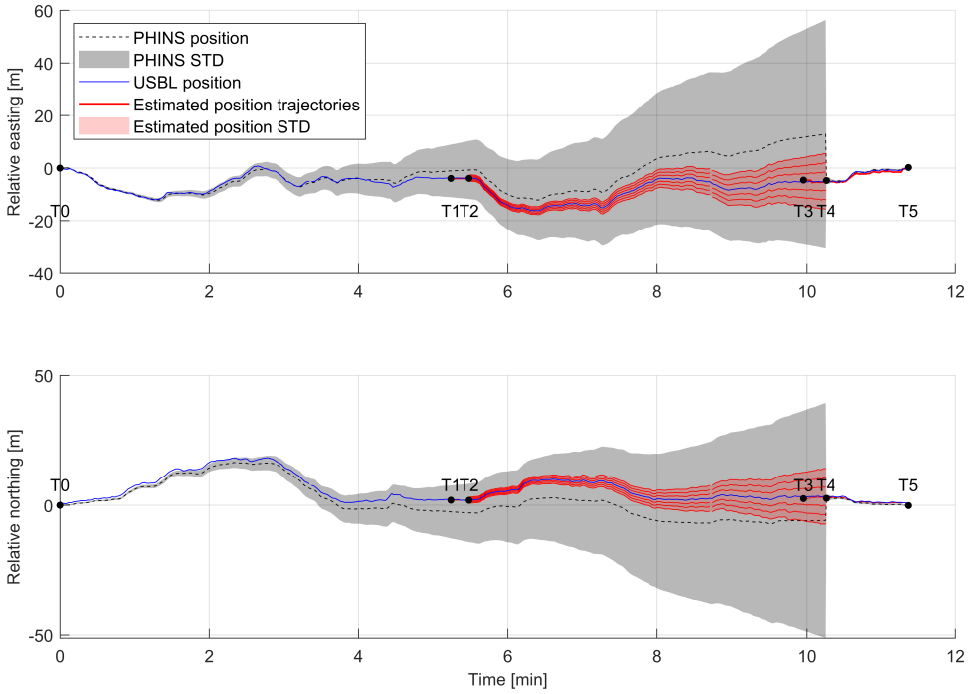

Fig. 7.4 Family of position estimation trajectories (red continuous lines) from time T2 to T4 in the case of ROV position visual update between time T1 and T2.

7.4 Additional considerations and limitations

Position error estimates provided by PHINS are based on the INS accelerometers and gyroscopes theoretical models in pure inertial mode and on models of other aiding sensors when used in aiding, thus the models are not accurate physical

measurements. Although the relative difference of the initial position error was small across three tests initially, the difference grows exponentially after longer periods of time, as shown in Fig. 7.1. For that reason, the derived error propagation function is considered to describe the behaviour of the system's error propagation correctly for up to 6 minutes.

7.5 Closing remarks

This chapter shows experimental results of a developed vision-based localization system discussed in Chapter 4, with potential to be utilised to eliminate drift error from on-vehicle inertial navigation system position estimation. The proposed system is developed around the standard equipment found throughout the ROV sector. While INS operates without USBL/LBL, the visually estimated pose could be used as a position fix, thus reducing the position error uncertainty presented to the pilot.

The system has been tested in the North Atlantic Ocean during trials in January 2019. The propagation of position error of PHINS system operating in pure inertial mode is measured and modelled as a function of time and initially estimated position error. This function is used to simulate family of possible position trajectories in the case that a reliable/known vision-based position fix is acquired during the test. The visually-based pose estimation method with IMU relative angle correction discussed in Chapter 4.4.1, was used to determine the relative pose between the ROV and deployed subsea asset. The results showed that the proposed system performed well and can improve the ROV/AUV localization underwater as presented to the pilot. In automated navigation systems such improved position knowledge on passing known visual position fix locations would aid in trajectory flight control between assets within a remote fields.

High precision INS system with DVL aiding provides a strong navigation system platform, however with the complexities involved in UUV based IMR activities this is not accurate enough for the transition of resident systems between assets or for close quarter operations on subsea installations. The position drift of such

configuration is typically 0.1% of the travelled distance for the PHINS system as shown in Table 3.3. However, in close proximity to a known marker, visual pose estimation is shown to be a reliable system for an absolute position fix. Since resident ROVs/AUVs operate in the structured environment, this low-cost solution can provide an alternative more cost effective solution or a valuable back-up and compliment to acoustic-based positioning systems.

Chapter 8

Discussion, conclusions and future work

8.1 Discussion and conclusions

This thesis has presented development, implementation and testing of multiple systems aimed towards expansion of unmanned underwater robot capabilities. The research presented here included work in a variety of engineering disciplines such as software, electronic and mechanical engineering. The motivation for this research and the desired objectives have been presented in the introduction of the thesis. This was followed by a review of the resident UUV projects and recent trends in the industry in Chapter 2. Chapter 3 presented hardware used during the offshore autonomous ROV docking trials, and problems and challenges associated with the ROV operations. Development and implementation of visual based pose estimation system has been presented and discussed in Chapter 4, while autonomous docking of a work-class ROV, using developed pose estimation system has been presented in Chapter 5. This is followed by TMS position prediction using ANFIS in Chapter 6.

One of the objectives has been creating a solution suitable for deployment on the global fleet of work-class ROVs. The work presented in this thesis addresses that and is readily implementable on the majority of ROVs equipped with the necessary devices. For the active light marker, suitable lights can be used in any geometrical

configuration, as long as a minimum of four light beacons are used in an asymmetrical pattern so that ambiguity is avoided. Regarding choice of vision system, any suitable camera in underwater housing can be used.

The following lists the objectives stated in Chapter 1.2 and achieved results:

- **Identification of the gaps in the current ROV technology for performing inspection, maintenance and repair tasks at challenging MRE sites.** Offshore operations in general are particularly expensive and with the rapid expansion of MRE sites and transition to deeper waters, the costs associated with operation, maintenance and repair are inevitably rising. One of the primary OPEX costs relate to ROV and support vessel day rates. Chapter 2 presented a review of the recent advances in the ROV industry, and relevant related research projects including recent trends in research. While resident ROV solutions are becoming more popular, they are more orientated towards the O&G sector, without considering the large geographical spread of the offshore MRE farms, and IMR operations in deep-water energy production sites. This is partially addressed through collaborative ROV-ASV platforms, however with small commercial uptake of the technology due to the platform relying on high bandwidth, low latency communication links. Therefore, high levels of automation are needed. Some initial research on this topic has been published by the author of this thesis in conference paper (see Appendix D) (Trslic et al., 2018).

- **Development, implementation and experimental validation of the visual pose estimation solution based on the active light marker.** The visual pose estimation solution has been developed. The system's hardware includes conventional subsea lights found throughout the sector arranged in an asymmetrical pattern to form a navigational marker, which is attached to the TMS. The marker is then observed by machine vision camera attached to the ROV stern. Frames captured by the camera are processed on the dedicated topside-PC located in the ROV control cabin. Chapter 4.2 presented the system's hardware, while the image acquisition and processing method is discussed in

Chapter 4.3, and pose estimation is discussed in Chapter 4.4. The results of the system performance on dry and in the real-world environment are given in Chapter 4.6. The results showed that the accuracy of the developed pose estimation solution depends on the distance between the navigational marker and the camera. This is mostly due to the system low angle measurements sensitivity at larger ranges from the marker. However, it has been shown that fusing data from the onboard inertial navigation sensor with vision-based pose estimation system contributes to system robustness and accuracy.

- **Development, implementation and real-world experimental validation of the work-class ROV docking to both static, seabed-deployed TMS, and to dynamic suspended TMS.** The system has been designed, developed and tested. The autonomous ROV docking has been successfully performed multiple times. First the ROV was docked to a static docking station, then docking to the TMS suspended from a surface vessel was performed. The developed vision-based position estimation system was used as a navigational solution. The system has been tested during the offshore trials in the North Atlantic Ocean, where the autonomous docking to static and suspended TMS has been successfully performed. The developed system presents a major contribution towards use of ROVs in deep-water offshore operations. The outcome of the trials has been presented in Chapter 5 and published in a journal paper (see Appendix D) (Trslic et al., 2020).

- **Development and implementation of a suspended TMS heave motion position prediction method.** A TMS suspended from a floating platform presents a highly dynamic system, with the TMS heave being the most prominent motion element and usually the limiting docking factor. Work-class ROVs are relatively heavy and not very dynamic, thus matching a TMS heaving motion is often not viable except in conditions of low or slow heave. To overcome this problem a method for TMS position prediction has been developed. The method based on an Adaptive Neuro-Fuzzy Inference System (ANFIS) enables the ROV docking manoeuvre to start before the TMS aligns with the ROV

for docking. The method has been presented in Chapter 6, with details about the implemented ANFIS system given in Chapter 6.2. Experimental results presented and discussed in Chapter 6.3 showed that the ANFIS used here has captured the essential components of the underlying TMS dynamics and can be used as a TMS heave motion prediction tool which extends current underwater robot's capabilities. The developed method is the subject of a published journal paper (see Appendix D) (Trslić, Omerdic, Dooly and Toal, 2020), and has a dual benefit of being used as an aiding tool for ROV pilot or as part of autonomous ROV docking solution.

- **Implementation of the method for elimination of the drift in the ROV navigation solution, utilising the developed active light marker system.** UUVs operating as resident vehicles performing IMR tasks will operate in partially structured environments, with known subsea structures which can facilitate navigational markers. The fact that the position and orientation of these structures is known can be utilized. The method has been introduced in Chapter 4.4.1, with initial results discussed in Chapter 4.6.2. The method is based on fusion of onboard INS relative angle measurements and camera estimated position. The results showed that the method significantly reduced the pose estimation error, due to precise INS-based relative angle measurements. The use of the method has been further tested for elimination of the drift in the ROV navigation solution, which is discussed in Chapter 7, and with the results presented in Chapter 7.3. The results showed that the proposed system can improve the UUV localization underwater and provide additional robustness and redundancy to the navigational system. This method is the subject of the published paper (see Appendix D) (Trslić, Weir, Riordan, Omerdic, Toal and Dooly, 2020).

8.2 Future work

The robotic advancements described in this thesis have a variety of potential applications. However, to further improve the presented system some suggestions are provided for future research and development.

As described in Chapter 3, the navigational light marker used during the autonomous ROV docking has been placed at the back of the TMS in order to remain in the camera FOV until the ROV is within TMS frame close to the fully home position. One possible primary future developments includes augmenting this system with the use of a markerless pose estimation algorithm when in close proximity to the docking station and recognisisng the pose of the ROV relative to the dock directly from the dock structure rather than using the light markers. Such a markerless method would utilise the StereoFusion algorithm which has been developed within CRIS as part of another project, and has been presented in Rossi et al. (2018). By utilising such an augmented method, the navigational light marker can be placed to the front of the docking station to avoid light marker occlusions by the TMS frame. When the ROV approaches the docking station entrance, and the light marker is no longer in the camera FOV, the markerless method can be used for ROV navigation or flight control for the final stage of docking. In addition, an approach utilising a 3D sonar could be developed and used to make the system more robust. This would be especially important in highly turbid water, which is still a significantly unresolved challenge for underwater vision systems.

The TMS heading control should be used despite good results achieved during the autonomous ROV docking to suspended TMS without such a system. While the ROV easily compensates for heading disturbances and is relatively agile around the yaw axis, lateral movements are slow due to large cross section area which introduces large drag forces. In the case of rotation of the TMS around the yaw axis, the ROV has to correct the heading and move laterally, which leads to extended and protracted docking times. Therefore, implementing TMS heading control with the addition of two thrusters to the TMS is recommended as an important future development.

Ongoing work includes implementing ANFIS based TMS heave position estimation with the ROV autonomous docking. The method presented in Chapter 6 showed great performance. However, it has yet to be integrated with the ROV control system. This future development for improvement would include detailed analysis of the ROV system response to thruster inputs, and implementation of higher-level features such as path planning and decision making processes in close quarter routing of the ROV to the dock.

References

Albiez, J., Joyeux, S., Gaudig, C., Hilljegerdes, J., Kroffke, S., Schoo, C., Arnold, S., Mimoso, G., Alcantara, P., Saback, R., Britto, J., Cesar, D., Neves, G., Watanabe, T., Merz Paranhos, P., Reis, M. and Kirchnery, F. (2015), FlatFish - a compact subsea-resident inspection AUV, *in* 'OCEANS 2015 - MTS/IEEE Washington', pp. 1–8.

Allen, B., Austin, T., Forrester, N., Goldsborough, R., Kukulya, A., Packard, G., Purcell, M. and Stokey, R. (2006), Autonomous Docking Demonstrations with Enhanced REMUS Technology, *in* 'OCEANS 2006', pp. 1–6. ISSN: 0197-7385.

Aoki, T., Murashima, T., Tsukioka, S., Nakajyoh, H. and Ida, M. (1999), Development of deep sea free swimming ROV "UROV7K", Vol. 3, IEEE & Marine Technol. Soc, pp. 1307–1311.
URL: http://ieeexplore.ieee.org/document/800181/

ASV Global (2020), 'The Design and Development of a Revolutionary Autonomous Subsea Inspection Capability'.
URL: https://www.asvglobal.com/the-design-and-development-of-a-revolutionary-autonomous-subsea-inspection-capability/

Balasuriya, B., Takai, M., Lam, W., Ura, T. and Kuroda, Y. (1997), Vision based autonomous underwater vehicle navigation: underwater cable tracking, *in* 'Oceans '97. MTS/IEEE Conference Proceedings', Vol. 2, pp. 1418–1424 vol.2. ISSN: null.

Barnatt, A. (2013), 'Guidelines for installing ROV Systems on vessels or platforms', p. 20.

Beckman, J. (2019), "World-first' resident subsea drone to operate at Njord for Equinor'.
URL: https://www.offshore-mag.com/subsea/article/14072745/worldfirst-resident-subsea-drone-to-operate-at-njord-for-equinor

Bowen, A. D., Yoerger, D. R., German, C. C., Kinsey, J. C., Jakuba, M. V., Gomez-Ibanez, D., Taylor, C. L., Machado, C., Howland, J. C., Kaiser, C. L., Heintz, M., Pontbriand, C., Suman, S., O'Hara, L., Bailey, J., Judge, C., McDonald, G., Whitcomb, L. L., McFarland, C. J. and Mayer, L. (2014), Design of Nereid-UI: A remotely operated underwater vehicle for oceanographic access under ice, IEEE,

pp. 1–6.
URL: http://ieeexplore.ieee.org/document/7003125/

Bowen, A. D., Yoerger, D. R., Taylor, C., McCabe, R., Howland, J., Gomez-Ibanez, D., Kinsey, J. C., Heintz, M., McDonald, G., Peters, D. B., Fletcher, B., Young, C., Buescher, J., Whitcomb, L. L., Martin, S. C., Webster, S. E. and Jakuba, M. V. (2008), The Nereus hybrid underwater robotic vehicle for global ocean science operations to 11,000m depth, IEEE, pp. 1–10.
URL: http://ieeexplore.ieee.org/document/5151993/

Boyacioglu, M. A. and Avci, D. (2010), 'An Adaptive Network-Based Fuzzy Inference System (ANFIS) for the prediction of stock market return: The case of the Istanbul Stock Exchange', *Expert Systems with Applications* **37**(12), 7908–7912.
URL: http://www.sciencedirect.com/science/article/pii/S0957417410003453

Brignone, L., Perrier, M. and Viala, C. (2007), A fully autonomous docking strategy for Intervention AUVs, IEEE, pp. 1–6.
URL: http://ieeexplore.ieee.org/document/4302290/

Brignone, L., Raugel, E., Opderbecke, J., Rigaud, V., Piasco, R. and Ragot, S. (2015), First sea trials of HROV the new hybrid vehicle developed by IFREMER, IEEE, pp. 1–7.
URL: http://ieeexplore.ieee.org/document/7271682/

Buffagni, M., Gasparoni, F., Bergseth, N. H., Bjornbom, E. and Broccia, P. (2014), Development and Test of an AUV for Environmental Monitoring and Asset Integrity in Offshore O&G Scenarios: CLEAN SEA Project, Society of Petroleum Engineers.

Buragohain, M. and Mahanta, C. (2008), 'A novel approach for ANFIS modelling based on full factorial design', *Applied Soft Computing* **8**(1), 609–625.
URL: http://www.sciencedirect.com/science/article/pii/S1568494607000464

Caiti, A., Ciaramella, E., Conte, G., Cossu, G., Costa, D., Grechi, S., Nuti, R., Scaradozzi, D. and Sturniolo, A. (2016*a*), OptoCOMM: Introducing a new optical underwater wireless communication modem, IEEE, pp. 1–5.
URL: http://ieeexplore.ieee.org/document/7583431/

Caiti, A., Ciaramella, E., Conte, G., Cossu, G., Costa, D., Grechi, S., Nuti, R., Scaradozzi, D. and Sturniolo, A. (2016*b*), Optocomm: introducing a new optical underwater wireless communication modem, *in* '2016 IEEE Third Underwater Communications and Networking Conference (UComms)', IEEE, pp. 1–5.

Capocci, R., Omerdic, E., Dooly, G. and Toal, D. (2018), 'Fault-Tolerant Control for ROVs Using Control Reallocation and Power Isolation', *Journal of Marine Science and Engineering* **6**(2), 40.
URL: https://www.mdpi.com/2077-1312/6/2/40

Carreras, M., Ridao, P., Garcia, R. and Nicosevici, T. (2003), Vision-based localization of an underwater robot in a structured environment, *in* '2003 IEEE International Conference on Robotics and Automation (Cat. No.03CH37422)', Vol. 1, pp. 971–976 vol.1. ISSN: 1050-4729.

Catapult (2018), 'Modus inspection robot could save wind farms £1bn | News'.
URL: https://ore.catapult.org.uk/press-releases/modus-autonomous-subsea-survey-system/

Chan, R. H., Ho, C.-W. and Nikolova, M. (2005), 'Salt-and-pepper noise removal by median-type noise detectors and detail-preserving regularization', *IEEE Transactions on image processing* **14**(10), 1479–1485.

Christ, R. D. and Sr, R. L. W. (2013), *The ROV Manual: A User Guide for Remotely Operated Vehicles*, Butterworth-Heinemann.

Cieslak, P., Ridao, P. and Giergiel, M. (2015), Autonomous underwater panel operation by GIRONA500 UVMS: A practical approach to autonomous underwater manipulation, *in* '2015 IEEE International Conference on Robotics and Automation (ICRA)', pp. 529–536. ISSN: 1050-4729.

Conte, G., Scaradozzi, D., Mannocchi, D., Raspa, P., Panebianco, L. and Screpanti, L. (2016), 'Experimental testing of a cooperative ASV-ROV multi-agent system', *IFAC-PapersOnLine* **49**(23), 347–354.
URL: https://linkinghub.elsevier.com/retrieve/pii/S2405896316320158

Cowen, S., Briest, S. and Dombrowski, J. (1997), Underwater docking of autonomous undersea vehicles using optical terminal guidance, *in* 'Oceans '97. MTS/IEEE Conference Proceedings', Vol. 2, pp. 1143–1147 vol.2.

CRIS UL (2019), 'Work Class ROV vision based autonomous docking [Video file]'.
URL: https://www.youtube.com/watch?v=ypgwMfDN6rU&feature=youtu.be

Curtin, T., Bellingham, J., Catipovic, J. and Webb, D. (1993), 'Autonomous Oceanographic Sampling Networks', *Oceanography* **6**(3), 86–94.
URL: https://tos.org/oceanography/article/autonomous-oceanographic-sampling-networks

de Costa Sousa, J. and Setnes, M. (1999), 'Fuzzy predictive filters in model predictive control', *IEEE Transactions on Industrial Electronics* **46**(6), 1225–1232.

Dineen, D. (2019), 'Energy in Ireland 2019 Report', p. 96.
URL: https://www.seai.ie/publications/Energy-in-Ireland-2019-.pdf

Dooly, G., Omerdic, E., Coleman, J., Miller, L., Kaknjo, A., Hayes, J., Braga, J., Ferreira, F., Conlon, H., Barry, H. et al. (2016), 'Unmanned vehicles for maritime spill response case study: Exercise cathach', *Marine pollution bulletin* **110**(1), 528–538.

References

Dudley, B. (2019), BP Statistical Review of World Energy, Technical report, British Petroleum.
URL: https://www.bp.com/content/dam/bp/business-sites/en/global/corporate/pdfs/energy-economics/statistical-review/bp-stats-review-2019-full-report.pdf

Duncan, N. (1986), ROVs and Moonpools - An Operator's Viewpoint, *in* R. L. Wernli and R. Chapman, eds, 'ROV '86: Remotely Operated Vehicles', Springer Netherlands, Dordrecht, pp. 41–50.

Duntley, S. Q. (1963), 'Light in the sea', *JOSA* **53**(2), 214–233.

ECA Group (2019), 'Successfully demonstration USV/ROV interoperability for subsea inspections'.
URL: https://www.ecagroup.com/en/business/eca-group-successfully-demonstrates-usv-rov-interoperability-for-subsea-inspections-for-total-and-technipfmc

Energy Northern Perspective (2019), 'Saipem continues with Shell license for subsea robotics development – Energy Northern Perspective'.
URL: https://energynorthern.com/2019/01/10/saipem-continues-with-shell-license-for-subsea-robotics-development/

Equinor (2019), 'Equinor E-ROV Concept, SV version [Video file]'.
URL: https://www.youtube.com/watch?v=OdLSBTlHkU0

Esakkirajan, S., Veerakumar, T., Subramanyam, A. N. and PremChand, C. (2011), 'Removal of high density salt and pepper noise through modified decision based unsymmetric trimmed median filter', *IEEE Signal processing letters* **18**(5), 287–290.

Evans, J., Keller, K., Smith, J., Marty, P. and Rigaud, O. (2001), Docking techniques and evaluation trials of the SWIMMER AUV: an autonomous deployment AUV for work-class ROVs, Vol. 1, Marine Technol. Soc, pp. 520–528.
URL: http://ieeexplore.ieee.org/document/968776/

Evans, J., Redmond, P., Plakas, C., Hamilton, K. and Lane, D. (2003), Autonomous docking for Intervention-AUVs using sonar and video-based real-time 3D pose estimation, IEEE, pp. 2201–2210 Vol.4.
URL: http://ieeexplore.ieee.org/document/1282820/

Fahrni, L., Thies, P. R., Johanning, L. and Cowles, J. (2018), 'Scope and feasibility of autonomous robotic subsea intervention systems for offshore inspection, maintenance and repair', p. 9.

Feezor, M. D., Sorrell, F. Y., Blankinship, P. R. and Bellingham, J. G. (2001), 'Autonomous underwater vehicle homing/docking via electromagnetic guidance', *IEEE Journal of Oceanic Engineering* **26**(4), 515–521.

Fraile, D. and Komusanac, I. (2019), 'Wind Energy in Europe: Outlook to 2023', *Wind Europe* p. 40.
URL: https://windeurope.org/wp-content/uploads/files/misc/WindEurope-Market-Outlook-to-2023-exec-summary.pdf

Freedom ROV | Oceaneering [Video file] (2019).
URL: https://www.youtube.com/watch?v=MoKMwoX1jf0

Furuholmen, M., Hanssen, A., Carter, R., Hatlen, K., Siesjo, J. et al. (2013), Resident autonomous underwater vehicle systems–a review of drivers, applications, and integration options for the subsea oil and gas market, *in* 'Offshore Mediterranean Conference and Exhibition', Offshore Mediterranean Conference.

Gilmour, B., Niccum, G. and O'Donnell, T. (2012), Field resident AUV systems — Chevron's long-term goal for AUV development, *in* '2012 IEEE/OES Autonomous Underwater Vehicles (AUV)', pp. 1–5. ISSN: 1522-3167.

Grasso, T., Bruni, F., Filippini, M., Gasparoni, F., Maddalena, D., Miozza, L., Cioffi, P., Lainati, A., Rimoldi, A., Gentile, L. and Di Fede., G. (2016), Clean Sea hybrid ROV/AUV for Asset Integrity Operations, International Society of Offshore and Polar Engineers.

Gray, A. and Schwartz, E. (2016), 'Anglerfish: an ASV controlled ROV', p. 6.

Guth, F., Silveira, L., Botelho, S., Drews, P. and Ballester, P. (2014), Underwater SLAM: Challenges, state of the art, algorithms and a new biologically-inspired approach, *in* '5th IEEE RAS/EMBS International Conference on Biomedical Robotics and Biomechatronics', pp. 981–986. ISSN: 2155-1782.

Haltrin, V. I. (1999), 'Chlorophyll-based model of seawater optical properties', *Applied Optics* **38**(33), 6826–6832.

Hannon, M., Topham, E., Dixon, J., McMillan, D. and Collu, M. (2019), Offshore wind, ready to float? Global and UK trends in the floating offshore wind market, Technical report, Univesity of Strathclyde, Glasgow.

Hartley, R. and Zisserman, A. (2004), *Multiple View Geometry in Computer Vision*, Cambridge University Press. Google-Books-ID: e30hAwAAQBAJ.

Hidalgo, F. and Bräunl, T. (2015), Review of underwater SLAM techniques, *in* '2015 6th International Conference on Automation, Robotics and Applications (ICARA)', pp. 306–311. ISSN: null.

Hobson, B. W., McEwen, R. S., Erickson, J., Hoover, T., McBride, L., Shane, F. and Bellingham, J. G. (2007), The Development and Ocean Testing of an AUV Docking Station for a 21" AUV, *in* 'OCEANS 2007', pp. 1–6. ISSN: 0197-7385.

IEA (2019), Offshore Wind Outlook 2019: World Energy Outlook Special Report, Technical report, International Energy Agency.

References

IKM Subsea (2018), 'R-ROV and OCC from IKM [Video file]'.
URL: https://www.youtube.com/watch?time_continue=12&v=nvHS7aV5A8Q

Institute, M. (2019), 'Research Vessel RV Celtic Explorer'.
URL: https://www.marine.ie/Home/site-area/infrastructure-facilities/research-vessels/celtic-explorer

iXblue (2019), 'Subsea Inertial Navigation, iXblue', [online]. [Accessed 29 Feb 2020].
URL: https://www.ixblue.com/products/range/subsea-inertial-navigation

IxSea (2007), 'PHINS, user manual'.

Jang, J.-S. (1993), 'ANFIS: adaptive-network-based fuzzy inference system', *IEEE Transactions on Systems, Man, and Cybernetics* **23**(3), 665–685.

Jang, J.-S. (1996), Input selection for ANFIS learning, *in* 'Proceedings of IEEE 5th International Fuzzy Systems', Vol. 2, pp. 1493–1499 vol.2.

Karaboga, D. and Kaya, E. (2019), 'Adaptive network based fuzzy inference system (ANFIS) training approaches: a comprehensive survey', *Artificial Intelligence Review* **52**(4), 2263–2293.
URL: https://doi.org/10.1007/s10462-017-9610-2

Krupinski, S., Maurelli, F., Grenon, G. and Petillot, Y. (2008), Investigation of autonomous docking strategies for robotic operation on intervention panels, *in* 'OCEANS 2008', pp. 1–10.

Krupinski, S., Maurelliy, F., Malliosz, A., Sotiropoulosx, P. and Palmer, T. (2009), Towards AUV docking on sub-sea structures, IEEE, pp. 1–10.
URL: http://ieeexplore.ieee.org/document/5278144/

Köser, K. and Frese, U. (2020), Challenges in Underwater Visual Navigation and SLAM, *in* F. Kirchner, S. Straube, D. Kühn and N. Hoyer, eds, 'AI Technology for Underwater Robots', Intelligent Systems, Control and Automation: Science and Engineering, Springer International Publishing, Cham, pp. 125–135.
URL: https://doi.org/10.1007/978-3-030-30683-0_11

L3 ASV (2020), 'L3 Technologies Demonstrates Revolutionary Autonomous Subsea Inspection Capability'.
URL: https://www.asvglobal.com/l3-technologies-demonstrates-revolutionary-autonomous-subsea-inspection-capability/

L3 ASV (n.d.), 'C-Worker 7'.
URL: https://www.asvglobal.com/product/c-worker-7/

Lachaud, E., Monbeig, Y., Nolleau, P., Hardy, A., Thompson, M. and Lardeux, M. (2018), Opportunities and Challenges of Remote Operating a ROV Embarked on a USV, Offshore Technology Conference.
URL: http://www.onepetro.org/doi/10.4043/29000-MS

Lee, D., Kim, G., Kim, D., Myung, H. and Choi, H.-T. (2012), 'Vision-based object detection and tracking for autonomous navigation of underwater robots', *Ocean Engineering* **48**, 59–68.

Leon, P., Roland, F., Brignone, L., Opderbecke, J., Greer, J., Khalighi, M. A., Hamza, T., Bourennane, S. and Bigand, M. (2017), A new underwater optical modem based on highly sensitive Silicon Photomultipliers, IEEE, pp. 1–6.
URL: http://ieeexplore.ieee.org/document/8084586/

Li, Y., Jiang, Y., Cao, J., Wang, B. and Li, Y. (2015), 'AUV docking experiments based on vision positioning using two cameras', *Ocean Engineering* **110**, 163–173.
URL: http://www.sciencedirect.com/science/article/pii/S0029801815005521

Liljebäck, P. and Mills, R. (2017), Eelume: A flexible and subsea resident IMR vehicle, *in* 'OCEANS 2017 - Aberdeen', pp. 1–4.

Liu, S., Ozay, M., Okatani, T., Xu, H., Sun, K. and Lin, Y. (2018), 'Detection and pose estimation for short-range vision-based underwater docking', *IEEE Access* **7**, 2720–2749.

Liu, S., Xu, H., Lin, Y. and Gao, L. (2019), 'Visual Navigation for Recovering an AUV by Another AUV in Shallow Water', *Sensors* **19**(8), 1889.
URL: https://www.mdpi.com/1424-8220/19/8/1889

Lwin, K. N., Mukada, N., Myint, M., Yamada, D., Minami, M., Matsuno, T., Saitou, K. and Godou, W. (2018), 'Docking at pool and sea by using active marker in turbid and day/night environment', *Artificial Life and Robotics* **23**(3), 409–419.
URL: https://doi.org/10.1007/s10015-018-0442-1

MacDonald, A. and Torkilsden, S. E. (2016), 'IKM Subsea wins contract for Statoil's Visund and Snorre B platforms', *Offshore Technology Magazine* .
URL: https://www.offshore-technology.com/uncategorised/newsikm-subsea-wins-contract-for-statoils-visund-and-snorre-b-platforms-4978250/

MacDonald, A. and Torkilsden, S. E. (2019), 'ROV in residence', *Offshore Engineer Magazine* .
URL: https://offshoreengineer.oedigital.com/magazines/OffshoreEngineer/201909/pdf/

Majumder, S., Scheding, S. and Durrant-Whyte, H. F. (2001), 'Multisensor data fusion for underwater navigation', *Robotics and Autonomous Systems* **35**(2), 97–108.
URL: http://www.sciencedirect.com/science/article/pii/S0921889000001263

Manley, J. E., Halpin, S., Radford, N. and Ondler, M. (2018), Aquanaut: A New Tool for Subsea Inspection and Intervention, IEEE, pp. 1–4.
URL: https://ieeexplore.ieee.org/document/8604508/

References

MarineTech - RSV Sea Observer [Video file] (2017).
URL: https://www.youtube.com/watch?v=L7OpMcMGPZc

Maslin, E. (2019*a*), 'Residency in Waiting', *Offshore Engineer Magazine* **44**(5), 68.
URL: https://offshoreengineer.oedigital.com/magazine/issue/201909

Maslin, E. (2019*b*), 'Steps Toward Freedom', *Offshore Engineer Magazine* **44**(5), 68.

McEwen, R. S., Hobson, B. W., McBride, L. and Bellingham, J. G. (2008), 'Docking Control System for a 54-cm-Diameter (21-in) AUV', *IEEE Journal of Oceanic Engineering* **33**(4), 550–562.
URL: http://ieeexplore.ieee.org/document/4769696/

McLeod, D. (2010), Emerging capabilities for autonomous inspection repair and maintenance, *in* 'OCEANS 2010 MTS/IEEE SEATTLE', pp. 1–4. ISSN: 0197-7385.

McPhee, D. (2019), 'Equinor awards Saipem £35m subsea service deal at Njord field - News for the Oil and Gas Sector', *Energy Voice* .
URL: https://www.energyvoice.com/oilandgas/208963/equinor-award-saipem-35m-subsea-service-deal-at-njord-field/

Menna, F., Nocerino, E., Fassi, F. and Remondino, F. (2016), 'Geometric and Optic Characterization of a Hemispherical Dome Port for Underwater Photogrammetry', *Sensors* **16**(1), 48.
URL: https://www.mdpi.com/1424-8220/16/1/48

Modus (2019), 'Subsea UK Subsea Supply Chain Capability Showcase'.
URL: https://www.subseauk.com/documents/documents2019/modus.pdf

Mordor Intelligence (2019), ROV Market - Segmented by Type, Activity, Application Industry, and Geography - Growth, Trends and Forecast (2019 - 2024), Technical report.
URL: https://www.mordorintelligence.com/industry-reports/rov-market

Murawski, S. A., Hollander, D. J., Gilbert, S. and Gracia, A. (2020), Deepwater Oil and Gas Production in the Gulf of Mexico and Related Global Trends, *in* S. A. Murawski, C. H. Ainsworth, S. Gilbert, D. J. Hollander, C. B. Paris, M. Schlüter and D. L. Wetzel, eds, 'Scenarios and Responses to Future Deep Oil Spills: Fighting the Next War', Springer International Publishing, Cham, pp. 16–32.
URL: https://doi.org/10.1007/978-3-030-12963-7_2

Nicosevici, T., Garcia, R., Carreras, M. and Villanueva, M. (2004), A review of sensor fusion techniques for underwater vehicle navigation, *in* 'Oceans '04 MTS/IEEE Techno-Ocean '04 (IEEE Cat. No.04CH37600)', Vol. 3, pp. 1600–1605 Vol.3. ISSN: null.

Oceaneering (2018), 'Freedom ROV'.
URL: https://www.oceaneering.com/datasheets/ROV-Freedom.pdf

Oceaneering (2019), 'E-ROV System'.
URL: https://www.oceaneering.com/brochures/e-rov-system/

Offshore Engineer (2020), 'Ocean Infinity Launches Armada'.
URL: https://www.oedigital.com/news/475288-ocean-infinity-launches-armada

Offshore magazine (2019), 'Deepwater leading the way in discovered oil and gas resources'.
URL: https://www.offshore-mag.com/deepwater/article/14036076/deepwater-leading-the-way-in-discovered-oil-and-gas-resources

Offshore magazine (n.d.), 'Trial proves autonomous ROV deployment capability'.
URL: https://www.offshore-mag.com/business-briefs/equipment-engineering/article/16790676/trial-proves-autonomous-rov-deployment-capability

Omerdic, E. and Toal, D. (2012), OceanRINGS: System concept applications, *in* '2012 20th Mediterranean Conference on Control Automation (MED)', pp. 1391–1396.

Omerdic, E., Toal, D. and Dooly, G. (2013), OceanRINGS: Smart Technologies for Subsea Operations, *in* 'Advanced in Marine Robotics', LAP LAMBERT Academic Publishing.

Ortiz, A., Simó, M. and Oliver, G. (2002), 'A vision system for an underwater cable tracker', *Machine Vision and Applications* **13**(3), 129–140.
URL: https://doi.org/10.1007/s001380100065

OSJ (2018), 'Resident robots could save money and remove ships from the equation', *OSJ - offshore support journal* **21**(4), 26–28.
URL: https://issuu.com/rivieramaritimemedia/docs/offshore_support_journal_may_2018

Palomeras, N., Vallicrosa, G., Mallios, A., Bosch, J., Vidal, E., Hurtos, N., Carreras, M. and Ridao, P. (2018), 'AUV homing and docking for remote operations', *Ocean Engineering* **154**, 106–120.
URL: http://www.sciencedirect.com/science/article/pii/S0029801818301367

Pan-Mook Lee, Bong-Hwan Jeon and Sea-Moon Kim (2003), Visual servoing for underwater docking of an autonomous underwater vehicle with one camera, IEEE, pp. 677–682 Vol.2.
URL: http://ieeexplore.ieee.org/document/1283350/

Park, J.-Y., Jun, B.-h., Lee, P.-m. and Oh, J. (2009), 'Experiments on vision guided docking of an autonomous underwater vehicle using one camera', *Ocean Engineering* **36**(1), 48–61.
URL: http://www.sciencedirect.com/science/article/pii/S0029801808002242

Paull, L., Saeedi, S., Seto, M. and Li, H. (2014), 'AUV Navigation and Localization: A Review', *IEEE Journal of Oceanic Engineering* **39**(1), 131–149.

References

Pontbriand, C., Farr, N., Ware, J., Preisig, J. and Popenoe, H. (2008), Diffuse high-bandwidth optical communications, *in* 'OCEANS 2008', IEEE, pp. 1–4.

Rajpurohit, V. S. and Pai, M. M. M. (2011), Efficient Object Motion Prediction Using Adaptive Fuzzy Navigational Environment, *in* V. V. Das, G. Thomas and F. Lumban Gaol, eds, 'Information Technology and Mobile Communication', Communications in Computer and Information Science, Springer, Berlin, Heidelberg, pp. 1–5.

Raspante, F. (2012), Underwater mobile docking of autonomous underwater vehicles, *in* 'Proceedings of the OCEANS 2012 Conference, Hampton Roads, VA, USA', pp. 21–24.

Raugel, E., Opderbecke, J., Fabri, M. C., Brignone, L. and Rigaud, V. (2019), Operational and scientific capabilities of Ariane, Ifremer's hybrid ROV, IEEE, pp. 1–7.
URL: https://ieeexplore.ieee.org/document/8867102/

Ribas, D., Ridao, P. and Neira, J. (2010), *Underwater SLAM for Structured Environments Using an Imaging Sonar*, Springer. Google-Books-ID: atJqCQAAQBAJ.

Rigaud, V. and Nicolas-Meunier, B. (2015), From manned to autonomous and hybrid underwater systems, *in* '2015 IEEE Underwater Technology (UT)', IEEE, Chennai, India, pp. 1–10.
URL: http://ieeexplore.ieee.org/document/7108268/

Robinson, L., Newe, T., Burke, J., Dooly, G., Coleman, J. and Toal, D. (2018), High Bandwidth Maritime Communication Systems – Review of Existing Solutions and New Proposals, *in* '2018 2nd URSI Atlantic Radio Science Meeting (AT-RASC)', pp. 1–3.

Rossi, M., Trslić, P., Sivčev, S., Riordan, J., Toal, D. and Dooly, G. (2018), 'Real-Time Underwater StereoFusion', *Sensors* **18**(11), 3936.
URL: https://www.mdpi.com/1424-8220/18/11/3936

Saab (2019), 'Saab Seaeye Sabertooth'.
URL: https://www.saabseaeye.com/uploads/seaeye_sabertooth_rev_3_(1).pdf

Saipem (2019), 'Sonsub Hydrone-R launched in water: the first dive of Saipem's Underwater Intervention Drone has made a splash | Saipem'.
URL: https://www.saipem.com/en/media/news/2019-07-31/sonsub-hydrone-r-launched-water-first-dive-saipems-underwater-intervention

Sarda, E. I. and Dhanak, M. R. (2017), 'A USV-Based Automated Launch and Recovery System for AUVs', *IEEE Journal of Oceanic Engineering* **42**(1), 37–55.

SEAI (2010), Strategic Environmental Assessment (SEA) of the Off shore Renewable Energy Development Plan (OREDP) in the Republic of Ireland, Technical report.

SEAI (2011), Wind energy roadmap, 2011-2050, Technical report.
URL: https://www.seai.ie/publications/Wind_Energy_Roadmap_2011-2050.pdf

Shoorehdeli, M. A., Teshnehlab, M. and Sedigh, A. K. (2007), Novel Hybrid Learning Algorithms for Tuning ANFIS Parameters Using Adaptive Weighted PSO, *in* '2007 IEEE International Fuzzy Systems Conference', pp. 1–6. ISSN: 1098-7584.

Singh, H., Bowen, M., Hover, F., LeBas, P. and Yoerger, D. (1997), Intelligent docking for an autonomous ocean sampling network, Vol. 2, IEEE, pp. 1126–1131.
URL: http://ieeexplore.ieee.org/document/624150/

Sivcev, S., Trslic, P., Adley, D., Robinson, L., Dooly, G., Omerdic, E. and Toal, D. (2019), Adaptive Neuro-Fuzzy Network Enhanced Automatic Visual Servoing Algorithm for ROV Manipulators, *in* 'OCEANS 2019', IEEE, Seattle, p. 7.

Sivčev, S., Rossi, M., Coleman, J., Dooly, G., Omerdić, E. and Toal, D. (2018), 'Fully automatic visual servoing control for work-class marine intervention ROVs', *Control Engineering Practice* **74**, 153–167.
URL: http://www.sciencedirect.com/science/article/pii/S0967066118300327

Smith, S. M. (1997), 'Experimental Results of an Inexpensive Short BaselineAcoustic Positioni System for AUV Navigation', p. 7.

Sonardyne (2019), 'SPRINT - Subsea Inertial Navigation System, Sonardyne', [online]. [Accessed 29 Feb 2020].
URL: https://www.sonardyne.com/product/sprint-subsea-inertial-navigation-system/

Sonardyne (2020), 'BlueComm 200 - Wireless Underwater Video and Vehicle Control'.
URL: https://www.sonardyne.com/product/bluecomm-200-wireless-underwater-video/

Statoil (2017), 'How we think UIDs will be used by Statoil in the future'.
URL: https://32zn56499nov99m251h4e9t8-wpengine.netdna-ssl.com/wp-content/uploads/2017/07/ID2017_Att09_Statoil_TomGlancy.pdf

Tampnet (2018), 'Tampnet complete major coverage milestone for the 4G LTE network in the Gulf of Mexico'.
URL: https://www.tampnet.com/news/tampnet-completes-major-coverage-milestone-for-the-4g-lte-network-in-the-gulf-of-mexico/

The Crown Estate (2018), 'Offshore wind operational report', p. 24.
URL: https://www.thecrownestate.co.uk/media/2950/offshore-wind-operational-report-2018.pdf

The Crown Estate (2019), 'Offshore Wind Leasing Round 4 | The Crown Estate'.
URL: https://www.thecrownestate.co.uk/en-gb/what-we-do/on-the-seabed/offshore-wind-leasing-round-4/

References

Tito, N. and Rambaldi, E. (2009), SWIMMER: Innovative IMR AUV, *in* 'Offshore Technology Conference', Offshore Technology Conference, Houston, Texas.
URL: http://www.onepetro.org/doi/10.4043/19930-MS

Toal, D., Nolan, S., Omerdic, E., Ahmad, H. and Horgan, J. (2010), 'EXTENDING ROVS – MEETING THE CHALLENGES IN OFFSHORE SCIENCE AND INDUSTRY', p. 6.

Toal, Omerdic, Ahmad and Nolan (2012), ROV LATIS: next generation smart underwater vehicle, *in* Roberts and Sutton, eds, 'Further Advances in Unmanned Marine Vehicles', Institution of Engineering and Technology, pp. 9–44.

Trslić, P., Omerdic, E., Dooly, G. and Toal, D. (2020), 'Neuro-Fuzzy Dynamic Position Prediction for Autonomous Work-Class ROV Docking', *Sensors* **20**(3), 693.
URL: https://www.mdpi.com/1424-8220/20/3/693

Trslić, P., Weir, A., Riordan, J., Omerdic, E., Toal, D. and Dooly, G. (2020), 'Vision-Based Localization System Suited to Resident Underwater Vehicles', *Sensors* **20**(2), 529.
URL: https://www.mdpi.com/1424-8220/20/2/529

Trslic, P., Rossi, M., Robinson, L., O'Donnel, C. W., Weir, A., Coleman, J., Riordan, J., Omerdic, E., Dooly, G. and Toal, D. (2020), 'Vision based autonomous docking for work class ROVs', *Ocean Engineering* **196**, 106840.
URL: http://www.sciencedirect.com/science/article/pii/S0029801819309369

Trslic, P., Rossi, M., Sivcev, S., Dooly, G., Coleman, J., Omerdic, E. and Toal, D. (2018), Long term, inspection class ROV deployment approach for remote monitoring and inspection, IEEE, pp. 1–6.
URL: https://ieeexplore.ieee.org/document/8604814/
uczyński et al.

Łuczyński, T., Pfingsthorn, M. and Birk, A. (2017), 'The Pinax-model for accurate and efficient refraction correction of underwater cameras in flat-pane housings', *Ocean Engineering* **133**, 9–22.
URL: http://www.sciencedirect.com/science/article/pii/S0029801817300434

uEye Camera Interface in Matlab (2016).
URL: http://matlabtidbits.blogspot.com/2016/10/ueye-camera-interface-in-matlab-mex.html

Under the Sea | Hydrone | Saipem [Video file] (2017).
URL: https://www.youtube.com/watch?v=nOQMpse36xQ

UT2 (2018), 'UT3 - Resident ROVs', *UT2* **12**(4), 26–31.
URL: https://issuu.com/ut-2_publication/docs/issuu_2108_4_front_cover

Vallicrosa, G., Bosch, J., Palomeras, N., Ridao, P., Carreras, M. and Gracias, N. (2016), 'Autonomous homing and docking for AUVs using Range-Only Localization and Light Beacons', *IFAC-PapersOnLine* **49**(23), 54–60.
URL: http://www.sciencedirect.com/science/article/pii/S2405896316319085

Whitcomb, L. L., Jakuba, M. V., Kinsey, J. C., Martin, S. C., Webster, S. E., Howland, J. C., Taylor, C. L., Gomez-Ibanez, D. and Yoerger, D. R. (2010), Navigation and control of the Nereus hybrid underwater vehicle for global ocean science to 10,903 m depth: Preliminary results, IEEE, pp. 594–600.
URL: http://ieeexplore.ieee.org/document/5509265/

Yaser, R. G. and Allah, H. R. (2019), 'Short Term Electricity Price Forecasting by Hybrid Mutual Information ANFIS-PSO Approach', **10**(10093), 63–72.
URL: https://www.sid.ir/en/Journal/ViewPaper.aspx?ID=693533

Yazdani, A., Sammut, K., Lammas, A., Clement, B. and Yakimenko, O. A. (2019), Cooperative Guidance System for AUV Docking with an Active Suspended Docking Station, *in* 'OCEANS 2019 - Marseille', pp. 1–6.

Zagatti, R., Juliano, D. R., Doak, R., Souza, G. M., de Paula Nardy, L., Lepikson, H. A., Gaudig, C. and Kirchner, F. (2018), FlatFish Resident AUV: Leading the Autonomy Era for Subsea Oil and Gas Operations, Offshore Technology Conference.
URL: http://www.onepetro.org/doi/10.4043/28881-MS

Zhong, L., Li, D., Lin, M., Lin, R. and Yang, C. (2019), 'A Fast Binocular Localisation Method for AUV Docking', *Sensors* **19**(7), 1735.
URL: https://www.mdpi.com/1424-8220/19/7/1735

Appendix A

The ROV control architecture

This appendix describes the control architecture of ROV Étaín. The appendix is based on (Omerdic et al. 2010; Omerdic et al. 2009).

In contrast to most common control architectures used in modern ROV industry (where ROV is equipped with basic I/O modules, while control synthesis is performed topside), ROV Étaín is equipped with a full real-time embedded control system, which performs all necessary data processing and synthesis online, aboard the vehicle in real-time.

The block diagram of the ROV control system is shown in Fig. A.1. The ROV control system utilises control allocation approach, where the actuator selection task (mapping of the total control efforts onto individual actuator settings) is separated from the regulation task (design of total control efforts) in the control design. The Mission Builder module, Arbitration module and Synthesis module perform the regulation task, while the Control Allocation module performs the actuator selection task. The main objective of the Mission Builder module is to transform the mission objective, pilot inputs and measured navigation data into the desired ROV trajectory, i.e. to formulate the trajectory planning problem. A description of the Arbitration module is given in the following. In order to achieve the desired trajectory under real-time constraints, a set of task executors (Exclusive Behaviours (only one active at a time) and Collaborative Behaviours (many active at a time)) have been developed. Each of these task executors is competing to control actuators. The control buffer

concept has been developed to provide transparency and easy fusion of different task executor demands. Each task executor produces its own control cluster inside the control buffer. A control cluster consists of Virtual Joystick components (to mimic direct controls generated by a virtual pilot) and a set of settings for Low-Level Controllers (set points, feed-forward inputs and on/off switches to enable/disable individual controllers). The Virtual Joystick components are normalised surge, sway and heave forces and roll, pitch and yaw moments. The Coordinator performs the fusion of these control clusters into the Standard Control Cluster.

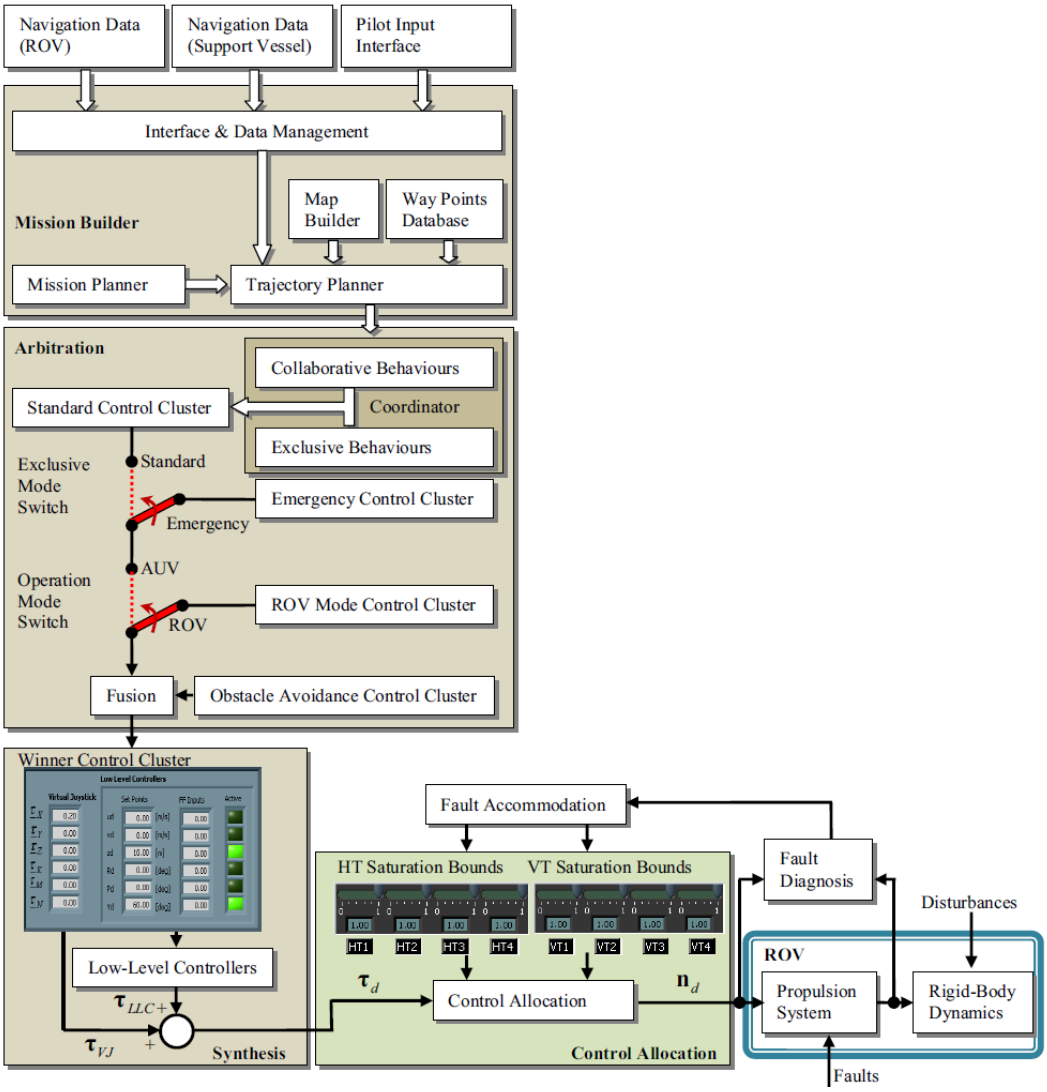

Fig. A.1 ROV Étaín control architecture.

The Operation Mode Switch is used to switch between AUV Mode and ROV Mode. In AUV Mode, control algorithms are exclusively used to create control actions (write values and set switches inside control clusters), while in ROV Mode the pilot has full freedom to generate these actions. However, the pilot should be aware not to "fight" low-level controller. For example, if the low-level heading controller is enabled to keep a set point (desired heading) of 60deg, any yaw moment created by the pilot using an input device, such as a joystick or gamepad, is considered as a disturbance by the heading controller. Therefore, the controller will create corresponding actions to reject this disturbance and keep the heading at 60°. The Exclusive Mode Switch is used to switch between Standard and Emergency Control Clusters in AUV Mode. In the case of any leakage (water penetration inside any bottle), two Leakage Answer Modes are available. In Auto-Answer mode the main state machine will activate the Emergency State setting the Exclusive Mode Switch to Emergency, setting the Operation Mode Switch to AUV Mode and initiating automatic ROV recovery to the surface. In Manual-Answer Mode the Operation Mode Switch is set to ROV Mode and the pilot is informed of the leakage, but no other automatic action is undertaken. Finally, the output control cluster is (optionally) blended with the Obstacle Avoidance Control Cluster to create the Winner Control Cluster, the ultimate "boss" with exclusive rights to control the actuators.

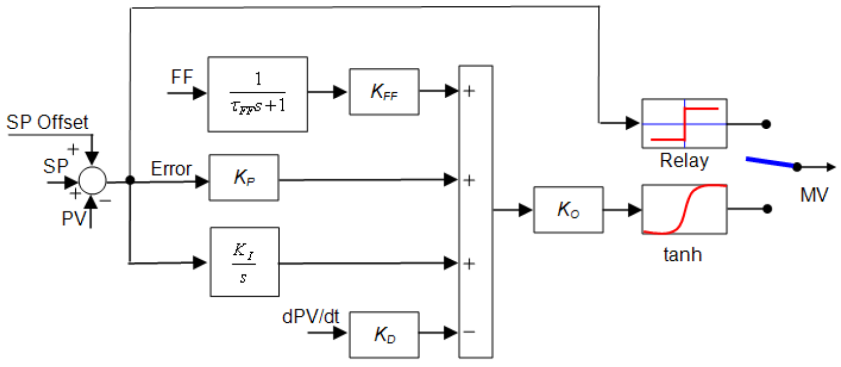

Fig. A.2 Low-level controller architecture.

Inside the Synthesis module the Winner Control Cluster is unbundled into Virtual Joystick components (vector T_{VJ}) and the Low-Level Controller (LLC) cluster, which is used as one of inputs to the LLC loop (Vectors *SP* and *FF* in Fig. A.2).

Other inputs include ROV navigation data (vectors *PV* and *dPV/dt*) and other parameters (vectors *SP Offset*, T_F, *KFF*, K_P, K_I, K_D and *Relay Amplitude*). There is a single controller for each degree of freedom. Surge and Sway controllers are velocity controllers, while Heave, Roll, Pitch and Yaw are position controllers. Each controller generates a manipulated variable MV to be applied to drive actuators, in order to keep process variable *PV* as close as possible to set point *SP*. Individual outputs are bundled into a vector of normalised forces and moments T_{LLC}. If a controller is disabled (not active), the corresponding *MV* is set to zero. Otherwise, the controller output is calculated as a normalised output of a modified PID controller. Feed-forward (FF) input improves the tracking performance in the case of the time-varying SP vector. Vector SP Offset is used to avoid integrator saturation problems. For example, the PID depth control algorithm has pure performance during the transition stage, since the ROV Étaín is slightly positively buoyant. However, much better performance is obtained using the PD control algorithm with SP Offset set to a positive value to compensate steady-state error due to positive buoyancy of the vehicle. In this case, depth change is fast, smooth, without overshoot and without steadystate error. However, this approach works well only in the case of smooth sensor signals, like in the case of ROV Étaín, where the depth sensor measurements are fused with the INS estimations using the Kalman filter.

Finally, in special "Autotuning" operation mode the controller output is generated using a relay (see Fig. A.2). Between successive ROV missions, it is likely that some of the onboard instruments/sensors/equipment will be added/removed/replaced, leading to changes in dynamic properties of the ROV (mass, moments of inertia, drag properties, etc). Controllers optimally tuned for a particular vessel configuration will not give the optimal performance in the case of a change in configuration. Autotuning of LLC is an advanced feature of the control system, yielding optimal controller performance, regardless of configuration changes. It is recommended that the autotuning is performed at the beginning of a mission. Two types of autotuning algorithms have been developed. Velocity controllers are tuned by recording and utilising the force-speed static characteristics. Autotuning of position controllers,

described in the following, utilises selfoscillations. Autotuning algorithms described in (Miskovic et al., 2006) have been expanded for 4 DOF controllers: Heave, Roll, Pitch and Yaw. The autotuning process involves the following steps: (1) Generate self-oscillations; (2) Wait for transient stage to finish; (3) Measure amplitude and period of steady-state oscillations; and (4) Find new values of controller gains using tuning rules. A novel set of tuning rules for underwater applications has been developed, which provides the optimal performance of low-level controllers in the case of configuration changes and the presence of disturbances (waves & sea currents).

The Control Allocation module in Fig. A.1 performs the actuator selection task. The thruster fault-tolerant control system consists of two subsystems: (1) The Fault Diagnosis Subsystem (FDS) uses fault detector units to monitor the states of thrusters (Omerdic and Roberts, 2003). (2) The Fault Accommodation Subsystem (FAS) uses information provided by the FDS to accommodate faults and perform control reallocation. The output of FAS controls the HT/VT Saturation Bounds sliders. A hybrid control allocation approach is implemented inside the LabVIEW Control Allocation Express VI. A hybrid approach for control allocation (Omerdic et al., 2004) is based on integration of the pseudoinverse and the fixed-point iteration method. It is implemented as a two-step process. The pseudoinverse solution is found in the first step. Then the feasibility of the solution is examined analysing its individual components. If violation of actuator constraint(s) is detected, the fixed-point iteration method is activated in the second step. In this way, the hybrid approach is able to allocate the exact solution, optimal in the l2 sense, inside the entire attainable command set.

A.1 References

Miskovic, N., Vukic, Z., Barisic, M. and Tovornik, B., 2006, June. Autotuning autopilots for micro-ROVs. In 2006 14th Mediterranean Conference on Control and Automation (pp. 1-6). IEEE.

Omerdic, E. and Roberts, G., 2003. Thruster fault diagnosis and accommodation for open-frame underwater vehicles. Control engineering practice, 12(12), pp.1575-1598.

Omerdic, E. and Roberts, G.N., 2004. Extension of feasible region of control allocation for open-frame underwater vehicles. IFAC Proceedings Volumes, 37(10), pp.315-320.

Omerdic, E. and Toal, D., 2009, January. Smart ROVLATIS: from design concepts to test trials. In IFAC 8th Conference on Manoeuvring and Control of Marine Craft (MCMC'2009).

Omerdic, E., Toal, D., Nolan, S. and Ahmad, H., 2010. Smart ROVLATIS: control architecture.

Appendix B

ROV Étaín technical specification summary

MRE-ROV

CRIS Centre for Robotics & Intelligent Systems

Fully electric Observation Class ROV configured for high thrust and lifting capability.

Great for long tether excursions and deep Free Swimming Operations.

Additional hydraulic power unit for underwater operations using manipulators.

Technical Specifications for Comanche ROV

Base Vehicle	
Chassis	Marine grade Aluminium frame with skid expansion
Max Payload	285kg
Max operating depth	2000m depth rating (LARS/TMS operations); 600m Free Swimming
Thrusters	Seven 100 kgf / 220 lbf Brushless DC Thrusters using StatorshieldTM Technology (4 horizontal, 3 vertical)
Weight in Air	1130kg
Forward speed (max)	2 m/s / 4 Knots
ROV Power supply	35kW, 3000V 400Hz
Embedded control & acquisition system	SubCAN Control System with MMRRC software OceanRINGS
Fibre/media converters	4 Pass Fibre Optic Connection with Focal CWDM

LARS/TMS Operations & Free Swimming Winch	
Length	2200m LARS Umbilical; 400m TMS tether 600m neutral Free Swimming tether
TMS frame	Type 3B Garage 316L Stainless Steel Frame

Instruments & Payload Sensors	
Multibeam sonar	Reson SeaBat 7125/7128 multibeam echsounder system
Forward Looking Sonar	Tritech SeaKing Dual Frequency Scanning Sonar
Sound velocity probe	Valeport UV-SVP (temperature & SVP)
Depth & altitude	Tritech PA500
Doppler Velocity Log	Nortek DVL 500kHz
GNSS (surface)	Applied Acoustics 106G RTK GNSS
Inertial navigation	iXBlue PHINS 6000 (High precision fibre optic INS)
Cameras	1 x Bowtech Explorer Pro (4000m) - Low Light monochrome Camera 3 x Sub-C 1Cam MK6 UHDF w/LiquidOptics – UHDF Colour Zoom Wide Angle Camera
Lights	4 x Bowtech 3200 LED Dimmable LED Light (3000m) 3 x Sub-C Lights for HD Cameras
Safety Systems	Novatech RF-700AR – VHF Beacon – Battery & Remote Antenna Novatech ST-400AR Xenon Flasher – Battery & Remote Flash Lamp
Manipulators	2 x Schilling Orion 7P
Hydraulic Power Unit	10kW HPU (13.4 HP, 207 BAR), Inc CARDEV filter

For more information visit: www.cris.ul.ie

ROVs for inspection and intervention in MRE

Ireland's European Structural and Investment Funds Programmes 2014-2020
Co-funded by the Irish Government and the European Union
European Union
European Regional Development Fund
Science Foundation Ireland sfi For what's next
MaREI Marine Renewable Energy Ireland
University of Limerick

Appendix C

The ROV navigation system - technical specification

This appendix contains the technical specification of the main components of the ROV navigation system:

- C.1 Phins 6000 Inertial Navigation System
- C.2 Nortek 500 Doppler Velocity Log
- C.3 Valeport UV-SVP sound velocity probe, temperature and depth sensor
- C.4 Okeanus GPSR-3015G

C.1 Phins 6000 INS

Phins Subsea

FOG-based high-performance subsea inertial navigation system for deep water

Phins Subsea is a subsea inertial navigation system providing position, true heading, attitude, speed, depth and heave. Its high-accuracy inertial measurement unit is coupled with an embedded digital signal processor that runs an advanced Kalman filter.
Phins Subsea can be pre-assembled and pre-calibrated with a doppler velocity log version, making the system easy to install and ready to use for more precise navigation.

FEATURES

- All-in-one high-accuracy 3D positioning with heading, roll and pitch
- FOG, unique strap-down technology
- Multiple aiding sensors available: (DVL, USBL, LBL, RAMSES, GPS, depth sensor)
- Options: DVL or RAMSES easy coupling
- Ethernet, web server (GUI)

APPLICATIONS

- AUV navigation
- Towfish navigation
- Metrology
- Precise positioning
- Out-of-straightness survey

BENEFITS

- High grade INS performance
- High reliability and maintenance free
- Rugged design for water depths up to 6,000 m
- Ultimate sub-metric performance using sparse array transponders and on-the-fly calibration
- Ease of use and quick installation

2017-03-DS-Phins6000

contact@ixblue.com | www.ixblue.com
EMEA +33 1 30 08 88 88 | Americas +1 781 937 8800 | APAC +65 6747 4912

iXblue

TECHNICAL SPECIFICATIONS

Performance

Position accuracy	
With USBL / LBL	Three times better than USBL / LBL
DVL-aided lowest expected performance	0.05 %TD (CEP 50)
DVL-aided optimal performances in typical conditions	0.01 %TD (CEP 50)
No aiding for 60s / 120s	0.06m / 0.3m
Heading accuracy	
With GPS	0.01 deg secant latitude RMS [1]
With DVL	0.02 deg secant latitude RMS [1]
Roll and pitch dynamic accuracy (no aiding)	0.01 deg RMS

Operating range/environement

Operating / storage temperature	-20°C to 55 °C / -40°C to 80 °C
Rotation rate dynamic range	Up to 750 deg/s
Acceleration dynamic range	± 15 g
Heading / roll / pitch	0 to +360 deg / ±180 deg / ±90 deg
MTBF	100,000 hours (System observed) 500,000 hours (FOG + Accelerometers)
Depth	6 000 m

Physical characteristics

	without DVL	with RDI DVL
Material	Titanium	Titanium
Weight in air / water	23 / 13 kg	43,7-48.5 / 27-28.5 kg
Mounting	6 Ø 6.5 holes	6 Ø 11 holes
Dimensions (L x W x H)	Ø 255 x 288 mm	Ø 298 x 543 mm
Connector	3 x 12 pins, 1 x 19 pins,1 x 26 pins SEACON	

Interfaces

Serial	RS422 or RS232
Ethernet	100 MBit - UDP / TCP server / TCP client / web server (GUI)
Pulse	3 inputs / 2 outputs
Inputs / outputs	Configurable 7i / 5o - Pulse[2] 3i / 2o - Configuration port
Baud rates	Up to 460 kbaud
Data output rate	0.1 Hz to 200 Hz
Power supply / consumption	24 VDC (20 - 32 V) / < 20 W

(1) Secant latitude = 1/cosine latitude
(2) Input GPS PPS pulse for accurate time synchronization of PHINS 6000

contact@ixblue.com | www.ixblue.com
EMEA +33 1 30 08 88 88 | Americas +1 781 937 8800 | APAC +65 6747 4912

iXblue

C.2 Nortek 500 DVL

DVL 1MHz/500kHz

UNDERWATER NAVIGATION

TECHNICAL SPECIFICATIONS

Bottom Velocity	1 MHz		500 kHz	
Single ping std @ 3m/s	0.5 cm/s		0.5 cm/s	
Long term accuracy	±0.2% / ±0.1 cm/s		±0.2% / ±0.1 cm/s	
Minimum altitude	0.2 m		0.3 m	
Maximum altitude	50 m		200 m	
Velocity resolution	0.01 mm/s		0.01 mm/s	
Maximum ping rate*	8 Hz max		8 Hz max	
*) Inquire for more options				
Water Tracking				
Minimum accuracy	1% of measured value / ±0.5 cm/s		1% of measured value / ±0.5 cm/s	
Minimum range	2.0 m		4.0 m	
Current Profiling				
Minimum accuracy	1% of measured value / ±0.5 cm/s		1% of measured value / ±0.5 cm/s	
Velocity resolution	0.1 cm/s		0.1 cm/s	
Interval	User specified nth ping		User specified nth ping	
Maximum range	30 m		70 m	
Blanking	0.1 m		0.5 m	
Cell size	0.2-2.0 m		0.5-4.0 m	
Max # cells	150		140	
Environmental				
Operating temperature	-4 to 40 °C			
Storage temperature	-20 to 60 °C			
Mechanical	**Head & electronics**		**Titanium DVL**	
	1 MHz	**500 kHz**	**1 MHz**	**500 kHz**
Depth rating	4000 m	6000 m	4000 m	6000 m
Weight	1.7 kg	3.5 kg	2.7 kg	5.9 kg
Weight in water	-	-	1.7 kg	3.1 kg
Height (see drawing)	(see drawing)		(see drawing)	
Diameter	(see drawing)		(see drawing)	

Hardware	1 MHz	500 kHz
Frequency of operation	1 MHz	500 kHz
Configuration	4-beam Janus array convex transducer, 25° beam angle	4-beam Janus array convex transducer, 25° beam angle
Internal memory	16 GB / 64 GB optional	16 GB / 64 GB optional
Interfaces		
Serial (either serial or Ethernet)	Configurable RS232 or RS422 Subconn connector, 8 pin male	
Ethernet	10/100 Mbits Auto MDI-X TCP/IP, UDP, HTTP protocols Fixed IP/DHCP client/AutoIP, UPnP IEEE1588/PTP for absolute time stamping Subconn connector, 8 pin male	
Data formats	Nortek proprietary w/ 1 ms time stamp accuracy, NMEA0183, Variants of PD0.	
Trigger	Internal 1, 2, 3, 4, 5, 6, 7 or 8 Hz Trigger option through command (Ethernet or serial) External TTL or 485 lines: - 1 input trigger (configurable Rising/Falling/Edges)	
Sensors		
Pressure	0.1%FS /precision better than 0.002% of full scale per sample	
Temperature	-4° to 40°C ±0.1°C	
Power	**1 MHz**	**500 kHz**
DC input	12-48 v	12-48 v
Maximum Peak Current	1.0 A	1.0 A
Average power	1.3 W	3.0 W
Materials		
Standard models	All materials Titanium and Delrin	

True innovation makes a difference

NORTEK

DVL 1MHz/500kHz

UNDERWATER NAVIGATION

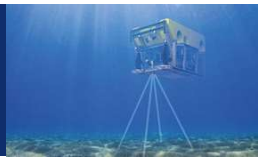

DVL 1 MHz

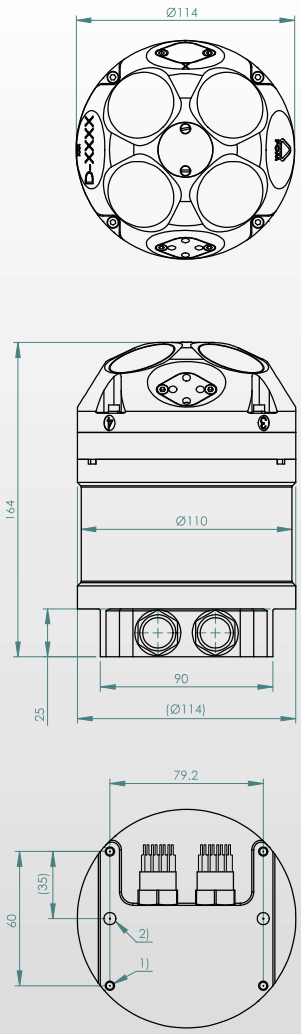

Inquire for optional mounting plates.

DVL 500 kHz

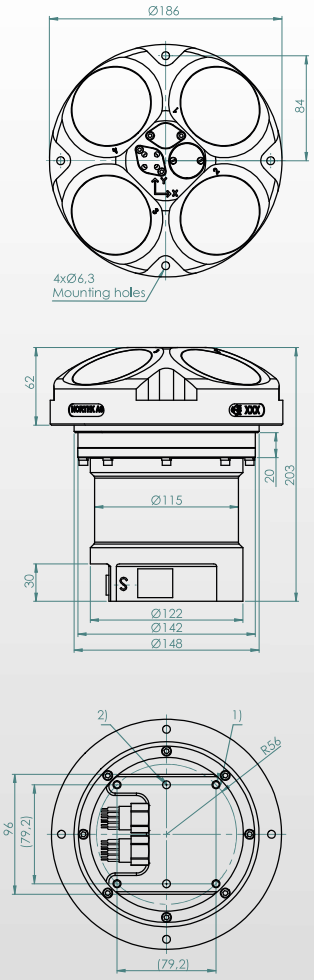

1) Mounting holes: 4x 1/4-20UNC 12 deep
2) Guide pin holes: Ø6,3 x 10 deep

All dimensions in mm.

DVL datasheet, 04.17 Rev. 04

NORTEK

Nortek AS
Vangkroken 2
1351 Rud, Norway
Tel: +47 6717 4500
inquiry@nortek.no

Nortek Japan
jpinquiry@nortek.jp
Tel: +81 03 6435 3270

Nortek China
inquiry@nortek.com.cn
Tel: +86-532-85017270

Nortek Netherlands
info@nortek-bv.nl
Tel +31 206543 600

Nortek France
info@nortekmed.com
Tel + 33 (0) 4 94 31 70 30

Nortek UK
inquiry@nortekuk.co.uk
Tel: +44 (0) 2380 596 428

Nortek Brazil
nortek@nortekbrasil.com.br
Tel: +55 (22) 2765-7630

Nortek USA
inquiry@nortekusa.com
Tel: + 1 617-206-5750

For representatives in other countries, please refer to www.nortek.no.

C.3 Valeport UV-SVP

UV-SVP Sound Velocity, Temperature and Pressure for an Underwater Vehicle

Based on the Valeport miniSVS, the UV-SVP offers a form-factor designed for Underwater Vehicles where space is at a premium. Incorporating Valeport's class leading time of flight sound speed sensor, a PRT temperature sensor and a 0.01% pressure sensor in a compact package weighing just 750 grams (in air), the lightweight titanium housing gives a depth rating of 3000m. A wide range (9-30V DC) isolated power supply and RS232 communications complete the package.

Sensors

Sound Velocity

Each sound velocity measurement is made using a single pulse of sound travelling over a known distance, so is independent of the inherent calculation errors present in all CTDs. Our unique digital signal processing technique virtually eliminates signal noise, and gives an almost instantaneous response; the digital measurement is also entirely linear, giving predictable performance under all conditions.

Range:	1375 - 1900m/s
Resolution:	0.001m/s
Accuracy:	±0.020m/s

Temperature

Range:	-5°C to +35°C
Resolution:	0.001°C
Accuracy:	±0.01°C

Pressure

Range:	10, 30, 100, 300
Resolution:	0.001% range
Accuracy:	±0.01% range

Data Output

RS232 & RS485 output, selected by command code. RS232 data may be taken directly into a PC over cables up to 200m long, whereas RS485 is suitable for longer cables (up to 1000m) and allows for multiple addressed units on a single cable.

Baud Rate:	19200 - 115200
Protocol:	8 data bits, 1 stop bit, No parity, No flow control

Electrical

Voltage:	8 – 30V DC Isolated
Power:	0.35W
Connector:	SubConn MCBH6F

Physical

Depth Rating:	3000m
Weight:	0.75 kg (in air)
Housing & Bulkhead:	Titanium

Ordering

06520549-XX	Supplied with: • 0.5m interface cable • Operation manual and transit case
Note:	XX denotes pressure transducer range. Select from 10, 30, 50, 100, 300, or 600 Bar

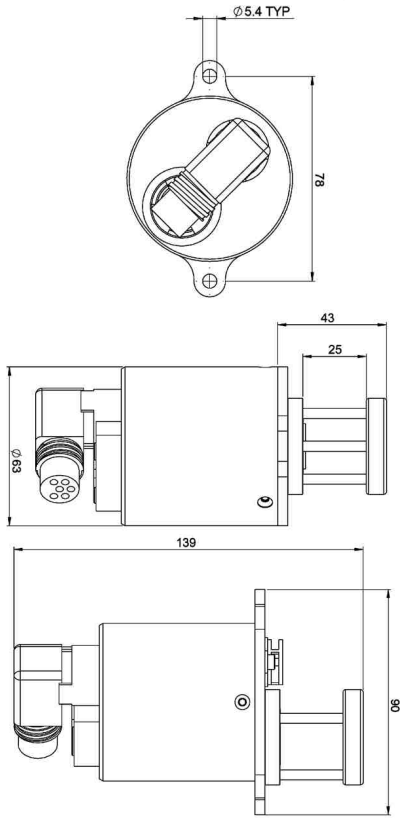

Data Sheet Reference: UV-SVP - June 2016

Valeport Limited, St. Peter's Quay Totnes, Devon, TQ9 5EW UK
t. +44 (0)1803 869292 f. +44 (0)1803 869293 e. sales@valeport.co.uk w. www.valeport.co.uk

C.4 Okeanus GPSR-3015G

OKEANUS
SCIENCE & TECHNOLOGY

SOSI

GPS RECEIVER

The SOSI Series GPSR-X015G Satellite Differential GPS Receivers are designed for use with deep diving AUVs, buoys or other autonomous systems that are required to operate at depth—but periodically surface to determine position and reset their navigation system. These receivers and antennas are designed to receive GPS satellite data only while on the surface, but can survive routine submergence to depth. The GPSR- X015G is available in depth ratings of 3000 or 6000 meters. The rugged 12 channel GPS engine is compatible with WAAS, EGNOS, JCAB and RTCM SC-104 Differential Correction Systems.

MECHANICAL SPECIFICATIONS

- Depth Rating: 3,000m or 6,000m
- Weight: 20 oz. (air)
- Weight: 8 oz. (seawater)
- Height: 3.25 in.
- Material: 6061 AL, Glass
- Finish: Hard coat anodize
- Connector: AWM-6-BCR-GRE
- Interface: RS232

TECHNICAL SPECIFICATIONS

- GPS Standard Positioning Service
  - Position: <15m, 95% typical
  - Velocity: 0.1kt RMS steady state
- DGPS (WAAS)
  - Position: <3m, 95% typical
  - Velocity: 0.1kt RMS steady state
- PPS Time: +/- 1 microsecond
- Operating Temp: -30 to +80oC
- Storage Temp: -40 to +80oC
- Geodetic Datum: 108 predefined, 1 userv

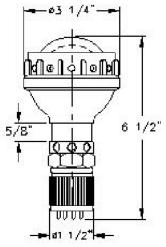

OKEANUS SCIENCE & TECHNOLOGY, LLC +1 (425) 869-1834 INFO@OKEANUS.COM WWW.OKEANUS.COM

Appendix D

Publications

1. Trslić, P., Omerdic, E., Dooly, G., and Toal, D. (2020), 'Neuro-Fuzzy dynamic position prediction for autonomous work-class ROV docking', *Sensors* 20(3), 693.
   DOI: 10.3390/s20030693. *Available online*

2. Trslić, P., Weir, A., Riordan, J., Omerdic, E., Toal, D. and Dooly, G.(2020), 'Vision-based localization system suited to resident underwater vehicles', *Sensors* 20(2), 529.
   DOI: 10.3390/s20020529. *Available online*

3. Trslić, P., Rossi, M., Robinson, L., O'Donnel, C.W., Weir, A., Coleman, J., Riordan, J., Omerdic, E., Dooly, G. and Toal, D.(2020), 'Vision Based Autonomous Docking for Work Class ROVs', *Ocean Engineering* 196, 106840.
   DOI: 10.1016/j.oceaneng.2019.106840. *Available online*

4. Omerdic, E., Trslić, P., Kaknjo, A., Weir, A., Rao, M., Dooly, G. and Toal, D., 2020. Geometric Insight into the Control Allocation Problem for Open-Frame ROVs and Visualisation of Solution. *Robotics*, 9(1), p.7.
   DOI: 10.3390/robotics9010007. *Available online*

5. Sivcev, S., Trslić, P., Adley, D., Robinson, L., Dooly, G., Omerdic, E. and Toal, D., 2019, October. Adaptive Neuro-Fuzzy Network Enhanced Automatic Visual Servoing Algorithm for ROV Manipulators. In OCEANS 2019

MTS/IEEE SEATTLE (pp. 1-7). IEEE.
DOI: 10.23919/OCEANS40490.2019.8962868. *Available online*

6. Rossi, M., Trslić, P., Sivčev, S., Riordan, J., Toal, D. and Dooly, G., 2018. Real-time underwater StereoFusion. *Sensors*, 18(11), p.3936.
DOI: 10.3390/s18113936. *Available online*

7. Trslić, P., Rossi, M., Sivčev, S., Coleman, J., Dooly, G., Omerdic, E. and Toal, D.(2018), 'Long term, inspection class ROV deployment approach for remote monitoring and inspection',*in* 'OCEANS 2018 - MTS/IEEE Charleston'.
DOI:10.1109/OCEANS.2018.8604814. *Available online*

sensors

MDPI

Article

Neuro-Fuzzy Dynamic Position Prediction for Autonomous Work-Class ROV Docking

Petar Trslić *, Edin Omerdic, Gerard Dooly and Daniel Toal

Centre for Robotics & Intelligent Systems, University of Limerick, Limerick V94 T9PX, Ireland; edin.omerdic@ul.ie (E.O.); gerard.dooly@ul.ie (G.D.); daniel.toal@ul.ie (D.T.);
* Correspondence: petar.trslic@ul.ie; Tel.: +353-61-213-102

Received: 21 December 2019; Accepted: 23 January 2020; Published: 27 January 2020

Abstract: This paper presents a docking station heave motion prediction method for dynamic remotely operated vehicle (ROV) docking, based on the Adaptive Neuro-Fuzzy Inference System (ANFIS). Due to the limited power onboard the subsea vehicle, high hydrodynamic drag forces, and inertia, work-class ROVs are often unable to match the heave motion of a docking station suspended from a surface vessel. Therefore, the docking relies entirely on the experience of the ROV pilot to estimate heave motion, and on human-in-the-loop ROV control. However, such an approach is not available for autonomous docking. To address this problem, an ANFIS-based method for prediction of a docking station heave motion is proposed and presented. The performance of the network was evaluated on real-world reference trajectories recorded during offshore trials in the North Atlantic Ocean during January 2019. The hardware used during the trials included a work-class ROV with a cage type TMS, deployed using an A-frame launch and recovery system.

Keywords: ANFIS; ROV docking; Position prediction

1. Introduction

In recent years, operations undertaken by unmanned underwater vehicles (UUVs) in the offshore energy sector are changing rapidly. This is driven by both offshore oil & gas (O&G) and the offshore wind sector where production platforms are pushed further off the coast, into areas of higher energy potential. However, considering significant expenditures related to the cost of the surface support vessel and crew, and with the production platforms in remote locations, the cost related to inspection, maintenance, and repair (IMR) tasks inevitably rise. Rising costs have resulted in the development and use of permanently deployed resident vehicle systems. Although the concept of permanently deployed vehicles exists in the literature for many years [1], only recently have we seen the introduction of commercial resident vehicles [2], with Oceaneering and IKM being industry leaders. Oceaneering developed E-ROV [3], a battery-powered, self-contained, work-class remotely operated vehicle (ROV), whereas IKM developed a fully electric R-ROV based on electric work-class ROV Merlin [4]. In general, such systems include a permanently deployed docking station which serves as a charging point, download/upload data link, and as mechanical protection for the resident vehicle [5].

However, within the O&G, and especially the offshore wind production field, multiple assets can be spread across more than 100 km^2, which need to be continuously inspected for condition monitoring purposes. This has been partially addressed through the development of resident autonomous underwater vehicles (AUV) [6,7]. However, due to the limited intervention capabilities of resident AUV systems, many energy-intensive applications still require ROVs [8]. These restrictions are recognized, and use of collaborative platforms consisting of an autonomous surface vehicle (ASV) and ROV are seen as a potential solution [9,10]. Although commercially available solutions based on observation class ROVs exist [11], significant commercial uptake of the technology is not yet recorded.

sensors

MDPI

Article

Vision-Based Localization System Suited to Resident Underwater Vehicles

Petar Trslić [1,*], Anthony Weir [1], James Riordan [2], Edin Omerdic [1] and Daniel Toal [1] and Gerard Dooly [1]

[1] Centre for Robotics & Intelligent Systems, University of Limerick, V94 T9PX Limerick, Ireland; anthony.weir@ul.ie (A.W.); edin.omerdic@ul.ie (E.O.); daniel.toal@ul.ie (D.T.); gerard.dooly@ul.ie (G.D.)
[2] School of Computing, Engineering, and Physical Sciences, University of the West of Scotland, Glasgow G72 0AG, UK; james.riordan@uws.ac.uk
* Correspondence: petar.trslic@ul.ie; Tel.: +353-61-213-102

Received: 9 December 2019; Accepted: 16 January 2020; Published: 18 January 2020

check for updates

Abstract: In recent years, we have seen significant interest in the use of permanently deployed resident robotic vehicles for commercial inspection, maintenance and repair (IMR) activities. This paper presents a concept and demonstration, through offshore trials, of a low-cost, low-maintenance, navigational marker that can eliminate drift in vehicle INS solution when the vehicle is close to the IMR target. The subsea localisation marker system is fixed on location on the resident field asset and is used in on-vehicle machine vision algorithms for pose estimation and facilitation of a high-resolution world coordinate frame registration with a high refresh rate. This paper presents evaluation of the system during trials in the North Atlantic Ocean during January 2019. System performances and propagation of position error is inspected and estimated, and the effect of intermittent visual based position update to Kalman filter and onboard INS solution is discussed. The paper presents experimental results of the commercial state-of-the-art inertial navigation system operating in the pure inertial mode for comparison.

Keywords: resident UUVs; localization; subsea navigation

1. Introduction

In recent years, we have seen the conceptual introduction of resident robotic platforms to underwater inspection, maintenance and repair (IMR) activities within the oil and gas sector. This is being driven by cost saving activities to reduce the levelized cost of energy (LCOE) for the sector and in an effort to compete with emerging sectors such as hydraulic fracturing. Traditionally, subsea IMR activities are carried out using a work-class hydraulic remotely operated vehicle (ROV). Vehicles are tethered and controlled directly from a surface support vessel and generally incur significant expenditures associated with the cost of the vessel and crew. The concept of permanently deployed ROV systems has been in the literature for many years [1]; however, only in recent years have we seen the introduction of these system to commercial marine activities offshore. IKM Subsea [2] were one of the first commercial entities to bring this from the proof-of-concept prototype stage to full operational system enactments. IKM developed their fully electric Merlin UCV ROV, modifying their manipulator protocols along with umbilical connectors for shore-based distance piloting and long-term deployment [3]. This was developed and deployed under a breakthrough ten-year contract for Statoil's Visund and Snorre B field assets where one resident ROV

Ocean Engineering 196 (2020) 106840

Contents lists available at ScienceDirect

Ocean Engineering

journal homepage: www.elsevier.com/locate/oceaneng

Vision based autonomous docking for work class ROVs

Petar Trslic *, Matija Rossi, Luke Robinson, Cathal W. O'Donnel, Anthony Weir, Joseph Coleman, James Riordan, Edin Omerdic, Gerard Dooly, Daniel Toal

Centre for Robotics and Intelligent Systems (CRIS), University of Limerick, Limerick, Ireland

ARTICLE INFO

Keywords:
Resident ROV
Autonomous docking
Computer vision

ABSTRACT

This paper presents autonomous docking of an industry standard work-class ROV to both static and dynamic docking station (Tether Management System — TMS) using visual based pose estimation techniques. This is the first time autonomous docking to a dynamic docking station has been presented. Furthermore, the presented system does not require a specially designed docking station but uses a conventional cage type TMS. The paper presents and discusses real-world environmental tests successfully completed during January 2019 in the North Atlantic Ocean. To validate the performance of the system, a commercial state of the art underwater navigation system has been used. The results demonstrate a significant advancement in resident ROV automation and capabilities, and represents a system which can be retrofitted to the current ROV fleet.

1. Introduction and background

There is constant growth in the world's energy consumption and an ever-increasing focus on energy security and diversification, with an emphasis on having energy production within home territorial regions. With expansion comes increased demand for all fuels and we have seen all variants except coal and hydroelectricity grow at above-average rates (Dudley, 2018). In recent years the trend in offshore power generation, both in oil & gas (O&G) and marine renewable energy (MRE), is to move production platforms further offshore where significant energy potential exists (W. Europe, 2017). This trend comes from a number of contributing factors including: need for increased energy farm footprint, technological advancements in ROV/AUV industry and significant savings in deep-water capital expenditure (CAPEX) and operational expenditure (OPEX) costs compared to 2014 levels (Intelligence, 2019). However and although higher energy potential and cost savings have resulted in deep-water sites becoming commercially viable, the costs associated with operations, maintenance, and repair are inevitably increasing with the move into deeper offshore regions. In downtime/failures, due to the remoteness of the production platform and associated transit times, weather windows for Inspection Maintenance and Repair (IMR) operations are significantly reduced. This represents a substantial issue in reducing and maintaining projected OPEX costs. This may not be overcome simply through predictive maintenance due to the growth in infrastructure planned within the future offshore blue economy. One of the primary OPEX costs including ROV deployment, is support vessel day rates. The day rate of an offshore maintenance vessel with a crew and equipped with ROV typically reaches at 100.000$ or more (Statoil, 2017; Christ and Sr, 2013). While production platform downtime can cause considerable costs in the O&G industry, geographic spread of infrastructure assets creates additional concerns within the MRE sector, which is currently undergoing huge expansion. Floating offshore MRE farms consist of seabed infrastructure, anchoring systems, flexible cable risers, floating platforms, towers, and distributed buoys/sensors that can be spread over an area of 100 km^2 or more. IMR tasks on a huge area demand more vessels, thus introducing higher OPEX. Furthermore, weather conditions onsite are more adverse further offshore, and considering that MRE sites are by their nature located in strong wind/current/tide areas, there can be narrow windows for IMR operations. The primary restriction in terms of ROV operations and associated operational weather windows, is in the launch and recovery of the vehicle, and the most demanding time for the pilot is within the first 15 m of water depth. These restrictions are recognised within the industry, particularly within the offshore wind sector, and as a solution to the problems resident, permanently deployed underwater vehicles are emerging as a potential solution to overcome these problems, expand operation weather windows and reduce OPEX costs. Using a permanently deployed vehicle, real-time, weather independent, onsite remote piloting is possible. This opens the path to year-round operations without the need for expensive vessels onsite and with reduced personnel transfers (OSJ, 2018).

ROVs have been the workhorse of the oil & gas industry since their introduction in the early 1970s, however the resident ROV concept is only recent, being born out of unprecedented cost saving demand

* Corresponding author.
E-mail address: petar.trslic@ul.ie (P. Trslic).

https://doi.org/10.1016/j.oceaneng.2019.106840
Received 10 July 2019; Received in revised form 24 October 2019; Accepted 7 December 2019
Available online 13 December 2019
0029-8018/

robotics

MDPI

Article

Geometric Insight into the Control Allocation Problem for Open-Frame ROVs and Visualisation of Solution

Edin Omerdic *, Petar Trslic, Admir Kaknjo, Anthony Weir, Muzzafar Rao, Gerard Dooly and Daniel Toal

Department of Electronics and Computer Engineering, Centre for Robotics and Intelligent Systems, University of Limerick, V94 T9PX, Limerick, Ireland; petar.trslic@ul.ie (P.T.); kaknjo.admir@gmail.com (A.K.); anthony.weir@ul.ie (A.W.); muzaffar.rao@ul.ie (M.R.); gerard.dooly@ul.ie (G.D.); daniel.toal@ul.ie (D.T.)

* Correspondence: edin.omerdic@ul.ie; Tel.: +353-0-61-202-355

Received: 8 November 2019; Accepted: 21 January 2020; Published: 29 January 2020

Abstract: The overall control system for an open-frame Remotely Operated Vehicle (ROV) is typically built from three subsystems: guidance, navigation and control (GNC). The control allocation plays a vital role in the control subsystem. Typically, open-frame underwater vehicles have p actuators (thrusters) for the motion in the horizontal plane, and the control allocation problem, in this case, is very complex and hard to visualise, because the normalised constrained control subset is a p-dimensional unit cube. The aim of this paper is to give a clear picture and a geometric interpretation of the problem and to introduce a hybrid method, based on the integration of a weighted pseudoinverse and the fixed-point method. The main idea of the hybrid method is visualised, and the deep geometric insight is provided using a "virtual" ROV in low-dimensional control spaces, including visualisation of the attainable command set, solution lines, control energy spheres and the role of pseudoinverse and fixed-point iterations. The same concepts are then extended to higher-dimensional cases, for open-frame ROV with four X-shaped (vectored) horizontal thrusters, which is one of the most common thruster configurations for commercial ROVs. The proposed hybrid method has been developed, integrated into a generic fault-tolerant ROV control system and evaluated in virtual and real-world environments off the west coast of Ireland using observation-class ROV Latis and work-class ROV Étaín.

Keywords: fault-tolerant control; control allocation; ROV

1. Introduction

In general, a fault is the primary cause of changes in the system structure or parameters that eventually leads to degraded system performance or even the loss of the system function. A Fault-Tolerant Control (FTC) system continuously analyses the behaviour of the plant in order to identify faults and changes the control law to hold the closed-loop system in a region of acceptable performance. Fault tolerance includes two steps [1]: (i) Fault diagnosis (the existence of faults has to be detected, and the faults have to be identified); (ii) Control re-design (the controller has to be adapted to the faulty situation so that the overall system continues to have satisfactory performance). Like faults, disturbances and model uncertainties change the plant behaviour and have similar effects on the system. Disturbances and model uncertainties are nuisances which are known to exist, but whose effects on the system performance are handled by appropriate measures like filtering or robust design. On another side, the FTC system is designed to detect the faults and remove their effects by remedial actions, i.e., it is aimed to change the control law in order to cancel the effects of the faults or to attenuate them to an acceptable level.

Adaptive Neuro-Fuzzy Network Enhanced Automatic Visual Servoing Algorithm for ROV Manipulators

Satja Sivcev, *Petar Trslic, David Adley, Luke Robinson, Gerard Dooly, Edin Omerdic, Daniel Toal
Centre for Robotics & Intelligent Systems
University of Limerick
Limerick, Ireland
petar.trslic@ul.ie

***Abstract*—This paper presents research and development for achieving advanced ROV manipulation systems with vision based servo control capable of being operated by pilots with auto assist in the dynamic subsea conditions. Underwater inspection and intervention operations are performed by work-class ROVs equipped with robotic manipulators. A standard offshore oil and gas setup includes a human pilot utilising telemanipulation technology to operate both vehicle and manipulators based on the work-site visual feedback provided by camera and sonar systems. For challenging applications in waves or currents where target devices are in motion a new approach is required. A position based visual servoing (PBVS) algorithm designed to follow a moving target with an underwater manipulator is proposed. The developed algorithm integrates Adaptive Neuro-Fuzzy Inference System (ANFIS) network framework for target motion prediction. The effectiveness of the developed software is verified through a series of experiments carried out with an off-the-shelf industrial hydraulic subsea manipulator in the laboratory conditions.**

***Index Terms*—visual servoing, ANFIS, subsea manipulation**

I. Introduction

This paper presents control system developments for subsea robotic manipulators beyond the current state-of-the-art in work-class Remotely Operated Vehicle (ROV) technology. The proposed methods are to enable ROVs to address challenging conditions encountered in Marine Renewable Energy (MRE) sites comprising of offshore wind, floating wind, wave energy conversion and tidal energy conversion devices. Development of enhanced robotic capability is essential to support large-scale operations for construction/roll out, Inspection Maintenance and Repair (IMR), monitoring and control of MRE installations. MRE devices are by design located in the dynamic real-world offshore conditions of high energy waves, currents, and winds. Service robots are necessary to allow the emerging MRE sector to develop and grow. Even though the workclass ROVs are the workhorse of subsea operations for the offshore oil and gas industry, the current intervention technology capabilities they integrate are not sufficient for operating in challenging MRE conditions. Moreover, oil and gas ROV operations are generally not performed in the top 20m - 40m splash zone, but rather the ROVs punch through the splash zone to operate in the relatively calm environment below or on the seabed. Additionally, cancelling ROV operations in unfavourable weather conditions is very common.

The MRE sector IMR operational conditions will under many circumstances be above operating limits of state-of-the-art commercial ROV technology [1]. Therefore, the motivation of this research is to investigate and develop ROV systems for intervention and inspection tasks in offshore conditions of increasing strength and deal with challenges in the performance of ROVs at high energy MRE sites [2]. Same systems could be used in an emerging sector of permanently deployed ROVs [3]. A broad range of subsea tasks undertaken by ROVs is done using underwater manipulators, including pipe inspection, salvage of sunken objects , mine disposal, surface cleaning, valve operating, drilling, rope cutting etc. The majority of commercial underwater manipulators are not servo controlled and none are supported with kinematic engine control approaches. They are predominantly hydraulically driven, and utilize traditional teleoperation approaches with an open loop control system, completely reliant on the human operator. The pilot who is located on the support vessel acquires visual feedback of the scene through camera and/or forward looking sonar systems and often simultaneously performs multiple tasks: manipulates the robot arm(s), flies the vehicle, or performs underwater inspection [4]. Sometimes ROV pilots face dangerous and stressful situations, e.g. British Petroleum ROV fleet working to shut off the well and stop the oil spill in the Deepwater Horizon disaster [5]. As motion disturbances affecting the underwater vehicle and the manipulator become significant the task execution with a human pilot in the loop becomes difficult and eventually impossible. This is especially the case in MRE sites where the target infrastructure is in the splash zone and in motion.

The majority of academic research experiments in the field of autonomous subsea manipulation have been carried out using prototype, all-electric robotic arms [6]–[8] which are either prototypes or recently commercialised. However, for work-class ROV intervention work, such electric manipulators are not designed or available with sufficient power as specified by ocean engineering contractor requirements, e.g. the manipulator-operated torque tool, which uses the wrist rotate

978-0-578-57618-3 ©2019 MTS

sensors

MDPI

Article

Real-Time Underwater StereoFusion

Matija Rossi [1,*], Petar Trslić [1], Satja Sivčev [1], James Riordan [2], Daniel Toal [1] and Gerard Dooly [1]

[1] Centre for Robotics & Intelligent Systems, University of Limerick, Limerick V94 T9PX, Ireland; petar.trslic@ul.ie (P.T.); satja.sivcev@ul.ie (S.S.); daniel.toal@ul.ie (D.T.); gerard.dooly@ul.ie (G.D.)
[2] School of Computing, Engineering, and Physical Sciences, University of the West of Scotland, Glasgow G72 0AG, UK; james.riordan@uws.ac.uk
* Correspondence: matija.rossi@ul.ie; Tel.: +353-61-213-102

Received: 14 September 2018; Accepted: 8 November 2018; Published: 14 November 2018

check for updates

Abstract: Many current and future applications of underwater robotics require real-time sensing and interpretation of the environment. As the vast majority of robots are equipped with cameras, computer vision is playing an increasingly important role it this field. This paper presents the implementation and experimental results of underwater StereoFusion, an algorithm for real-time 3D dense reconstruction and camera tracking. Unlike KinectFusion on which it is based, StereoFusion relies on a stereo camera as its main sensor. The algorithm uses the depth map obtained from the stereo camera to incrementally build a volumetric 3D model of the environment, while simultaneously using the model for camera tracking. It has been successfully tested both in a lake and in the ocean, using two different state-of-the-art underwater Remotely Operated Vehicles (ROVs). Ongoing work focuses on applying the same algorithm to acoustic sensors, and on the implementation of a vision based monocular system with the same capabilities.

Keywords: stereo; underwater; ROV; GPU; real-time; 3D; fusion; camera; tracking; vision

1. Introduction

Applications of computer vision are rapidly growing across a wide spectrum of underwater operations. Vision systems are increasingly being used as the primary tool for inspection of underwater sites, in disciplines ranging from archaeology [1] and biology [2], to offshore engineering [3] and pipeline inspection [4]. This has been facilitated by the increasing industry adoption of remotely operated vehicles (ROV) and autonomous underwater vehicles (AUV) [5–7], which opens the door to many new applications for machine vision. A common task is robot navigation, for which underwater is challenging for many reasons, such as the lack of radio communications, including global navigation satellite systems (GNSS), and limited sensing technology compared to land or airborne vehicles. For this purpose, camera and acoustic sensor systems can be used to implement simultaneous localisation and mapping (SLAM) algorithms to complement inertial navigation systems (INS), which inevitably suffer from drift. If such algorithms prove sufficiently robust, vision systems may obviate the need for inertial navigation systems and replace them with image-based target referenced navigation [8].

An even more demanding task is robotic intervention, where work class ROVs equipped with underwater manipulators have traditionally been teleoperated from support vessels by human operators. Significant effort is currently being put towards the automation of such operations using computer vision [9–12]. In order for an intervention task to be carried out autonomously, it is necessary to know the structure of the scene around the target and the position of the robot relative to it. This makes it possible to then implement higher level features such as path planning, obstacle avoidance, and target identification. Additionally, even in the case of manual operations, providing an

Long term, inspection class ROV deployment approach for remote monitoring and inspection

Petar Trslić, Matija Rossi, Satja Sivčev, Gerard Dooly, Joseph Coleman, Edin Omerdić, Daniel Toal
Centre for Robotics & Intelligent Systems
University of Limerick
Limerick, Ireland
Petar.Trslic@ul.ie

***Abstract*—Marine Renewable Energy (MRE) installations offshore will have significant challenges for operation, inspection, repair, maintenance and intervention activities beyond those for onshore renewable energy farms. To minimise operating expenses (opex) MRE installations must rely on remote monitoring and control (remote presence) with limited human intervention in the field. This paper presents an overview of the long-term, ROV deployment approach for remote monitoring and inspection of distributed assets within the offshore MRE farm, and focuses on one of the critical subsystems: the development of an autonomous offshore garaging system for an inspection class ROV, which will incorporate Smart Tether Management System (STMS).**

***Index Terms*—resident ROV, automatic TMS**

I. Introduction

MRE installations offshore face challenges beyond those in offshore oil and gas due to the scale of individual installation, i.e. plant is unmanned, and MRE must be located in areas of strong waves/current/wind. MRE installations must rely more on remote monitoring and control (remote presence) with limited human intervention in the field. With the growing trend of building offshore floating wind farms [1], being placed further offshore into deeper waters where stronger and more consistent winds conditions will produce greater energy levels, rising opex associated with operations and maintenance (O&M) in the splash zone (top 20m) is inevitable, and this must be minimised. Offshore MRE farms consist of floating platforms, towers, anchoring systems, flexible cable risers, seabed infrastructure, and distributed data buoys/sensor platforms. Using a permanently deployed ROV system, we are capable of providing onsite, real-time, remote inspection piloting allowing predictive maintenance and inspection tasks to be completed with the requirement for expensive vessels and personnel transfers significantly reduced. As the environmental impact of MRE installations, such as offshore wind farms, is known to a certain extent, a permanently deployed vehicle on such a farm with various sensors that are required for inspection of subsea structures can also be used for environmental monitoring. This will allow for an even greater understanding of the subsea biology and enable future studies by providing continuous long-term datasets.

This material is based upon works supported by Science Foundation Ireland (SFI) under the Research Centres Award 2012, SFI Centre for Marine & Renewable Energy Research (12/RC/2302 and 14/SP/2740).

In section II we describe vital parts of the resident ROV concept and the different deployment approaches of such a system. Equipment developed and acquired within the research group, which is to be used as a platform for resident ROV concept is presented here as well. Section III presents an ongoing development of the STMS, and in section IV we conclude and describe future work which is to be taken.

II. Background

Since ROV support vessels are costly and MRE installations are progressing further offshore, there is a considerable potential for resident ROVs as technology advances. There are a couple of research and development projects working on resident ROV system with different goals and approaches. Some examples include the Eelume project by Kongsberg [2], SAAB Sabertooth ROV/AUV [3], and recently two work-class resident ROV systems were developed, E-ROV from Oceaneering [4] and RROV from IKM [5]. These systems are based on work-class ROVs, and both are designed to perform a heavy intervention at the oil and gas field. The emphasis of our approach is on inspection of underwater assets, while a predictive maintenance approach dictates the intervention operation frequency.

A. Resident ROV subsystems

A system such as resident ROV consists of four major subsystems: (1) a garaging system consisting of TMS and docking station, (2) an autonomous power supply, (3) communication with the shore, and (4) a long-term deployed ROV. The subsystems can be placed above the water or subsea, in various configurations, which are defined by site type (existence of a floating platform), sea conditions, and power requirements. Fig. 1 shows different arrangements of these subsystems. The proposed arrangement for inspection-class ROV (I-ROV) is shown in Fig. 1a. It consists of a communication module, a power subsystem, and a TMS subsystem placed on a floating structure (wind turbine tower, buoy) while both the docking station and the ROV itself are submerged. This allows for launch and recovery of the ROV, which is the most critical part of the ROV operation, without a dependence on weather conditions on the surface. The power supplied to the system is generated on-site and communication is achieved through